David João Henriques Martins
Licenciado em Ciências de Engenharia Civil

PRECAST CONCRETE TRUSS TOWERS TO SUPPORT WIND ENERGY GENERATORS
- experimental analysis of column to column connections -

Dissertação para obtenção do Grau de Mestre
em Engenharia Civil – Perfil Estruturas

Orientador: Professor Doutor Válter José da Guia Lúcio
Professor Associado, FCT/UNL

Co-orientador: Professora Doutora Sueli Souza
Professor Auxiliar, UTFPR,

Júri:

Presidente: Prof. Doutor Filipe Pimentel Amarante dos Santos
Arguente: Prof. Doutora Carla Alexandra da Cruz Marchão
Vogal: Prof. Doutor Válter José da Guia Lúcio

FACULDADE DE CIÊNCIAS E TECNOLOGIA
UNIVERSIDADE NOVA DE LISBOA

Novembro de 2018

PRECAST CONCRETE TRUSS TOWERS TO SUPPORT WIND ENERGY GENERATORS: EXPERIMENTAL ANALYSIS OF COLUMN TO COLUMN

Acknowledgements

The present dissertation would not have been accomplished without the support from many people who have either helped me or encouraged me. For all those people, my most profound thanks.

I would like to express my great admiration, recognition and respect for my adviser, Professor Válter Lúcio. I am grateful to have had this opportunity to share with him his priceless scientific teachings, his wisdom and experience, and also thank him for his friendship and precious advices.

I would like express my great respect to my co-adviser, Professor Sueli Souza, who also helped me to complete this dissertation. I am grateful for her help, assistance and friendship.

I also thank to Professor Carlos Chastre and Professor Luiz Souza, for their priceless presence and assistance throughout the completion of this dissertation.

I would like thank CONCREMAT for having supplied the precast concrete elements and also for all their technical aptitude, competence and cooperation.

I thank to TREJOR for having supplied the anchor bolts used in connection between the precast concrete elements.

I would like to thank SOPROEL for having filled the connection joints of experimental models S2 and S3 with epoxy resin.

I also want to show my appreciation to my colleagues, Pedro Guerra, Davide Barbosa, Pedro Patrício, Tânia Simões, Ana Breia, Isabel Borba, Cinderela Plácido, Solange Cardoso, Catarina de Jesus, and Rita Geraldes, with whom I had the pleasure of sharing moments along my academic path.

A special thanks to Noel and Dinarte for the unconditional support and help in general problem solving throughout experimental tests in laboratory.

Lastly, thanks to my wife, to my family, to my great friends for all their love, support, patience and inspiration since nothing or almost nothing would be possible without them.

Abstract

Currently, with the evolution of the technology and increased demand for wind energy, it is clear there is a need to use larger wind turbines with longer blades and, consequently, taller towers. With this need to build taller towers, precast concrete solutions have become very competitive. Truss precast concrete towers is a solution that complies with the demands of the present and future wind energy production. The execution and structural behaviour of the connections between the tower elements remain an important research issue.

The main purpose of this dissertation is an experimental analysis of the behaviour of the column-column structural connection of a precast reinforced concrete lattice tower when exposed to seismic and wind actions, to ensure their enforceability in wind energy production industry. It is necessary to continue to increase the knowledge of then fragilities which still exist in the structural connections between precast concrete elements.

So, four experimental tests (S1, S2, S3 and S4) were performed. Both connections of experimental models S1 and S2 were tested using a mixed system with corrugated steel sleeves and protruding steel bars, and commercial anchor bolt connections. However, the connection of first model (S1) was tested with a joint 50 mm thick while in second model (S2) the joint thickness was reduced to the minimum (dry joint - “zero thickness joint”). The connection of the third experimental model (S3) was by a traditional connection system (corrugated sleeves and protruding steel bars) also with dry joint. In the last model (S4), the connection was only with commercial anchor bolts connections and with a 50 mm thick joint.

Keywords:
Precast concrete elements, structural connections, lattice tower.

Resumo

Actualmente, com a evolução da tecnologia e o aumento da procura da energia éolica, é evidente a necessidade de recorrer não só ao uso de turbinas com pás mais longas, mas também de torres mais altas. Com a necessidade de recorrer a torres mais altas, as soluções pré-fabricadas tornam-se muito competitivas. A torre treliçada pré-fabricada em betão é a solução que permite satisfazer as exigências actuais e futuras que incidem sobre a produção de energia eólica. A execução e o comportamento estrutural das ligações entre os elementos da torre continuam a ser uma tema importante de pesquisa.

O principal objetivo da presente dissertação é simular o comportamento das ligações estruturais entre elementos pré-fabricados em betão armado de uma torre eólica treliçada quando sujeita às ações sísmicas e do vento, de modo a validar e verificar a sua aplicabilidade na indústria de produção de energia eólica. É necessário continuar a ampliar os conhecimentos sobre as fragilidades que existem nas ligações estruturais entre elementos pré-fabricados de betão.

Para tal foram ensaiados quatro modelos experimentais (S1, S2, S3 e S4). Ambas as ligações dos modelos S1 e S2 foram asseguradas através de um sistema misto de ligações aparafusadas e ligações de continuidade (varões salientes com bainhas). A ligação no primeiro modelo foi executada com uma junta de 50 mm de espessura enquanto no segundo esta foi anulada ao mínimo (junta seca - "junta zero"). A ligação do terceiro modelo (S3) foi executada a partir de varões salientes e bainhas, e também com junta praticamente nula (junta seca). No último modelo (S4), a ligação foi assegurada apenas com um sistema de ligação aparafusada e com junta de 50 mm de espessura.

Palavras chave:

Elementos pré-fabricados em betão, ligações estruturais, torre eólica treliçada.

Contents

List of Figures

List of Tables

List of Abbreviations, Acronyms, and Symbols

Abbreviations

EC2	Eurocode 2
EC8	Eurocode 8

Acronyms

FCT	Faculdade de Ciências e Tecnologia
RC	Reinforced Concrete
UFRG	Unidirectional Fibre Reinforced Grout
UNL	Universidade Nova de Lisboa
UTFPR	Universidade Tecnológica Federal do Paraná

Symbols

A	Contact concrete area
A_{sw}	Cross sectional area of shear reinforcement
b_w	Width of the web
d	Effective depth of a cross section
E_{cm}	Secant modulus of elasticity of concrete
E_m	Mean experimental values of Young's modulus
f_c	Compressive strength of concrete
f_{cd}	Design value of concrete compressive strength
f_{cm}	Mean value of the compressive strength of concrete and grout

$f_{cm,cube}$	Mean value of concrete cubic compressive strength
f_{ct}	Value of axial tensile strength of concrete
f_{ctm}	Mean value of axial tensile strength of concrete
f_y	Tensile yield strength of steel
f_{ym}	Mean tensile yield strength of steel
f_{ywd}	Design yield of shear reinforcement
f_u	Ultimate strength of steel
M_{cr}	Cracking Moment
M_{rd}	Moment capacity
N_c	Axial force
P	Axial force
$V_{Rd,max}$	Strut capacity
$V_{Rd,s}$	Stirrups capacity
W	Elastc section modulus
α_{cw},	Coefficient taking account of the state of the stress in the compression chord.
ε	Strain
ε_{c1}	Strain at maximum compression stress for concrete
ε_{cu1}	Ultimate compression strain for concrete
ε_y	Yield strain
ε_u	Ultimate strain for steel
v	Strength reduction factor for concrete cracked in shear
σ_{cp}	Compressive stress in the concrete from axial load or prestressing
δ_{max}	Experimental maximum displacement
δ_{res}	Experimental residual displacement
θ,	Angle between concrete compression strut and beam axis perpendicular to the shear force

Chapter 1

Introduction

1.1 Background

The wind energy production is a growing industry, is the most sought-after renewable energy source and is a good option to replace non renewable energy sources that remain in use. According to wind global market statistics from Global Wind Energy Council [1], 51.473 MW of new wind capacity was added in 2014.

Currently the electricity production needs are increasing due to growing consumption, thus it is important to build structures able to respond to this need, but this is only possible with the help of engineering. An evolution in scale (tower height and blades length) is needed. Tower height increase raises the turbine to the highest possible position to achieve higher wind speeds (wind turbine power contributes to increase in energy production).

The precast reinforced concrete lattice tower solution (Figure 1.1), designed by Lúcio and Chastre [2], allows the construction of higher towers (between 80 to 120 meters), and it is competitive in relation to other structural systems.

Legend: 1 – column; **2** – beam; **3** – joint; **4** – bracing diagonals; **6** – foundation; **7** – base to support eolic turbine (**20**)

Figure 1.1: Precast reinforced concrete lattice tower solution, designed by Lúcio and Chastre [2]: onshore (left); offshore (middle); lateral view (right).

Compared with other structural systems adopted in Portugal, the "eolic truss tower" would have much higher production capacity and a costs reduction of about 15-20%. Furthermore, this solution is engineered for slender precast elements which simplifies their transportation and handing/elevation on site. In other words, the potential benefits with this solution designed by Lúcio and Chastre [2] (eolic truss tower) exist at the level of production, transportation, construction, application and for the environment. This is because the tower elements are prefabricated in concrete a durable material with strict quality control. In addition to this, the production of the structures with precast elements occurs in places which allow a high level of quality and durability control. Moreover, the concrete structures have much more durability when compared to steel towers, especially in maritime environments, due to the protective action of an appropriate reinforcement concrete cover. This durability increases with the use of high-performance concrete and this technique is commonly used in precast manufacturing companies.

The transportation of these elements is easy, simple and practical because for this tower solution the geometry of the tower is simpler and smaller thus not exceeding transportation limitations (Figure 1.2).

Figure 1.2: Transportation of tower elements of precast reinforced concrete lattice tower solution. [2]

In construction, because:

- the significant weight of the tower allows a reduction of the required foundation weight, leading to cost reductions. Moreover thanks to the use of long elements and fast structural connections, the assemblage speed is much bigger which also leads to cost reductions. (Figure 1.3)
- this system is not conditioned by current dimension limits in the transportation, so it is possible to optimize the geometry of the tower with less restrictions;
- the reduction of fatigue effects due to a significant improvement of the structural damping and dynamic behaviour;
- due to the high ductility of the tower elements and its structural damping which increases in situations of extreme loads, this system presents a good response to seismic actions. Unlike

steel towers, the behaviour of this structure is able to dissipate energy in the event of an earthquake;

- the connections between elements are reliable, maintenance free, easy and fast to implement on site;
- the connections of the columns to foundations, are simple, cheap and reliable.

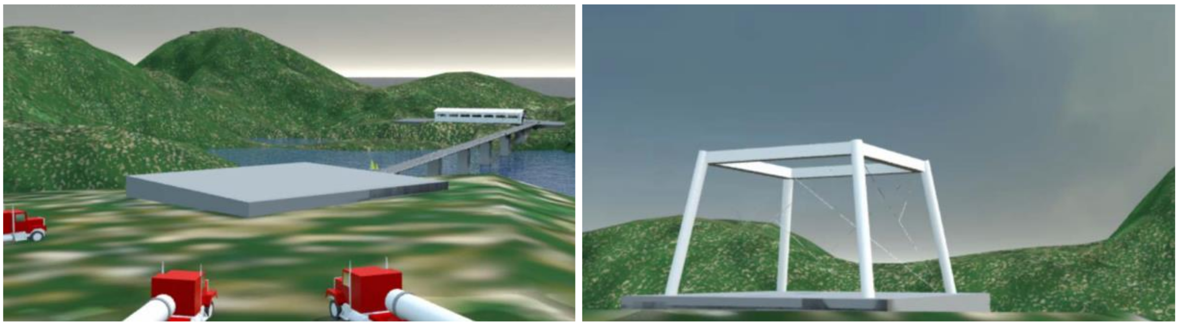

Figure 1.3: Assemblage of tower elements of precast reinforced concrete lattice tower solution. [2]

This structural system of eolic tower makes it possible for their use not only onshore but also offshore (Figure 1.4). Finally, at an environment level with this precast solution it will be possible to reduce the CO2 emissions in relation to the manufacture of a steel tower.

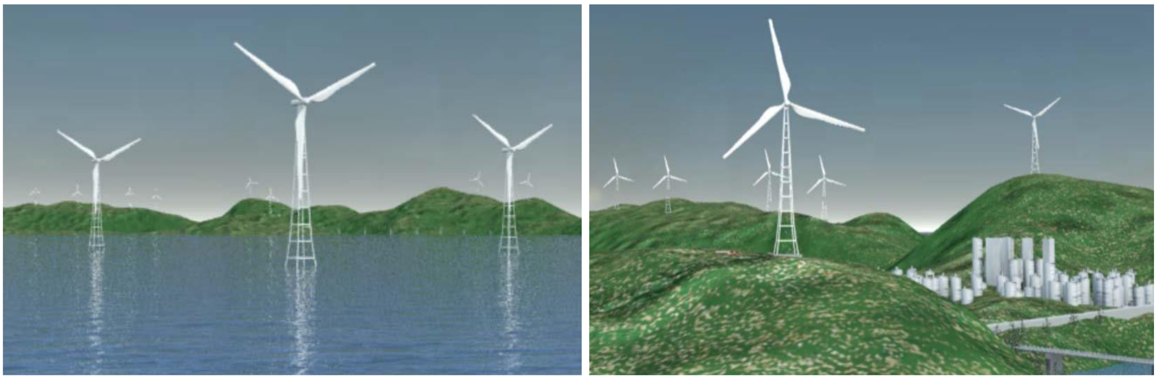

Figure 1.4: Precast reinforced concrete lattice tower solution (onshore and offshore). [2]

Therefore, based on a precast reinforced concrete lattice tower solution (Figure 1.1), designed by Lúcio and Chastre [2], the purpose of this dissertation (or research) will be to extend and deepen our knowledge about behaviour of connections between the precast elements, namely column to column connections.

The connections have a major importance in global behaviour of precast structures. When the connections are not properly designed or well-constructed they become a problem for precast structures. Thus, the study of connection behaviour between elements of the tower is of utmost importance. According to El Debs [3], the connections must have the same quality control as the elements in precast structures.

One very traditional and widely used solution is the connection system with corrugated steel ducts cast in one element and protruding bars in the other. In this system the connection is sealed with grout inside the ducts after insertion of the protruding bars and alignment of the connecting elements. According to experimental tests results from Reguengo, R. Lúcio, V., Chastre, C. [4], this is a good connecting solution, as long as the protruding bar anchorage length is designed according to current rules.

Moreover, there are also connection systems with anchor bolts. Currently, this connection system is considered as an alternative solution compared to the traditional connections adopted in reinforced precast concrete. This system is based on the mechanical connection between steel shoes embedded into one column and protruding anchor bolts anchored into the other column. According to studies performed by Fagà et al [5], the behaviour of the anchor bolts control the collapse mechanisms, without significant damage of the precast elements, regardless of the axial load level imposed on top of the column. Although the anchor bolts have reached the plastic level (yielding level) due to horizontal forces, no significant loss of connection stiffness was observed and neither was there any significant damage in the column base.

To enable the construction of the tower it is necessary to choose a type of connection that is easy to implement, economical and resistant to internal forces.

In this research, four experimental results of column to column connections with 50 mm and 3 mm joints are presented:

- experimental models S1 and S2 – mixed connection system with corrugated steel sleeves and protruding steel bars, and commercial anchor bolt connections;
- experimental model S3 - connection system with only corrugated sleeves and protruding steel bars;
- experimental model S4 - system with only commercial anchor bolt connections;

In models S1 and S4 a joint with a thickness of 50 mm was considered, while in connection systems of models S2 and S3 a dry joint - “zero joint” (almost null joint) was considered.

1.2 Objectives and scope

The present dissertation aims to extend and deepen knowledge about behaviour of connections between precast elements, namely between column to column. To this end, four connection systems between precast concrete elements (connection column to column) were tested, where two of them have a joint with 50 mm thick and the other two have a dry joint - “zero joint” (almost null joint). This simulation has the purpose of analysing the response of precast elements connections when subjected to axial and shear force, in order to validate and verify the applicability of this connection systems in precast elements of an “eolic truss tower”, engineered by Lúcio and Chastre [2].

1.3 Dissertation outline

The content of the dissertation is organized into the following six chapters:

- **Chapter 1 -** General approach to the subject of the dissertation
- **Chapter 2 -** Analysis of the state-of-the-art.
- **Chapter 3 -** Description of the experimental tests. Identification and depiction of experimental models, definition of testing system, instrumentation and test procedures.
- **Chapter 4 -** Characterization of the materials used in the production of the models.
- **Chapter 5 -** Report of experimental results obtained and subsequent analysis and comparison.
- **Chapter 6 -** Summary of the research, conclusions and suggestions for future work.

Chapter 2

State-of-the-art

2.1 Introduction

Structural connections in precast concrete guarantee the connection between independent elements. In the design, connections should have the capacity to transfer the forces between elements in order to guarantee the robust behaviour of the structure. Furthermore, it is fundamental to guarantee that the design has taken into account important aspects like the dimensional tolerances, connection requirements, simple execution and inspection/manutention [7].

According to Proença [8], Reis [9] and Albarran [10], the connections between precast elements must perform well in the following areas:

1. **Structural safety:**

   - **mechanical strength:** all the connections between structural elements must resist appropriately to shear and/or bending forces, as a result of the actions that may occur during the life of the structure;

   - **ductility:** this is the most demanding criteria in countries with high seismic activity. The structure must be able to withstand large deformations before failure. The ductility must be guaranteed not only in the connections but also in the precast elements themselves;

   - **durability:** All structural elements, specially the connections, must have appropriate durability characteristics according to the type of environmental exposure. The protection of the steel elements against corrosion can be ensured through adequate concrete cover or through an anti-corrosion treatment;

   - **fire resistance:** the fire resistance of the precast structural elements must reflect that of the structural elements cast on site; moreover, the material specifications must be in accordance with fire safety regulations [11];

- **stability and balance:** As the overall behaviour of the structure often differs from the service stage to the assembly stage, it is important to design the connections between precast elements, not only for service stages but also for assembly stages.

2. **<u>execution versus economy:</u>**

- Simplicity is the fundamental principle of a connection design. A simple connection is, generally, easy to design and execute, therefore it will have good chances of being more economical. This simplicity should be planned not only for the production phase, but also for the assembly phase. The work on site must be minimized because the processes in the factory are simpler. It is always more economic if during the assembly phase the processes are simple, fast and effective. Moreover, factory production, has a qualified workforce, better working conditions, better organization and quality control. Therefore, it is always be wiser to “complicate in the factory in order to facilitate the assembly phase”. Lastly, the choice of the type of connection must consider minimal tolerances between precast elements [12] and/or elements executed on site, otherwise this could lead to difficulties during the structures assembly and/or limit the adequate performance of the connections.

3. **<u>aesthetics:</u>**

- Generally speaking, the connections between precast concrete elements are not very appealing aesthetically, however, there are connection systems that are hidden inside the concrete elements.

2.2 Connections in precast concrete elements

According to Pompeu dos Santos [13], the classification of the type of connection one can be based on four criteria:

- type of precast elements to connect, i.e. connecting footing to column, column to column, beam to column, beam to beam and beam to slab;
- type of forces transmitted, i.e. connections for compression, for tension, for bending or for shear;
- type/process of execution, i.e. anchor bolt connections, welded connections, pre-stressed connections, connections for continuity cast on site;
- type of behaviour under bending:
  I. <u>Pinned Connections</u> - connections that do not transmit bending moments.

II. Rigid Connections – where a total transmission of the bending moment and, therefore, the continuity between elements is duly ensured (they exhibit strength and deformability similar to the monolithic structures).

III. Semi-Rigid Connections - cases where the transmission of the bending moment is partial, consequently, the continuity between elements is merely partial (the deformability is significantly higher than in-cast-in place structures).

Mokk (1969) [14] classifies the connections between precast elements as rigid or pinned. Rigid connections restrict the degree of freedom of the system. In other words, they allow the transmission of the bending moment between elements. This type of connection is suitable when the goal is to have a connection with a good performance in relation to tension, compression, shear and bending. These connections can be obtained through:

a) welded metal plates;
b) lap lengths between bars by:
    i. grout sealing;
    ii. welding;
    iii. couplers;
c) post-tension;
d) anchor bolts.

The pinned connections are used when there is no interest in maintaining the bending moment continuity. In the precast concrete industry, these connections are very common in beam to column connections in warehouses and factory buildings.

Columns are usually subjected to combinations of compression and bending, therefore it is fundamental that the transmission of the bending moments is assured in the column-column connections.

The column-column connection may occur close to the connection with the beam or at half distance between floors. The major advantage of the first hypothesis is by decreasing the number of connections needed to be carried out on site. However, in cases where the continuity of the beam is demanded, this connection type can be complex and can slow down the assembly phase. The great advantage of the second hypothesis is to guarantee that the connection is performed in a zone in which the bending moments on the column are small, so that its efficiency is less critical for the structure. In seismic areas, ideally all the column-column connections should be made at half way between the floors. This second hypothesis, makes it possible to construct a precast structure without connections in the columns critical zone, ensuring a global ductility similar to cast-in-place structures.

Therefore, when column-column connections are made in the critical zone, they must be oversized to remain within the elastic stage during an earthquake.

2.2.1 Connection with welding plates

The process of connection by welded plates consists of leaving a steel plate on the end of each precast element. This plate is welded to steel bars which stay embedded in the columns. Each column is positioned and the connection is obtained by the welding of the steel plates around the perimeter (see Figure 2.1 - a)). Alternatively, this connection can be made with steel bars protruding from each precast element which are welded to a steel section on site (see Figure 2.1 - b)). In both cases the strength of the welding must guarantee a rigid connection between the columns, effectively handling the forces that can be transmitted by the connection: mainly compression, shear and bending.

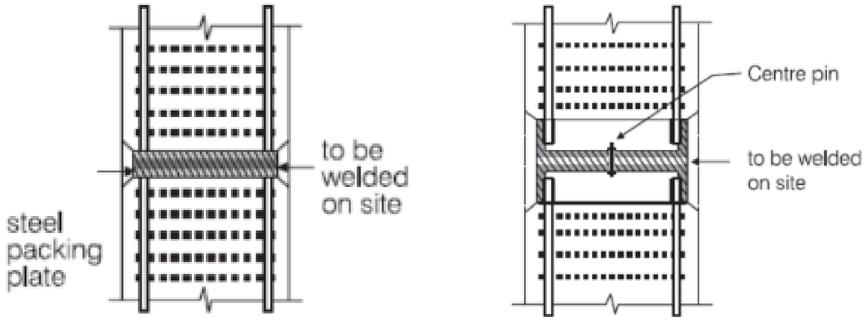

Figure 2.1: Column to column connection by welding steel plates (**a**) or steel section (**b**).[20]

This connection type is of a simple design and, allows the highest tolerances and high strength and is fast to execute. The fact that this construction process demands some technology and specialized workforce, makes it expensive to perform on site, so whenever possible, it should be used in the factory. For this reason, the bolted connections are more appealing solutions compared to welding connections, even though the requirements of stricter tolerances. Besides that, the welded connections has a brittle failure, and therefore it is not recommended in high seismic zones. Regarding fatigue, the welded connections have less resistant capacity in comparison to bolted connections.

In conclusion, despite being an alternative, the welded connection systems are not commonly used in the column-column connections due to the disadvantages described above.

2.2.2 Corrugated steel sleeves with grout

In this connection one of the elements has protruding steel bars, while the other has holes with the corrugated steel sleeves embedded in concrete. After inserting the bars inside the holes, they are filled up with fluid grout to guarantee the sealing of the steel bars. Therefore, the continuity of the connection is ensured by the anchorage of the longitudinal bars by overlay as shown in Figure 2.2.

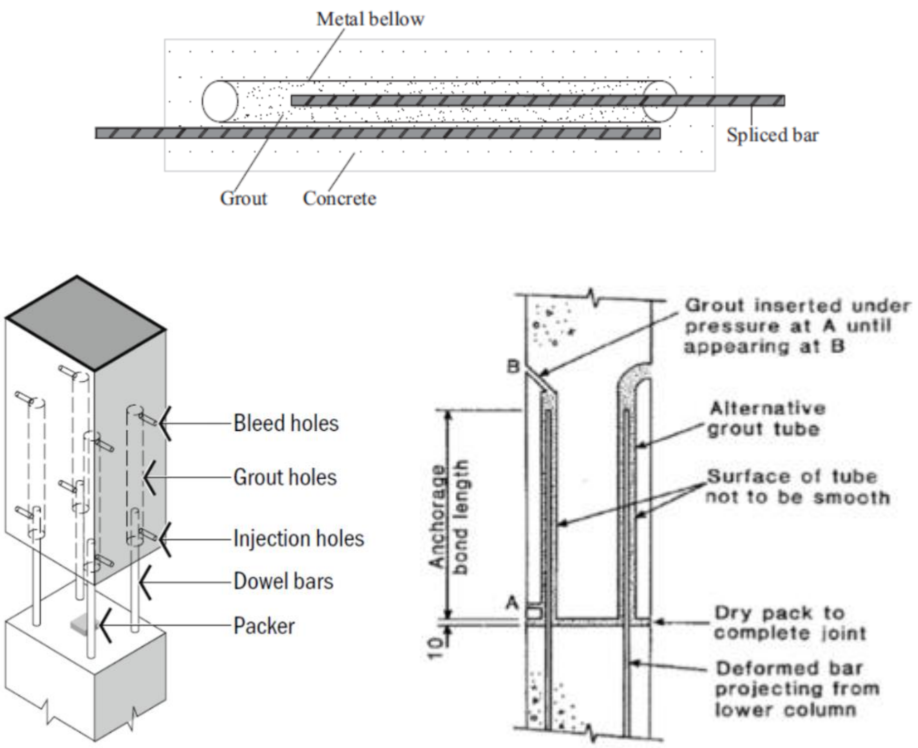

Figure 2.2: Column to column connection with continuity of reinforcement through overlap length (up-[21] and down-[19]).

Elliot [22] calls this system "columns on grouted sleeves". In his opinion the filler material should be similar to a fluid grout with compression strength higher than column concrete strength and never less than 40 MPa. The gap (the space between hole sleeve and steel bar) should have a nominal dimension of never less than 6 mm, in the case of grout injection, or 10 to 15 mm in case of grout filled by gravity.

The recommended sleeve minimum diameter is 2.5ø to 3ø, where ø is the protruding steel bars diameter. This rule guarantees a suitable tolerance for grout filling process. Eight protruding steel bars per column is the maximum recommended number. If more bars are necessary, a concrete with higher compression resistance and protruding steel bars with higher diameter should be used.
This connection process type has some disadvantages:

- the need for support to ensure the column remains vertical;

- curing time is required so that the bonding reaches its maximum strength;
- the protruding steel bars are sometimes bent / twisted during transportation and assembly operations;
- sometimes the tolerances between the holes and the protruding steel bars are not achieved, which leads to difficulties in assembly and, in turn, incomplete sealing of the steel bars, thus compromising the connection strength;
- for the protruding steel bars to be centered with the corrugated sleeves, it is necessary to reduce the effective depth (d) of the longitudinal reinforcement, therefore decreasing bending resistance at the connecting zone;
- in the section of the holes (corrugated sleeves), the interruption of the protruding steel bars is total (sharp transition of reinforcement), thus increasing a critical zone susceptible to failure (plastic hinge formation). This sharp transition should be made far away from the column cross section of maximum moments.
- in situations of high compression, the thickness of joint should be practically null, otherwise the buckling risk of protruding steel bars increases. Therefore, the cases illustrated in Figure 2.3, where the connecting joint is also used to ensure the continuity of slab and beams, are not suitable for earthquake regions.

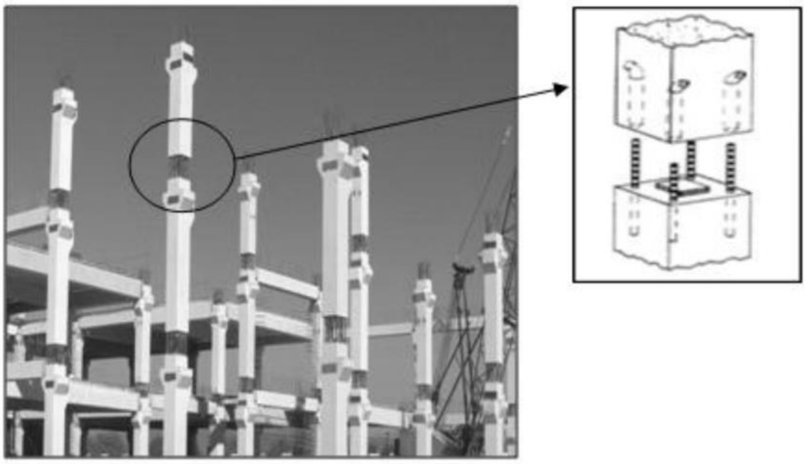

Figure 2.3: Column to column connection with on-site cast connection joint and corrugated steel sleeves [23].

However, despite these disadvantages, it is a very traditional and common process for connections between precast concrete elements. Notable advantages of this connection process include:

- In areas of high seismic activity, it is a recommended solution due to its ductility when compared to welded or anchor bolt connections.

- The connection is not external, therefore it is not necessary to apply protection against the action of environmental agents or fire. Moreover, this type of connection does not have any visual impact.

Figure 2.4 shows three situations using this type of connection. Situation (a) refers to an example of division of the elements, in which the connection of the columns is made floor level, allowing continuity for the beam. In (b) is represented the division of the elements with cross-shape, in which the connection of the columns is performed at half height of the floors. Finally, in (c) the elements have a T-shape, where the connection of the columns occurs at the level of the floors.

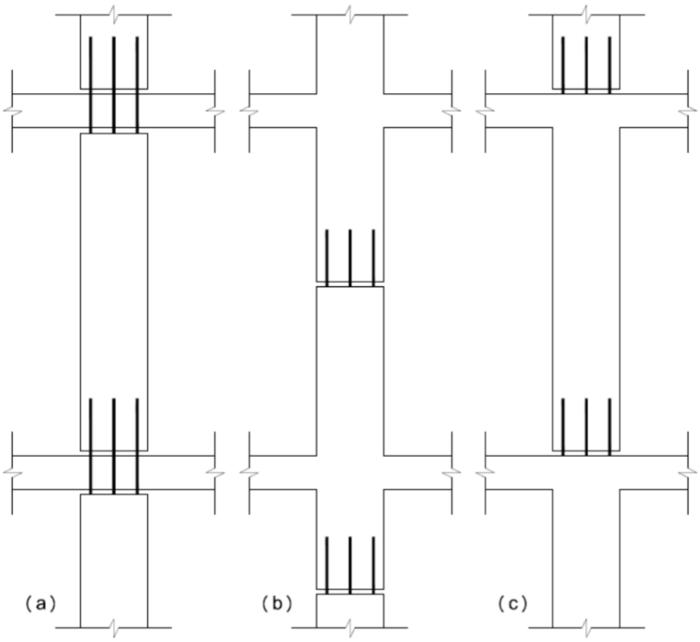

Figure 2.4: Column to column connection with continuity of reinforcement through grout sealing [24].

Connections with continuity of reinforcement, depending on location and number of protruding steel bars, can be designed and prepared for energy dissipation for cyclic actions [21]. For a good performance under dynamic actions (earthquakes), these connections should have: energy dissipation capacity, ductility and spiral reinforcements to prevent the steel bars buckling and the detachment or crushing of concrete in the areas of the plastic hinges [21].

2.2.3 Through bar welding

In this connection both columns have protruding steel bars and the continuity is ensured by lap length of the longitudinal bars through welding, and subsequently sealed with grout or concrete, as shown in Figure 2.5.

As with the welded plate solution (**section 2.2.1**), for the reasons already mentioned, this type of solution is not common in the execution of the column-column connections. Moreover, this type of solution, which can be observed in Figure 2.5, has low ductility. The lack of confinement of the continuity reinforcement in the weld zone makes this connection fragile and susceptible to failure by buckling phenomena, when it is subjected to dynamic actions (earthquake).

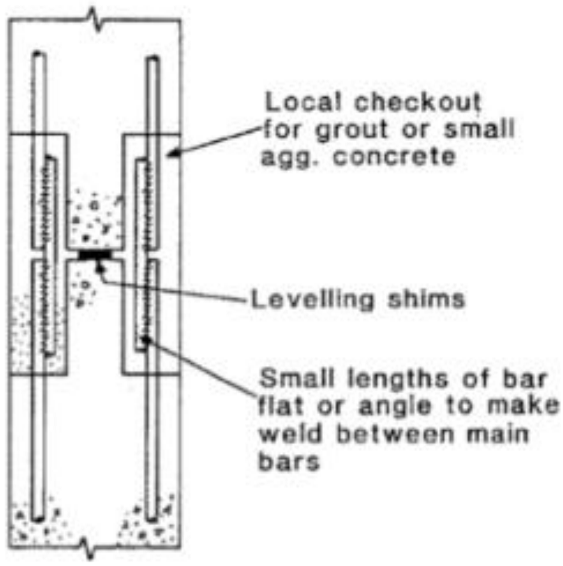

Figure 2.5: Column to column connection with continuity of reinforcement, using lap lengths through welding [19].

2.2.4 Through bar couplers

In some situations, the lap of the steel bars by overlapping is not feasible, and an alternative can be the use of mechanical coupling devices. Some of these techniques are illustrated in Figure 2.6.

The reinforcement continuity can be obtained with couplers, or by laying steel bars in metal sleeves, later filled with high resistance mortars (grout), in which the forces between the two steel bars are transmitted by their adhesion to the mortar. When the metal sleeve is filled with metallic materials, the connection behaviour turns out to be more fragile or similar to that of a weld.

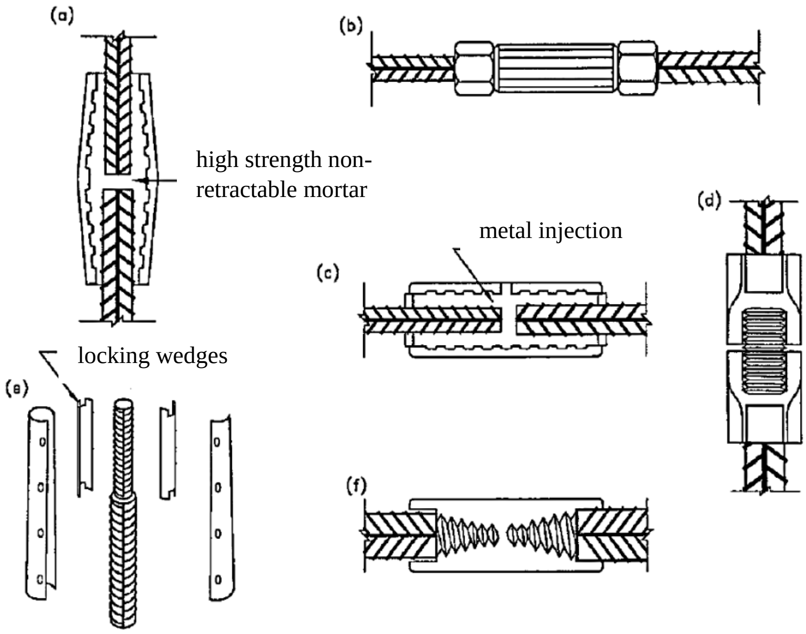

Legend: (**a**) – metal sleeve with injection of high strength non-retractable mortar; (**b**) – adjustable anchor coupler; (**c**) – metal sleeve with metal injection; (**d**) - connection with connecting screw; (**e**) metal coupler locking wedges, (**f**) simple anchor coupler.

Figure 2.6: Reinforcement continuity ensured by couplers [24].

In order to avoid failure through the coupler zone, these devices must be designed for tensile forces at least equal to the bar yield stress multiplied by 1.25 [26]. All systems illustrated in Figure 2.6 have a good mechanical resistance and performance. According to the author Pedro Reis [9], for this type of connection to be adopted for seismic actions it is very important that the system is able to withstand dynamic loads, and failure in the coupler zone is avoided.

The disadvantages of this type of connections are very similar to those described in the reinforcement overlapping process:

- need for support to ensure column remains vertical (in the case of systems with sleeves filled with grout);
- curing time is required for the connection to reach its maximum strength (in the case of systems with sleeves filled with grout);
- the protruding steel bars are sometimes bent/twisted during transport and assembly phases;
- sometimes the tolerances between the couplers and the elements to be connected (protruding steel bars from the column faces) are not achieved, which causes assembling difficulties;

- in situations of high compression, the joint between the two column faces should be very small, otherwise the danger of bending of the protruding steel bars increases. Therefore, cases identical to those illustrated in Figure 2.7 are not suitable for situations with high compressions.

The mechanical coupling systems have a more fragile behaviour, similar to that in welded connections when compared to the solutions of continuity due to reinforcement overlap. Two examples of column-column connection using couplers are illustrated in Figures 2.7 and 2.8.

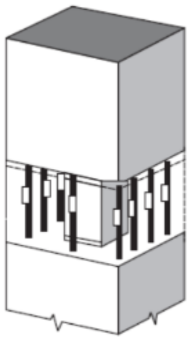

Figure 2.7: Column to column connection by reinforcement continuity using screwed couplers [20].

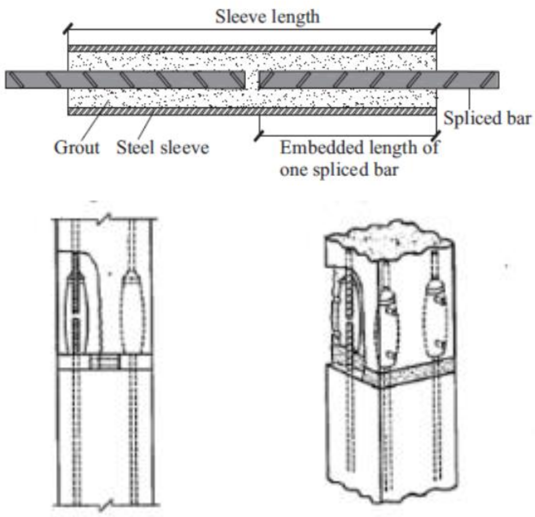

Figure 2.8: Column to column connection by reinforcement continuity using couplers filled with grout (left-[21]; right-[24]).

2.2.5 Connection by post-tensioning

This connection process (Figure 2.9) consists in guaranteeing the connection of two precast elements with the use of post-tensioning, which may be adherent or non-adherent. The post-tensioning can be done by using high strength steel strands.

The connection process consists of ensuring the verticality of the elements to be joined. Subsequently the connection joint is filled with grout/mortar and only after it acquires sufficient compressive strength, is the post tension is applied. For this reason, this process involves more assembly time. According to Pedro Reis [9] this solution is easy to implement and control quality and has a good structural performance, not only in terms of ductility but also strength.

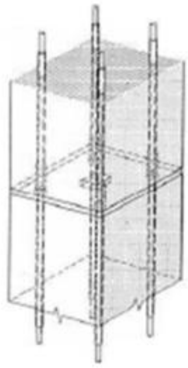

Figure 2.9: Column to column connection ensured through post-tensioned steel bars [27].

Figure 2.10 shows a column-column connecting system with two post-tensioned tendons. According to the authors P. Sideris, A. J. Aref and A. Filiatrault [28], this connection system is ideal for zones with moderate to high seismicity.

In this solution, the connection joint occurs at half height and no filling materials are applied (dry joint), i.e. the precast elements are placed in direct contact. Duct adapters are placed at the top of each face of the precast elements which increase the diameter of the sleeves of the post-tensioned tendons in this zone. The loads P2 and P1 applied at the top of column simulate, respectively, the gravitational load and the seismic action (Figure 2.10-a)). This solution allows the structure to suffer relative displacements through the slip between joints and the free rotation of each vertical element (Figure 2.10-b-3). This behaviour mitigates the effect of the seismic action, which is an advantage for these solutions in seismic zones.

According to Figure 2.10 (b-2), the slip amplitude is conditioned by the gap between the tendons and the duct adapters at the top and bottom of the joint, i.e., the diameter of the adapters is what defines the slip capacity. Slip between joints may also induce rotation phenomena. This rotation is caused by the eccentricity of the parts and the increase of the vertical load (Figure 2.10 b-3). The rotation of the upper part is conditioned, as in the previous case, by the contact of the tendons with the duct adapters. The stability of the vertical elements is therefore guaranteed by the tensioning of the tendons as well as by the applied axial load P2. The rotation of the elements does not allow a great dissipation of energy but allows the precast elements to remain stable. With the concrete crushing at the edges of the joint and with the possible yielding of the post tensioned tendons, the rotations increase and the vertical position of the structure is not so easily guaranteed.

This rotation causes low energy dissipation, as the only dissipation mechanisms are the crushing of the concrete and the yielding of the post-tensioned tendons. On the other hand, the slip between precast elements guarantees a good energy dissipation (due to friction), without significant structural damage, since this slipping only causes wear on the joint faces. In order for the joint to exhibit good friction properties, materials that guarantee these characteristics (epoxy materials, for example) should be applied over the joint.

Figure 2.10 (c.1) shows a solution with a non-linear post-stress plot, as an alternative to the linear plot shown in Figure 2.10 (a). In this situation, once the cables are post-tensioned they immediately come into contact with the duct adapters, which results in forces capable of preventing significant sliding between the joints. See Figure 2.10 (c.2).

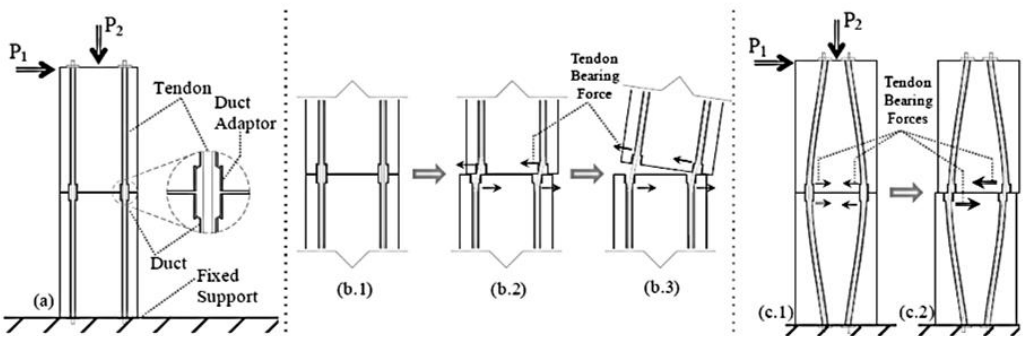

(a) Benchmark configuration (b) Slip-critical HSR joint: (b.1) Undeformed configuration, (b.2) Sliding capacity reached, and (b.3) Rocking response, after sliding capacity has been reached, and (c) Benchmark configuration with nonlinear PT geometry: (c.1) Undeformed configuration, and (c.2) Response against sliding

Figure 2.10: Ligação Pilar-Pilar por pós-tensão [28].

2.2.6 Connections using anchor bolts

Anchor bolt connection systems are often considered ideal for precast structures. This connection system guarantees a simple and fast installation (avoiding vertical shoring on site), which optimizes the assembly time. On the other hand, this solution has some disadvantages, namely small manufacturing tolerances and positioning, i.e. reduced capacity to accommodate dimensional deviations that may occur either at the level of the holes or at the level of the anchor bolts. The fact that its design is complicated means this connection system is not always compatible with geometrical and or architectural constraints. Finally, the fact that there are still few studies and references on this type of solutions, makes it not a preferable option in areas of high seismic activity.

At an economic level these solutions may also require the use of materials and accessories with high costs, however, the optimization of the assembly time can justify these costs.

This connection system is ensured by a male-female system. On one side of the column the anchor bolts (male) are properly embedded in the concrete. On the other side, the column shoes (female) are also properly embedded in the concrete. Both the male and female elements are usually welded to longitudinal bars (Figure 2.11). The number of anchors to be considered in the connection must always be as low as possible, therefore it is preferable to increase the section strength and or the strength class of the concrete in order to avoid congestion and simplify the assembly. Eight anchors per connection are the maximum number advisable.

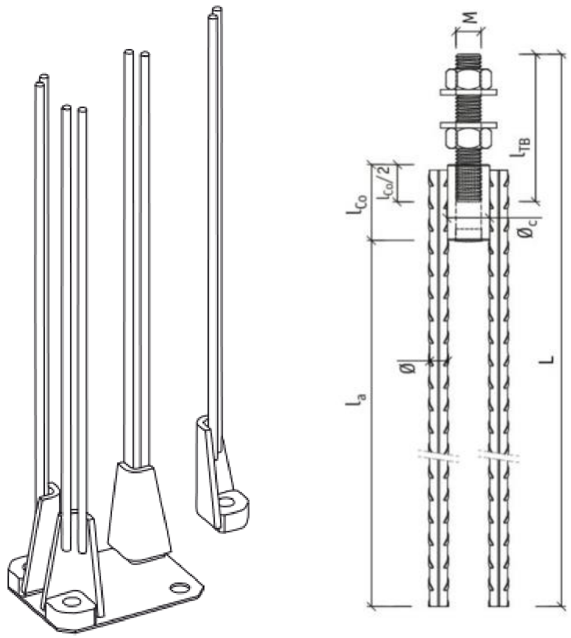

(a) Column Shoes (b) Anchor Bolts

Figure 2.11: Connection system with anchor bolt elements [29].

Regarding the assembly, it is very simple to assemble. The female column is positioned over the column with the anchors, and the vertical position is guaranteed through a system of nuts and locknuts. Once the connection is properly made the faces of the two precast elements are sealed with epoxy resin, in the case of a dry joint, or with non-retractable mortar (grout) if the thickness of the joint requires so. The low points of the areas where the bolted connection is made can be filled with non-retractable mortar in order to ensure good protection against fire and corrosion.

Figure 2.12 shows a column-column connection system using the anchor bolt system. Another example is illustrated in Figure 2.13, where in this case the column-column connection allows for the continuity of the beam.

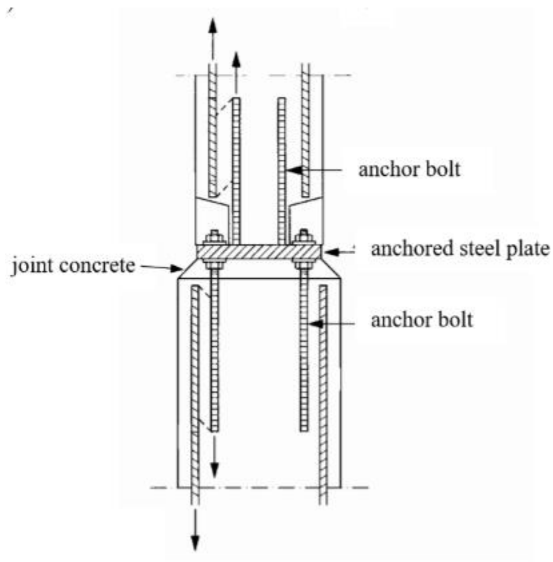

Figure 2.12: Column to column connection with anchor bolt systems [16].

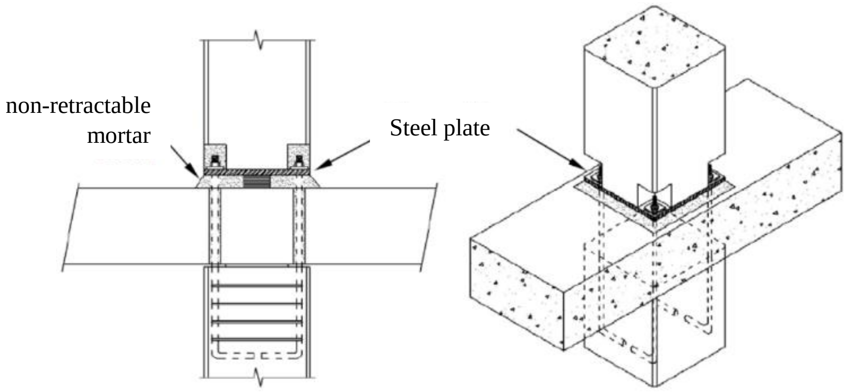

Figure 2.13: Column to column connection with continuity in the beam, using anchor bolt systems [10].

2.2.7 Column to column joints

As regards to the presence of the filling material, the joint between precast elements may be "dry" or "wet". A joint is said to be “dry” when the connections between precast elements are performed without the addition of any filling materials at the contact face between the elements and or at the periphery of the same. Often steel or neoprene plates are incorporated in the contact faces to improve the contact and to correct any irregularities that may exist, avoiding the occurrence of possible concentrated stresses.

The "wet" connections result from the use of filler materials such as resin, grout, mortar, among others, on the face of contact between the surfaces of the precast elements. These materials can be used in order to contribute to the structural strength of the connection, so they should be designed to withstand the vertical and or horizontal loads as well as possible rotations and translations (lateral displacements), or else they may simply have the function of absorbing the irregularities of the contact surfaces and or to protect the elements that ensure the connection.

The connections between columns are, in most situations, strongly demanded by compression. Dry joints should only be applied when the average stresses in the contact zone do not exceed 0.3.fcd, and the contact surfaces are completely regular (EC2 [30]). If the contact surfaces are not prepared with accuracy, the presence of irregularities in the surfaces can rise to stress concentrations. According to Santos Silva [24], these irregularities in the surfaces can sometimes lead to bending and twisting forces, as shown in Figure 2.14**.**

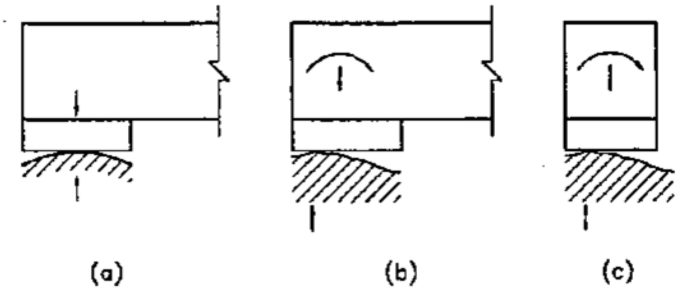

Legend: (a) Stress concentrations; **(b)** transmission of moments; **(c)** transmission of twisting forces;

Figure 2.14: Forces caused by contact surfaces with irregularities [24].

The filling of joints with concrete and mortar is mainly used to absorbing the irregularities of the surfaces, thus avoiding the phenomena shown in Figure 2.14. Moreover it also allows continuity between the precast elements avoiding the apparent joints. Even if the surfaces are perfectly regular, the sealing of the joints is always recommended, since this ensures a greater protection of the connection area against corrosion and fire.

The stress fields due to the transmission of compression between two elements, is usually influenced by the dimensions of the loaded area and the stiffness of the connection materials, as shown in Figure 2.15. The filling materials, when subjected to compression, can develop significant tensile stresses in the adjacent elements. When the elasticity module of the filling material is less than 70% of the adjacent elements material, the filling material shape suffers changes in the load application direction and perpendicularly by the Poisson effect, causing frictional forces between the two materials in contact and the splitting of the adjacent elements. In such situations, tensile transverse stresses must be absorbed by suitable reinforcements placed on the adjacent elements. The friction force value depends on the friction coefficient and the contact area between the two materials, the support transversal deformability and the value of the compressive force. In cases where the elasticity modulus of the filling material is equal or higher than 70% of the material modulus of the adjacent elements, the transmission of compression occurs in an area lower than the cross section area of the connecting elements, which increases the stresses in middle and unleash to failure in middle of support contact surface (bursting).

Legend: (a) Bursting; **(b)** Splitting

Figure 2.15: Stress fields due to compression on a column to column connection [24].

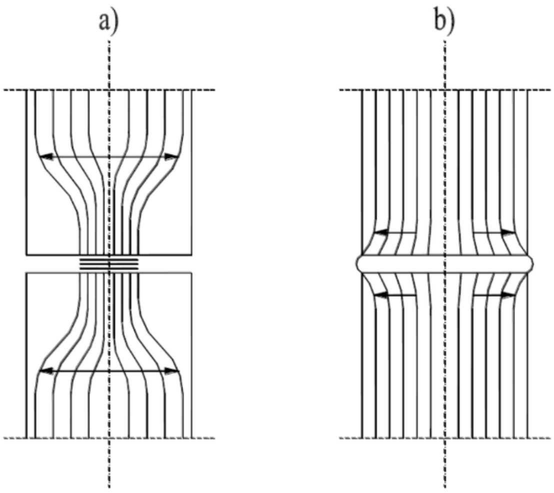

Figure 2.16 shows an example of bursting phenomena. The steel has an elastic modulus higher than the concrete, which unleash lateral compressive forces in the concrete.

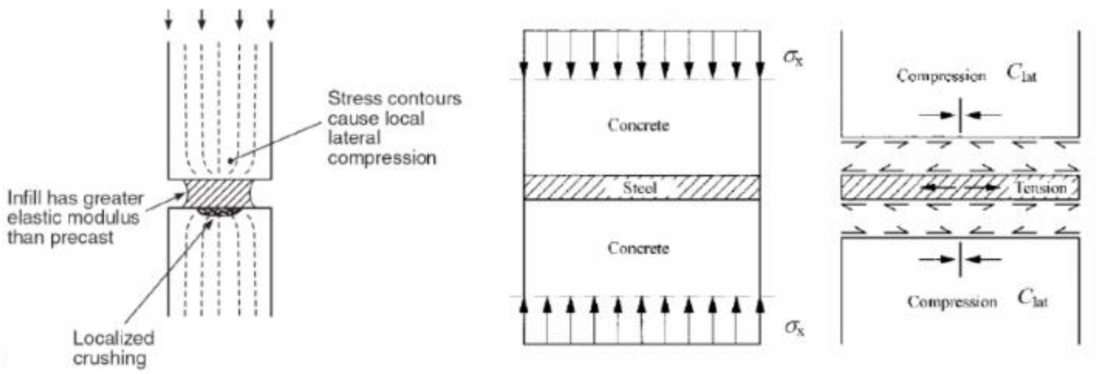

Figure 2.16: Bursting phenomena (compression between concrete elements using steel plate as connection joint [7]).

Figures 2.17 and 2.18 present two different situations. In the first, a compressed joint with grout, whose elasticity modulus is similar to the one of the adjacent precast concrete elements and in the second, a connection joint with a material with elastic modulus much lower than adjacent elements, causing splitting.

Figure 2.19 illustrates some examples of compression transmission in joints with different elastic modulus.

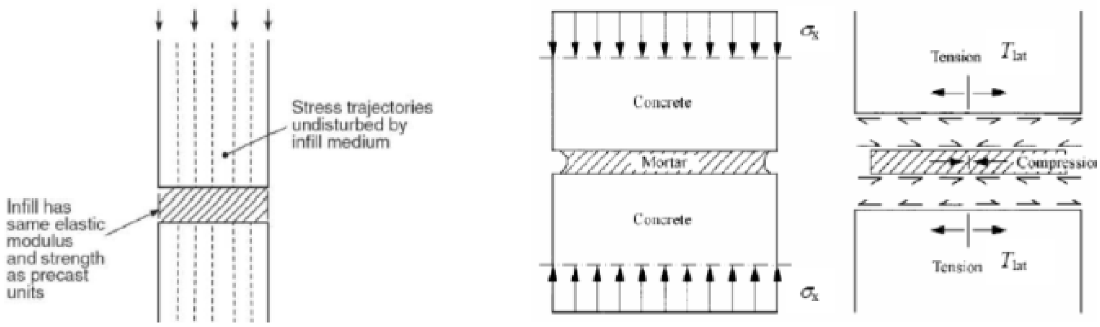

Figure 2.17: Splitting phenomena (compression between concrete elements using grout/mortar as connection joint [7]).

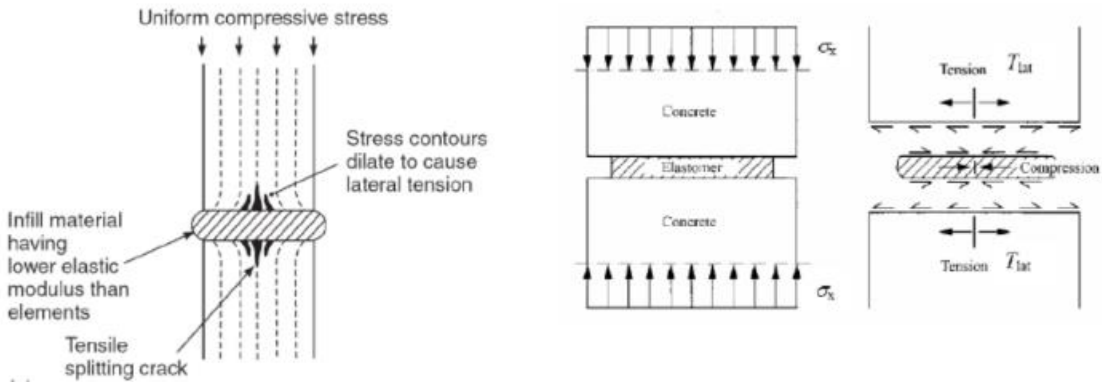

Figure 2.18: Splitting phenomena (compression between concrete elements using neoprene as connection joint [7]).

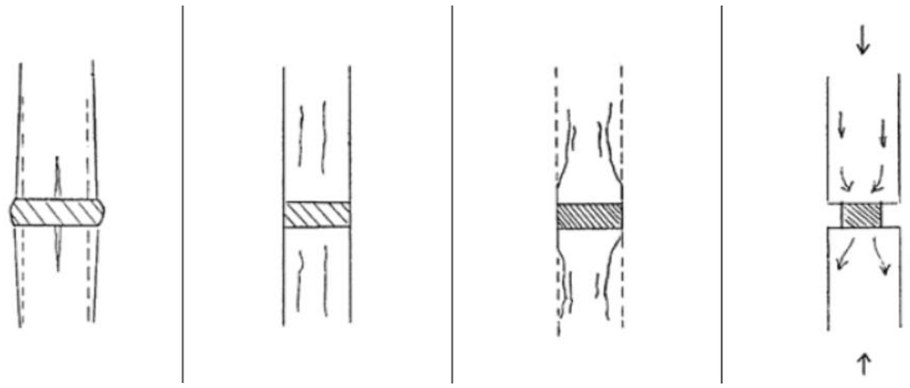

(a) Lower than precast elements

(b) Similar to precast elements

(c) Higher than precast elements

(d) Like (c) but with lower range

Figure 2.19: Compression between concrete elements using materials with different elastic modulus as joint [7].

Chapter 3

Experimental program

3.1 General aspects

The experimental component of this work aims to study the behaviour of precast concrete column-column connections for wind towers. To simulate the actions, bending with compression tests were carried out.

This chapter will describe the experimental specimens, their geometry and reinforcement, the testing system and the measuring equipment used in the tests.

The parameters analysed in the tests were the mechanical behaviour of connections, such as the reinforcement connections used, the type of connection joint and the type of material used to fill the connection joint.

Two types of reinforcement connections, with steel rebars protruding from one column end (Ø16) with corrugated steel sleeves in the other column end, and anchor bolt connections were tested. In the experimental specimens S1 and S2, the connection was constructed with six reinforcing bars Ø16 protruding and six anchor bolt connections. In the experimental specimen S3, the connection was made with twelve reinforcing bars Ø16 protruding and, in experimental specimen S4, the connection was made with twelve anchor bolt connections.

Two types of connection joints were used. In experimental specimens S1 and S4 connection joints with 50 mm of thickness were used. In the remaining experimental specimens S2 and S3, the connection joint thickness was reduced to the minimum thickness (dry joint), however, because of surface irregularities in precast concrete elements, it was not possible to reduce it entirely, so the thickness was reduced to approximately 3 mm. The joints with 50 mm of thickness were filled with cement slurry reinforced with steel fibres, whose composition was studied and developed by Reis [31], while the connection joints with 3 mm of thickness were filled with low viscosity epoxy resin for injecting (*Sikadur-52 Injection* [32]).

3.2 Experimental specimens description

Each experimental specimen is a single column that result from the connection between columns A and B. Four experimental specimens (S1, S2, S3 and S4) were produced and, due to their size, were tested in the horizontal position like a beam. All the experimental specimens were half scale (1:2) when compared with the dimensions of the column lattice tower, illustrated in Figure 1.1. Both columns A and B of each experimental specimen have the same geometry. The columns have a dominant circular cross section (Figure 3.1 – section B-B'), that represents the real geometry of wind towers' columns, and two rectangular cross sections (Figure 3.1 – section A-A'). The rectangular cross section zones were created to apply the vertical load at 1/3 of the span, and in the ends of the model (corbel) to provide support and to apply the compression force with prestress tendons.

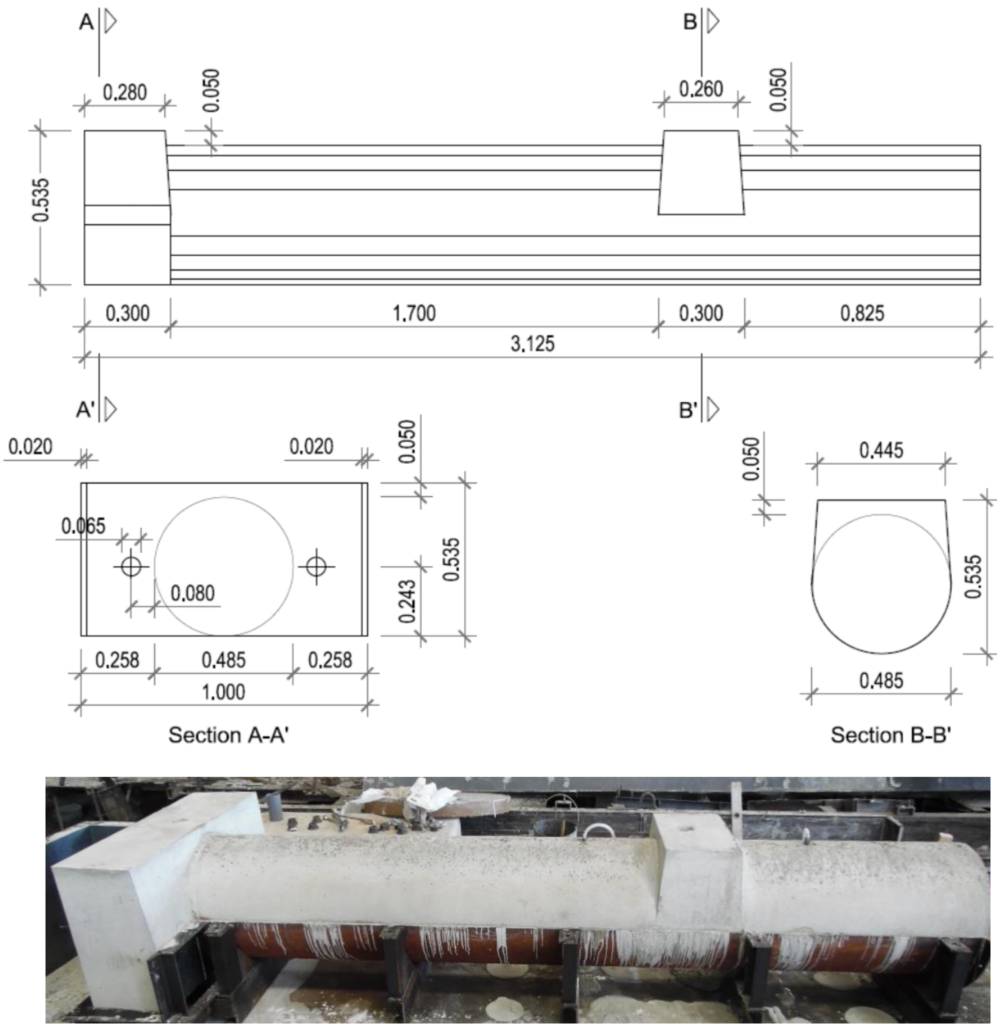

Figure 3.1: Geometry of columns, A and B, of each experimental specimens.

Table 3.1 presents the dimensions and connection type of the experimental specimens.

Table 3.1: Experimental specimens characteristics.

Experimental model	Corbel (rectangular section)		Circular section		Connection joint		
	Base (m)	Height (m)	Ø (m)	Total Length (m)	Thickness (mm)	Filling material	Connection reinforcement
S1	0.30x1.00	0.535	0.485	5.700	50	Mortar/ cement slurry	(6) Ø16 + (6) Anchor bolt connections
S2	0.30x1.00	0.535	0.485	5.653	3	Epoxy Resin	(6) Ø16 + (6) Anchor bolt connections
S3	0.30x1.00	0.535	0.485	5.653	3	Epoxy Resin	(12) Ø16
S4	0.30x1.00	0.535	0.485	5.700	50	Mortar/cement slurry	(6) Anchor bolt connections

The only geometric difference between the experimental specimens is the total length. This difference occurs because of the thickness of the connection joint used as shown in Figure 3.2.

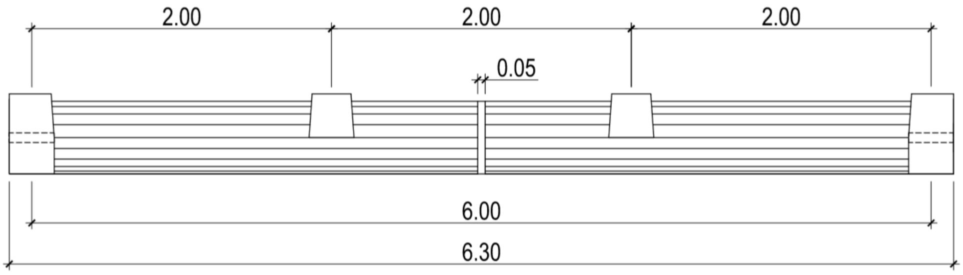

(a)

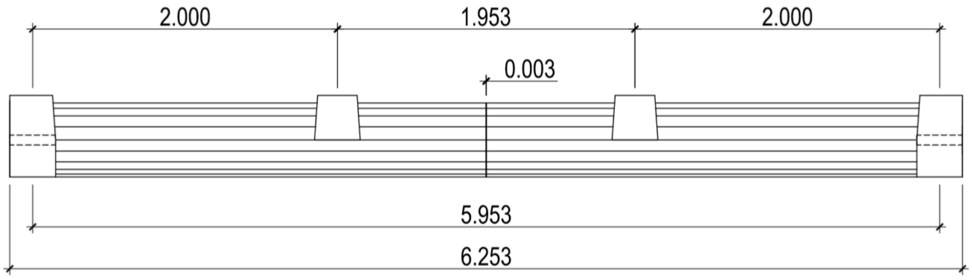

(b)

Figure 3.2: Experimental specimens' geometry, lateral view: (a) **S1** and **S4**; (b) **S2** and **S3**.

The links of column A in each experimental specimen, and in column B of the experimental specimen S3, were 10 mm diameter every 75 mm. The spacing was reduced for 50 mm to avoid buckling in longitudinal reinforcement adjacent to the connection (Figure 3.3 – (a)). The Figure 3.3 (b) presents a picture of the shear reinforcement considered in column A for specimens S1 and S2; The Figure 3.3 (c) presents a picture of the shear reinforcement considered in column A for experimental specimen S3.

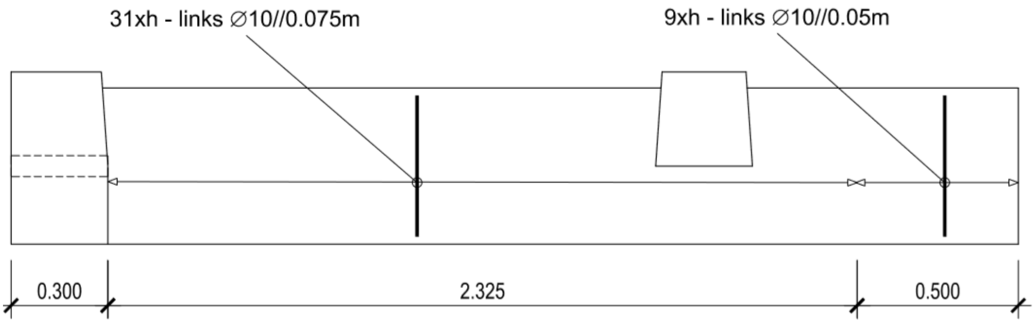

(a)

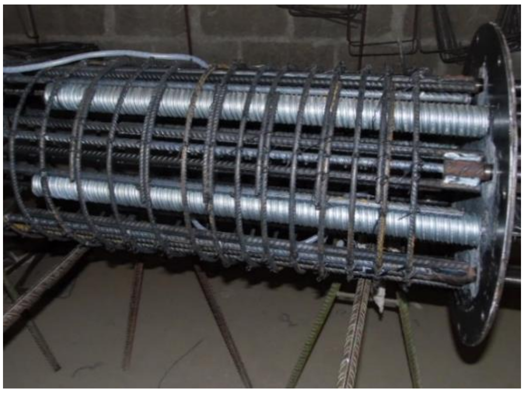

(b) (c)

Figure 3.3: Shear reinforcement in column A (all experimental specimens) and in column B (experimental specimen S3);

In column B of the specimens S1, S2 and S4, additional 6 mm diameter links were used to assemble the anchor bolt system (Figure 3.4-(a)). The holes done in column B for allow the bolted connection is can also be seen in Figure 3.4-(a). The Figure 3.4 (b) presents a picture of the shear reinforcement considered in column B for experimental specimens S1 and S2, while the Figure 3.3 (c) presents a picture of the shear reinforcement considered in column B for experimental specimen S4.

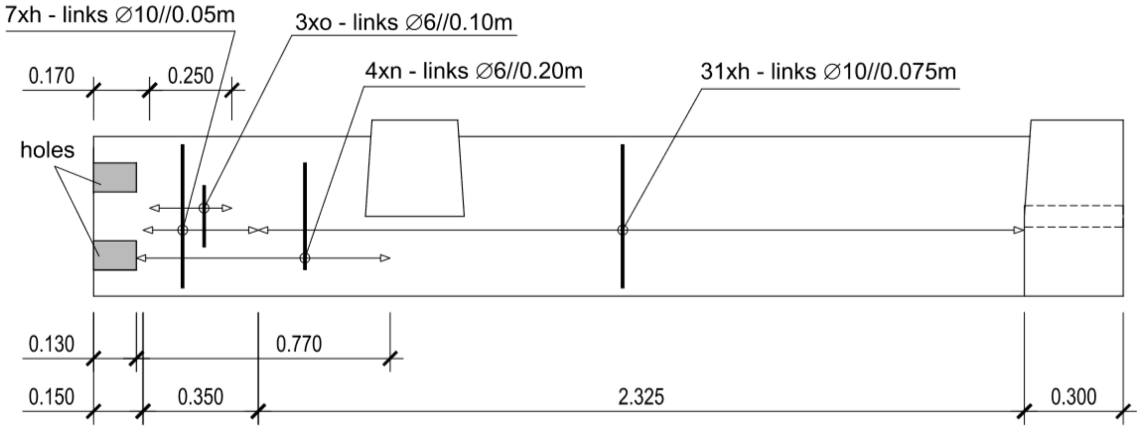

(a)

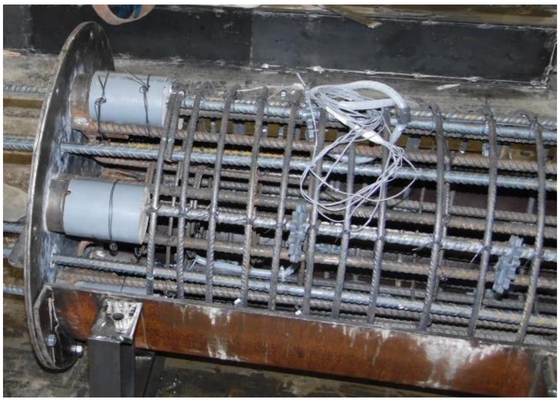

(b)

(c)

Figure 3.4: Shear reinforcement in column B for experimental specimens S1, S2 and S4.

The anchor bolt system, used in experimental specimens S1, S2 and S4, is detailed in Figure 3.5. The Figures 3.6 to 3.9 represent the joint reinforcements detailing of columns A and B.

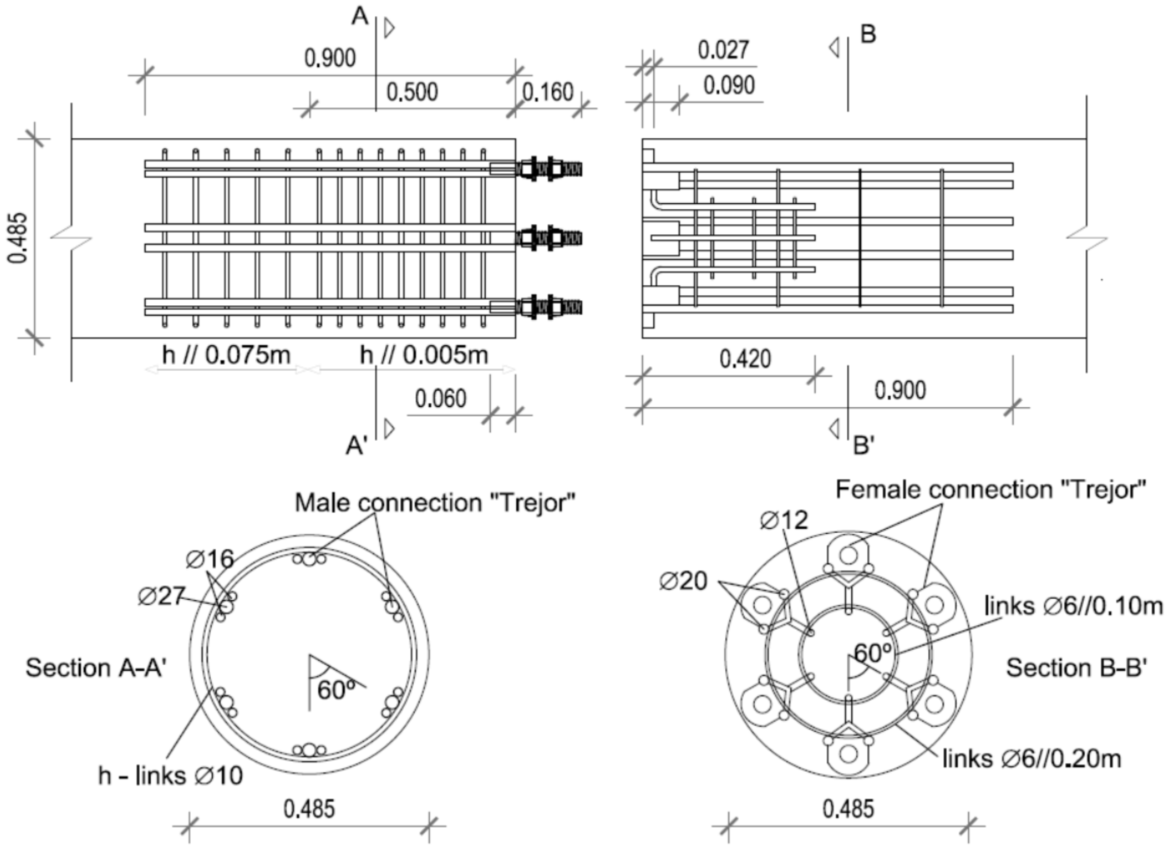

Figure 3.5: Anchor bolt connections (male and female connection Trejor) used in experimental specimens S1, S2 and S4.

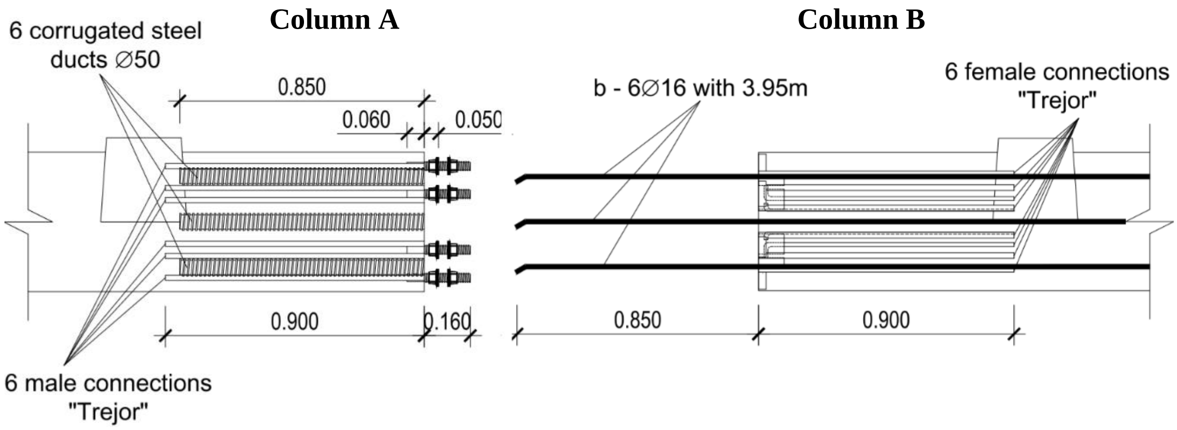

Figure 3.6: Detailing of connection reinforcement used in experimental specimen S1, lateral view.

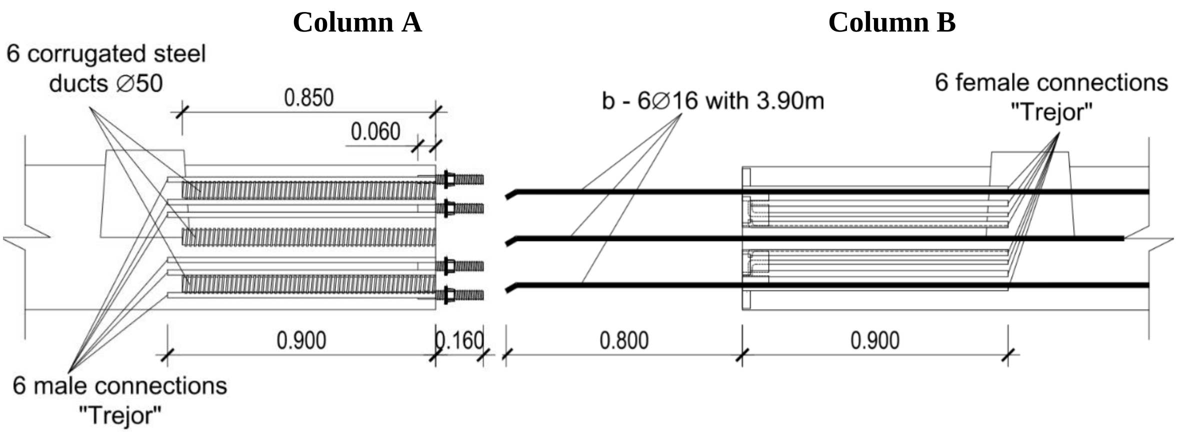

Figure 3.7: Detailing of connection reinforcement used in experimental specimen S2, lateral view.

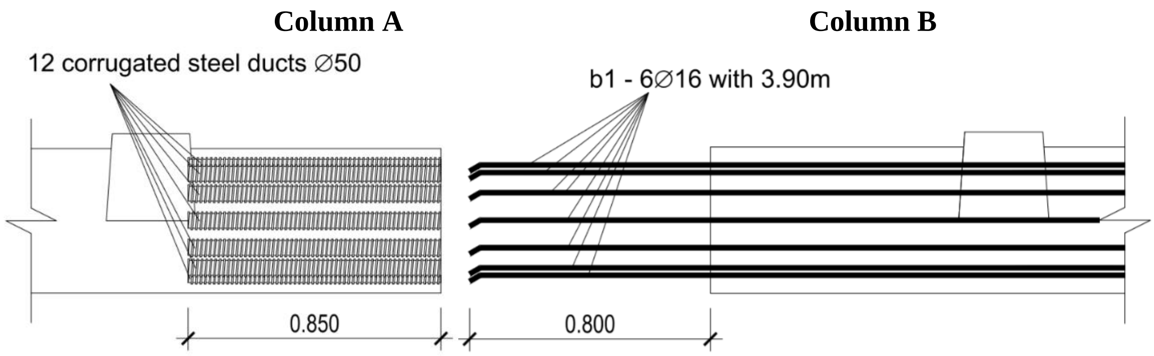

Figure 3.8: Detailing of connection reinforcement used in experimental specimen S3, lateral view.

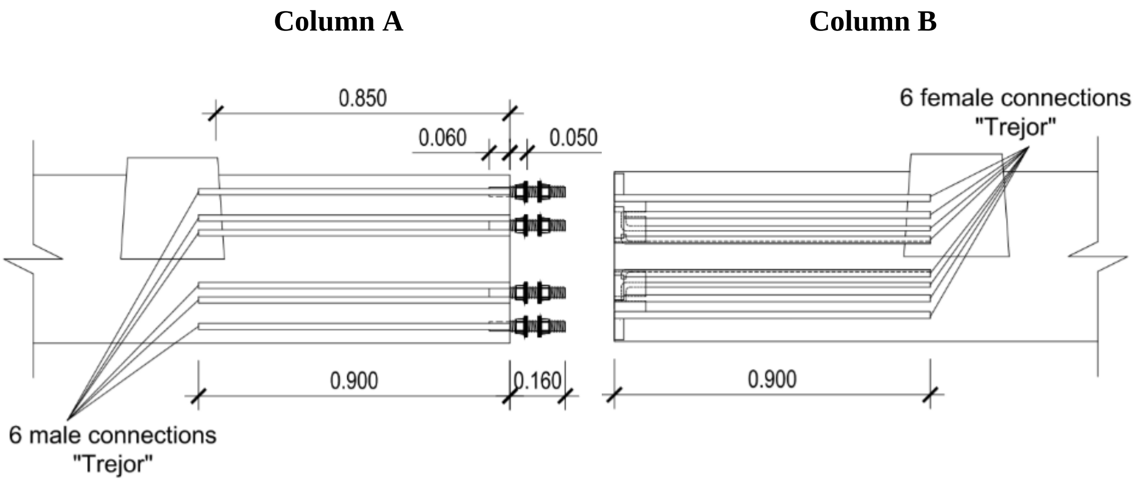

Figure 3.9: Detailing of connection reinforcement used in experimental specimen S4, lateral view.

Table 3.2 summarizes the material used in the joints of columns A and B. Note that the longitudinal reinforcement used in column B of experimental specimen S3, is also responsible for guaranteeing the connection between columns A and B.

Table 3.2: Description of longitudinal connection reinforcement used in column A and column B of each experimental specimen.

Experimental specimens	**Longitudinal connection reinforcement**													
	Column A							Column B						
	Corrugated steel ducts			Male-connection Trejor				Protruding steel bars			Female-connection Trejor			
	(a)	Ø (mm)	Length (m)	**(b)**	**(c)**	Ø (mm)	Length (m)	**(d)**	Ø (mm)	Length (m)	**(b)**	**(c)**	Ø (mm)	Length (m)
S1	6	50	0.85	6	2	16	0.90	6	16	0.85	6	1	12.5	0.42
												2	16	0.90
S2	6	50	0.85	6	2	16	0.90	6	16	0.80	6	1	12.5	0.42
												2	16	0.90
S3	12	50	0.85	-	-	-	-	12	16	0.80	-	-	-	-
S4	-	-	-	6	2	16	0.90	-	-	-	6	1	12.5	0.42
												2	16	0.90

Legend: **(a)** – amount of corrugated steel ducts; **(b)** – amount of anchor bolt connections (male/female); **(c)** – amount of steel bars in each anchor bolt connection (male/female); **(d)** – amount of protruding steel bars.

The detailing of longitudinal reinforcement (ordinary + connection) dimensioned to column A of the experimental specimens S1 and S2, is shown in Figure 3.10-(a). Figure 3.10-(b) shows a picture of the cross-section of column A (direction: connection surface-corbel) and Figure 3.10-(c) shows a picture of cross-section of column A (direction: corbel-connection surface).

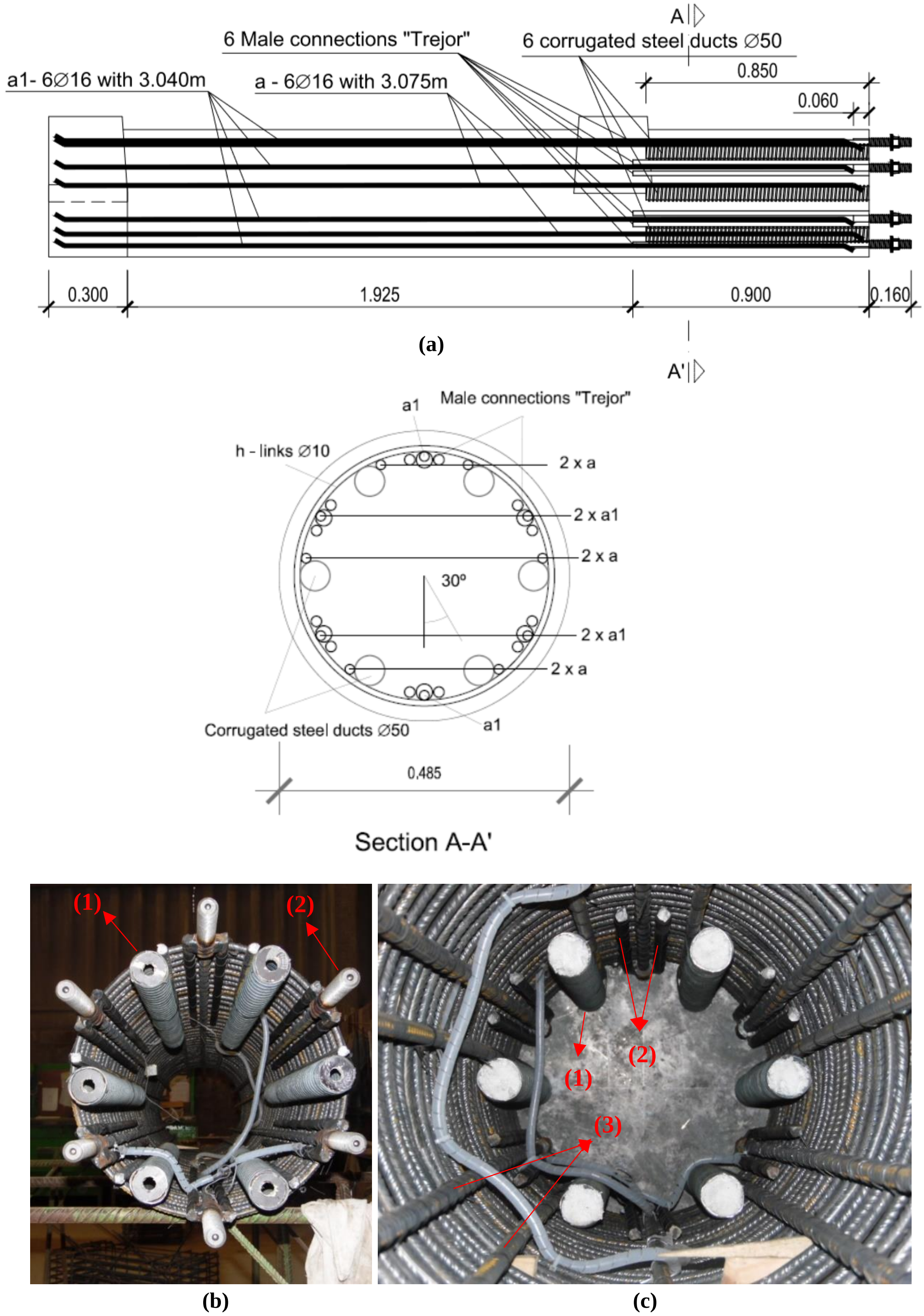

Legend: **(1)** – Corrugated steel ducts; **(2)** - male connections Trejor; **(3)** – Ordinary reinforcement;

Figure 3.10: Longitudinal reinforcement (ordinary + connection) of column A to experimental specimens S1 and S2.

The detailing of longitudinal reinforcement (ordinary + connection) dimensioned to column B of the experimental specimens S1 and S2, is shown in Figure 3.11-(a). Figure 3.11-(b) shows a picture of the cross-section of column B (direction: connection surface-corbel) and Figure 3.11-(c) shows a picture of cross-section of column B (direction: corbel-connection surface)

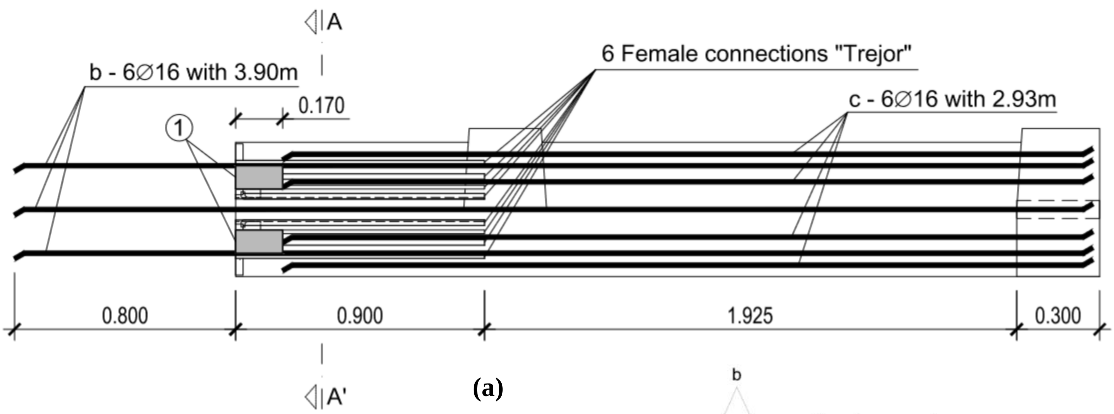

(a)

Legend: **1** - holes;
2 – protruding longitudinal bars (connection reinforcement);
3 – female connections Trejor(connection reinforcement);
4 – ordinary reinforcement;

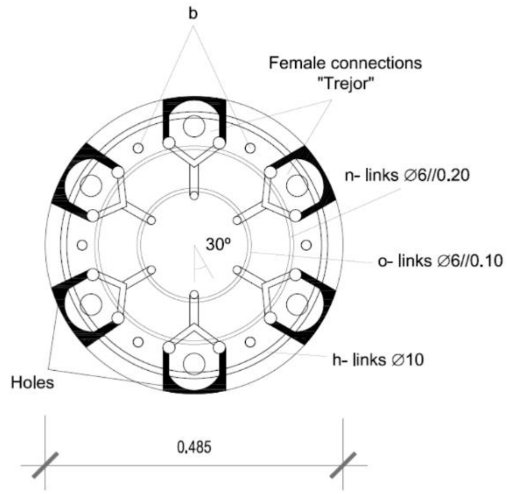

Section A-A'

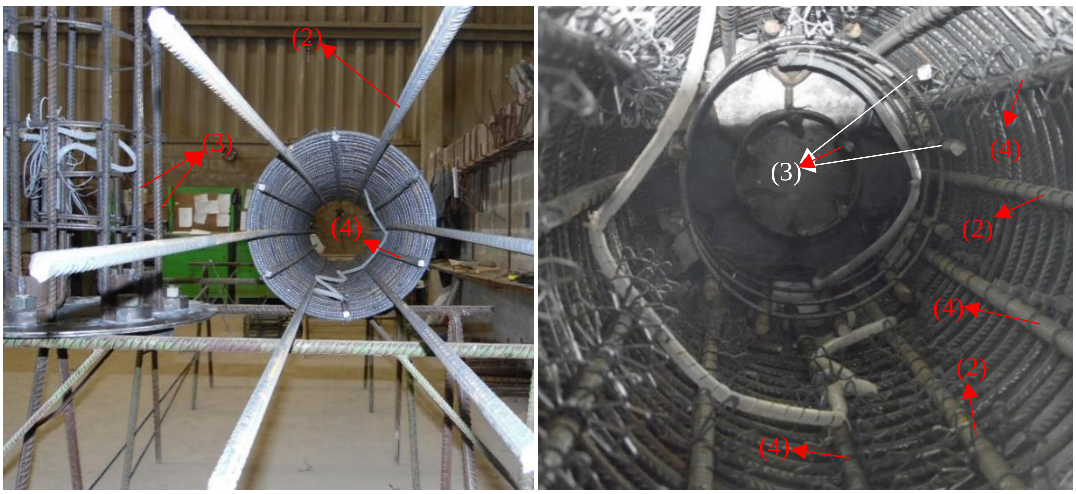

(b) **(c)**

Figure 3.11: Longitudinal reinforcement (ordinary + connection) of column B to experimental specimens S1 and S2.

The detailing of longitudinal reinforcement (ordinary + connection) dimensioned to column A of the experimental specimen S3, is shown in Figure 3.12-(a). Figure 3.12-(b) shows an image of the cross-section of column A (direction: corbel-connection surface) and Figure 3.12-(c) shows an aerial view of the longitudinal reinforcement.

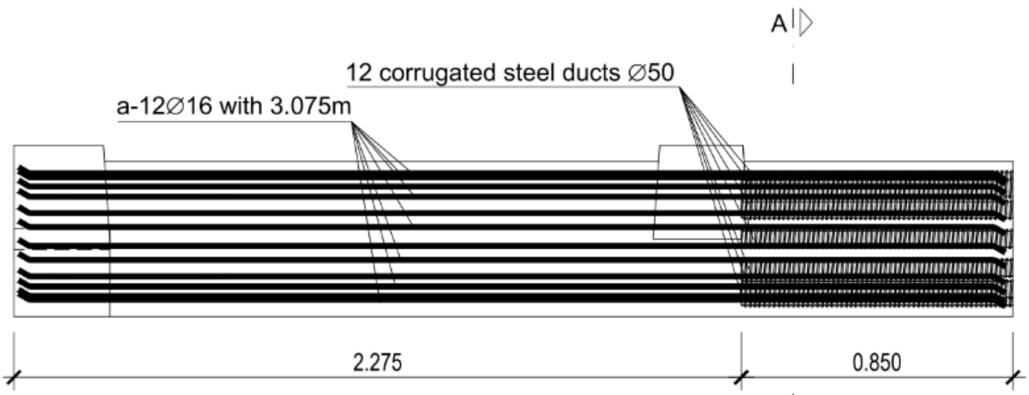

(a)

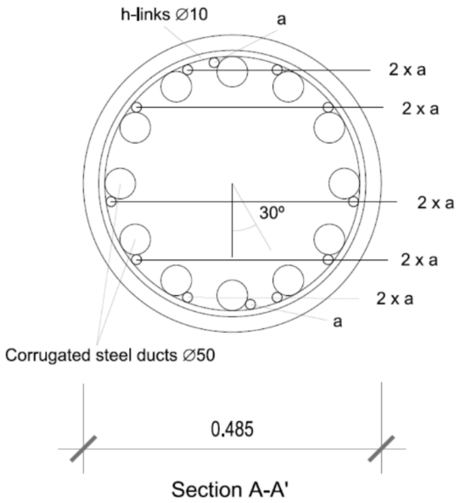

Legend: **1** – Corrugated steel ducts;

2 – Ordinary reinforcement;

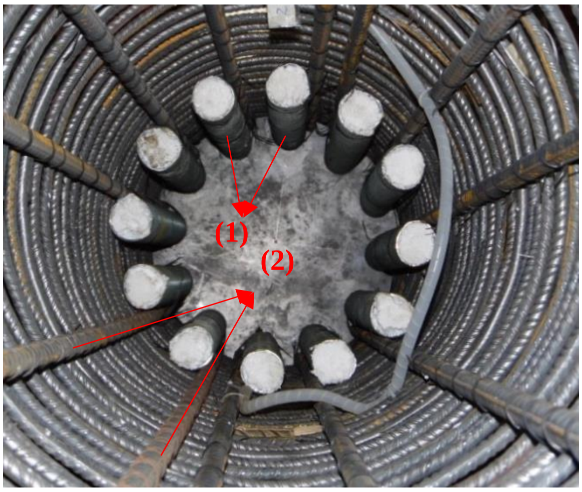

(b) **(c)**

Figure 3.12: Longitudinal reinforcement (ordinary + connection) of column A to experimental specimen S3.

The detailing of the longitudinal reinforcement (ordinary + connection) dimensioned to column B of the experimental specimen S3, is shown in Figure 3.13-(a). Figure 3.13-(b) presents a picture of the cross-section of column B (direction: connection surface-corbel) and Figure 3.13-(c) shows a picture of longitudinal disposition of reinforcement.

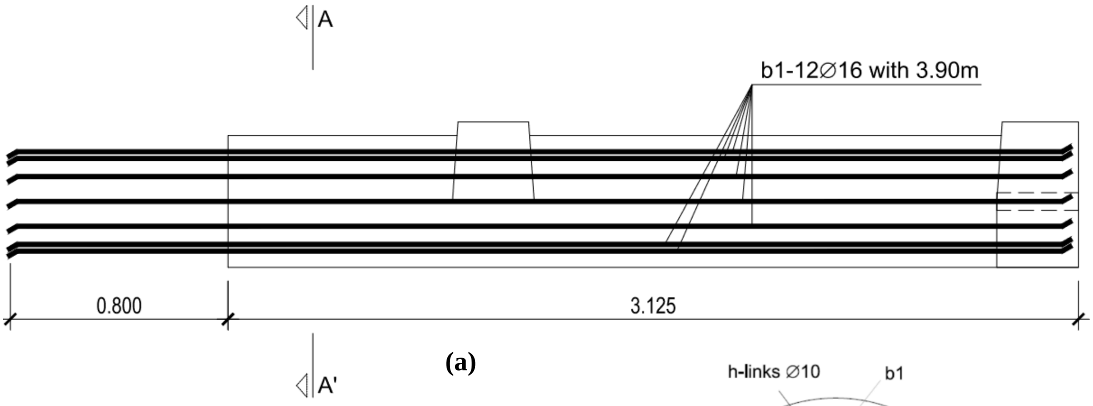

(a)

Legend: **1** – Protruding longitudinal bars.

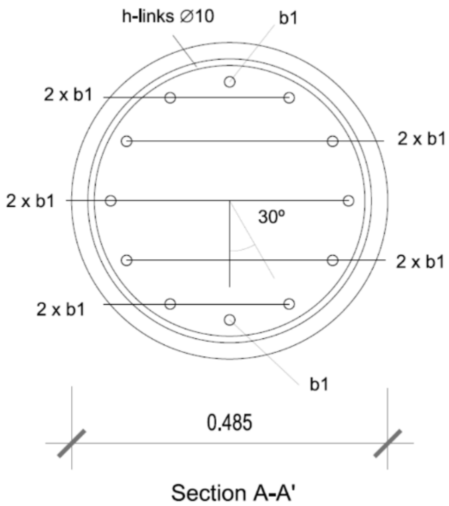

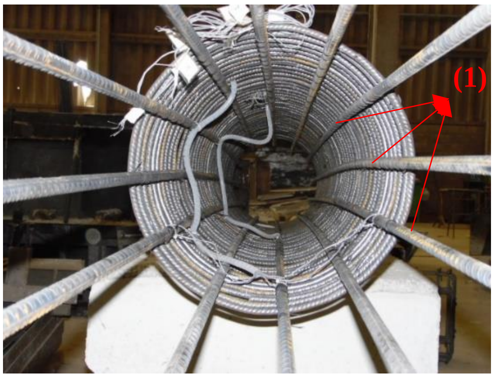

(b) **(c)**

Figure 3.13: Longitudinal reinforcement (ordinary + connection) of column B to experimental specimen S3.

The detailing of longitudinal reinforcement (ordinary + connection) dimensioned to column A of the experimental specimen S4, is shown in Figure 3.14-(a). Figure 3.14-(b) illustrates the cross-section of column A (direction: corbel-connection surface) and Figure 3.14-(c) shows the longitudinal disposition of the reinforcement of column A. In this specimen (S4), the distribution of longitudinal reinforcement in column B is the same as that of column B of experimental specimens S1 and S2 (Figure 3.11) but, in this case, there are no protruding longitudinal bars and the bars end at the column surface.

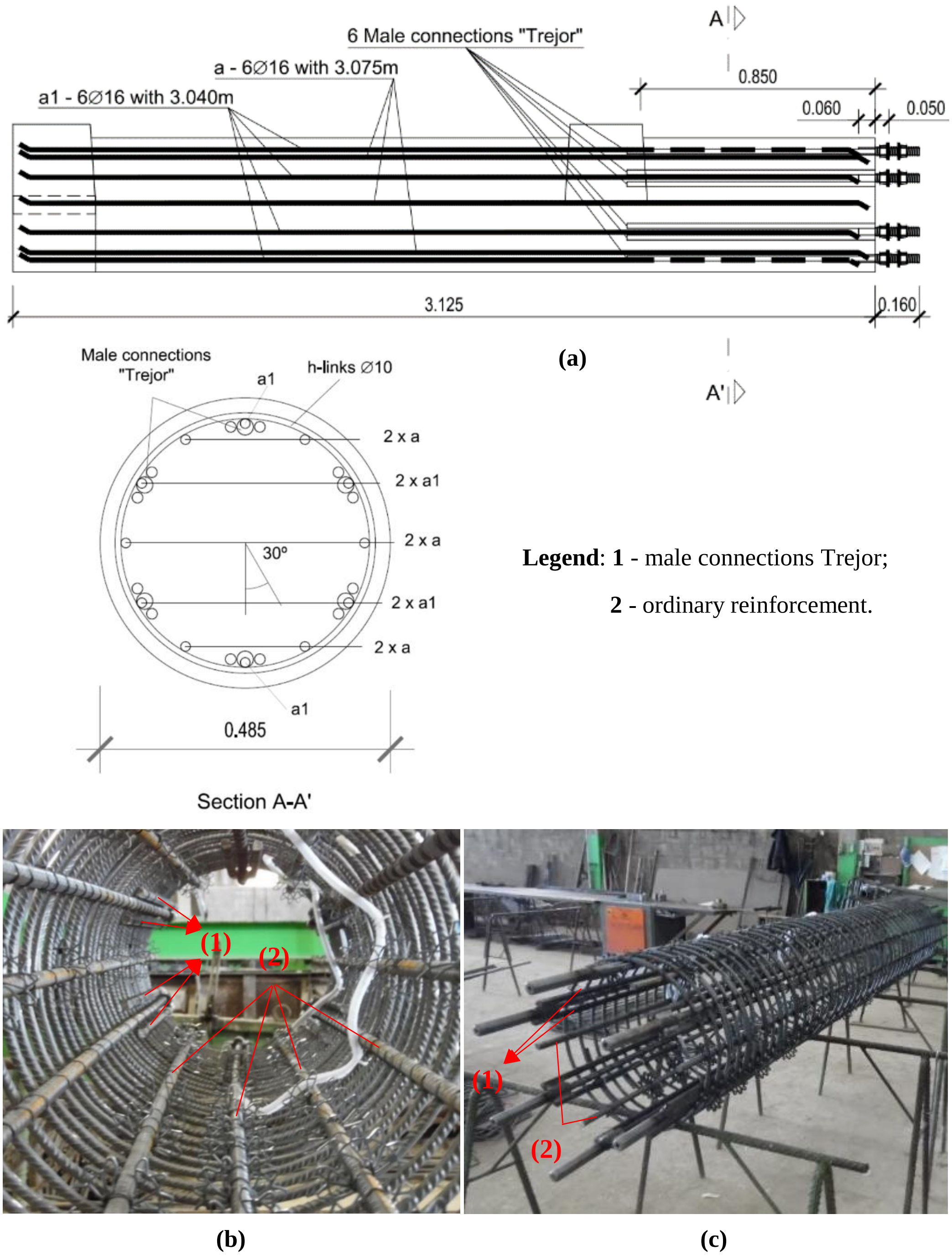

Figure 3.14: Longitudinal reinforcement (ordinary + connection) of column A to experimental specimen S4.

Table 3.3 presents the longitudinal reinforcement. The differences in length of the reinforcement in Table 3.3 are the result of the different geometry of the anchor bolt connections (male and female connections) used in the connection between columns A and B of specimens S1, S2 and S4.

Table 3.3: Longitudinal reinforcements' characteristics (ordinary)

<table>
<tr><th rowspan="3">Experimental specimen</th><th colspan="6">Longitudinal ordinary reinforcement</th></tr>
<tr><th colspan="3">Column A</th><th colspan="3">Column B</th></tr>
<tr><th>Nº steel bars (uni.)</th><th>Ø (mm)</th><th>Length (m)</th><th>Nº steel bars (uni.)</th><th>Ø (mm)</th><th>Length (m)</th></tr>
<tr><td rowspan="2">S1</td><td>6</td><td>16</td><td>3.040</td><td rowspan="2">6</td><td rowspan="2">16</td><td rowspan="2">2.930</td></tr>
<tr><td>6</td><td>16</td><td>3.075</td></tr>
<tr><td rowspan="2">S2</td><td>6</td><td>16</td><td>3.040</td><td rowspan="2">6</td><td rowspan="2">16</td><td rowspan="2">2.930</td></tr>
<tr><td>6</td><td>16</td><td>3.075</td></tr>
<tr><td>S3</td><td>12</td><td>16</td><td>3.075</td><td>-</td><td>-</td><td>-</td></tr>
<tr><td rowspan="2">S4</td><td>6</td><td>16</td><td>3.040</td><td>6</td><td>16</td><td>2.930</td></tr>
<tr><td>6</td><td>16</td><td>3.075</td><td>6</td><td>16</td><td>3.075</td></tr>
</table>

3.3 Test setup and instrumentation

The tests of the experimental specimens were made in the laboratory of heavy structures of the Faculty of Sciences and Technology of Universidade NOVA de Lisboa. Figure 3.15 shows the assembly of the test setup.

Figure 3.15: Picture of the test setup.

The experimental specimens are single columns that result from the connection between columns A and B (Figure 3.16). The final length of the column, with a 50 mm joint, was 6.30 m (model S1 and S4) and 6.253 m for joints 3mm thick (model S2 and S3). As previously mentioned, due to the large dimensions, the columns were tested in the horizontal position like supported beams over roller supports.

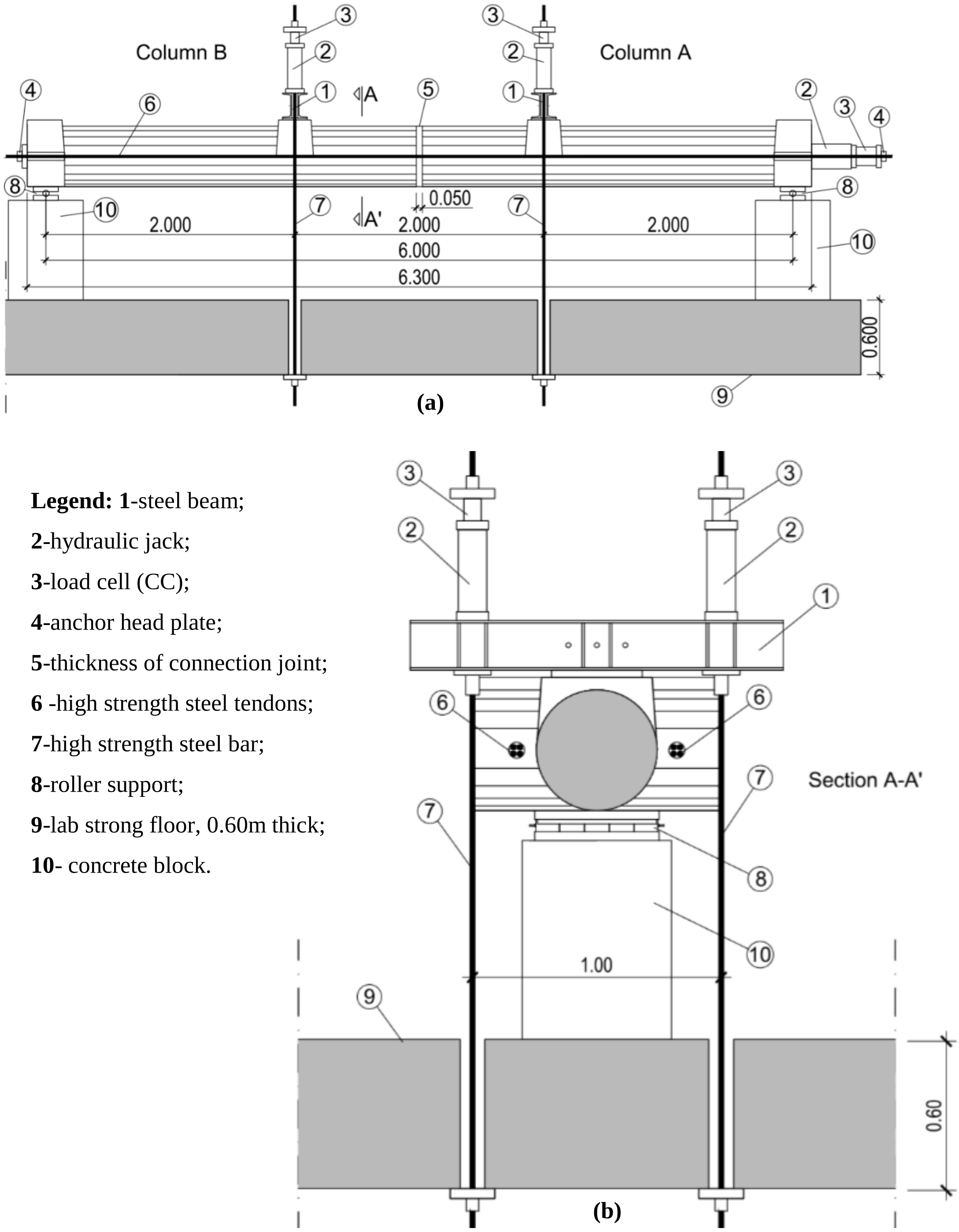

Legend: **1**-steel beam;
2-hydraulic jack;
3-load cell (CC);
4-anchor head plate;
5-thickness of connection joint;
6 -high strength steel tendons;
7-high strength steel bar;
8-roller support;
9-lab strong floor, 0.60m thick;
10- concrete block.

Figure 3.16: Test setup: **(a)** lateral View; **(b)** cross section A-A’.

3.3.1 Test procedure

An axial force was applied and kept constant until the end of the test, while cycles of vertical load were applied. The vertical load seeks to simulate the cyclical actions of earthquakes or wind, while axial force sought to simulate the compression applied to the column due to the structure's weight.

The vertical load, was applied using four hydraulic jacks and four load cells, with 200 kN and 500 kN capacity, respectively. The load was applied on two corbels of the experimental specimen, at 1/3 of the span, as shown in Figure 3.16. To apply the compression force, 2 hydraulic jacks and 2 load cells were used, with 1000 kN and 2000 kN capacity, respectively.

To measure vertical displacements displacement transducers were used, whose location will be shown in section 3.3.3. To measure crack openings, TML transducers type PI (relative displacement transducers) were used. A Datalogger UPM100 from HBM, associated with software the Catman 4.0 from HBM, were used for data acquisition.

The axial load was applied through high strength steel tendons on the corbels cast in the experimental specimen ends. The pre-stressing system adopted used 2 x 4 strands with 7 wires of 15.2 mm diameter (0.6"). A compression force of 1000 kN was applied in the column, resulting in a normal compressive-stress of about 5 MPa. The pre-stress application can be seen in Figures 3.16 and 3.22.

To apply the cyclic vertical loading, 2 steel beams were used and each one of them was placed on a steel plate above rectangular sections (small corbels) located at 1/3 of the span. Over each steel beam two hydraulic jacks, with 200 kN capacity, and two load cells, with 500 kN capacity, were placed (Figures 3.19 and 3.35). The cyclic loading consisted in the application of various loading and unloading phases. In each load phase, the vertical load level increased. This procedure was performed until model's failure (Figure 3.17).

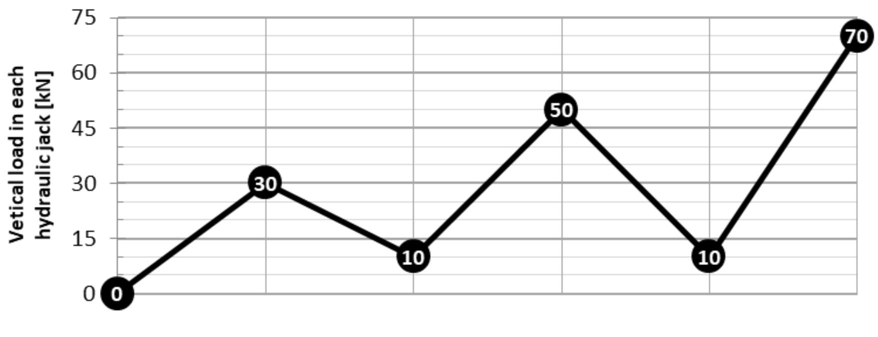

Figure 3.17: Vertical loading sequence applied to each hydraulic cylinder during the experimental tests.

3.3.2 Assembly of the test setup

The assembly of test setup, for each experimental specimen, was performed in the following way:

i. preparation and positioning of the reaction concrete blocks used to support the experimental specimen, with roller supports on top. The supports were levelled with a layer of gypsum plaster (Figure 3.18);
ii. positioning of the experimental specimen over the roller supports (Figure 3.18);
iii. placement of rectangular steel plates on the two small corbels (protruding rectangular sections) at 1/3 of the column span. These plates were levelled with gypsum plaster. Above these plates were placed the steel beams, the hydraulic cylinder and load cells. This equipment was fixed to the laboratory strong floor with high strength steel bars (*Dywidag* Ø26 mm), as shown in Figure 3.19.
iv. preparation and positioning of the vertical displacement transducers and the *TML* transducers (relative displacement transducers). See Figures 3.20 and 3.21.
v. preparation and placement of the pre-stressing system, comprising the high strength steel tendons, the hydraulic jacks, the load cells, the anchor head plates, and the wedges. See Figures 3.22.

After completing all the described steps, the equipment was calibrated before the test commenced.

Figure 3.18: Assembly phase of test setup – Experimental specimen positioning

Figure 3.19: Assembly phase of test setup – Vertical loading system preparation.

Figure 3.20: Assembly phase of test setup – vertical displacement transducers preparation and positioning.

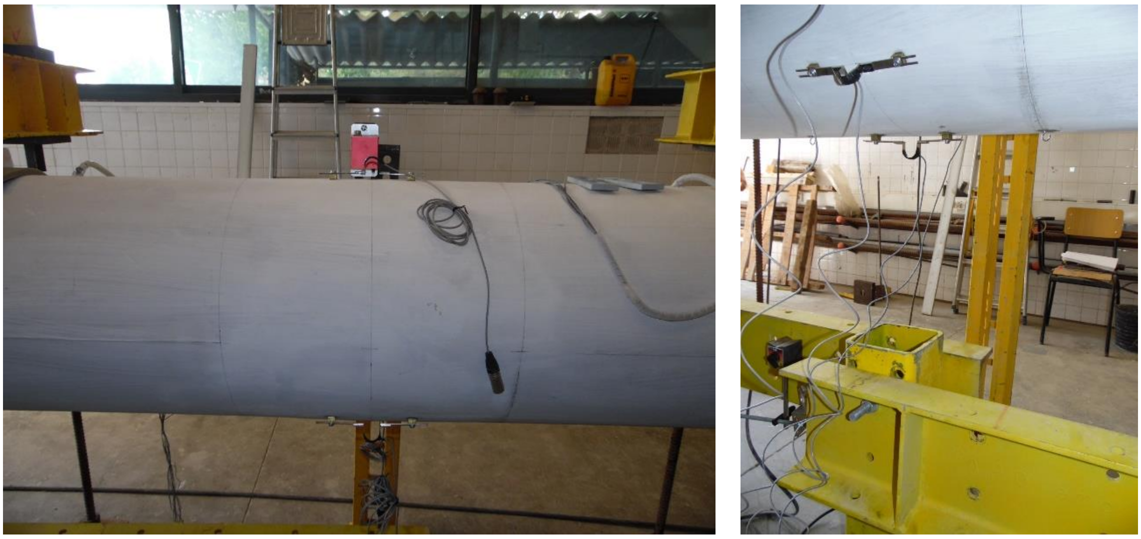

Figure 3.21: Assembly phase of test setup – *TML* transducers positioning.

Figure 3.22: Assembly phase of test setup – pre-stressing system preparation.

3.3.3 Experimental instrumentation

Strain gauges

Figures 3.23 and 3.24 show the location of the strain gauges placed on longitudinal reinforcement in each column A of specimens S1 and S2. These devices made it possible to measure the strains of longitudinal reinforcement during the experimental tests.

Sections A-A' and B-B', indicated in Figure 3.24, show the distribution and identification of the strain gauges placed at a distance of 150 mm and at 1025 mm, respectively, from the connection surface of each column A of specimens S1 and S2. The section A-A' shows the strain gauges used on ordinary longitudinal reinforcement (Ext.1/2; Ext.3/4 and Ext.5/6) while section B-B' indicates the strain gauges adopted on connection longitudinal reinforcement (Ext.17/18).

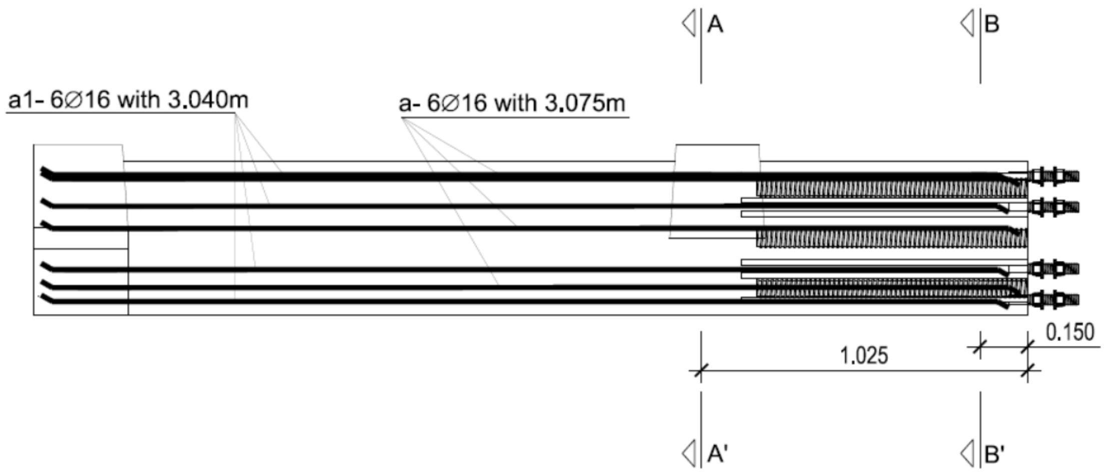

Figure 3.23: Column A of specimens S1 and S2, lateral view.

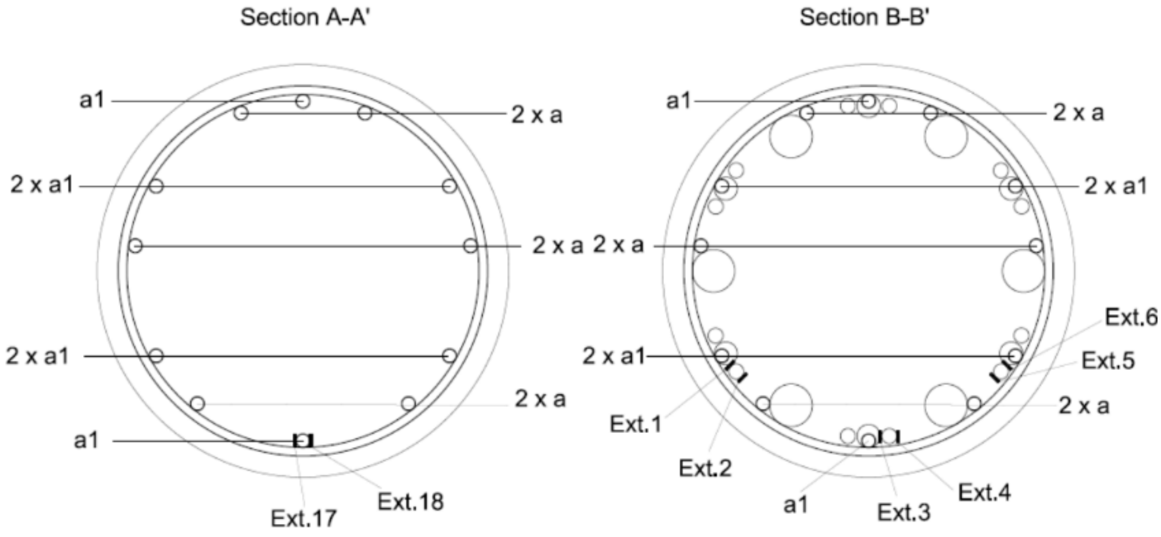

Figure 3.24: Column A of specimens S1 and S2 - Positioning and identification of strain gauges placed in longitudinal reinforcement.

The location of strain gauges used in each column B, of specimens S1 and S2, is specified in Figures 3.25 and 3.26.

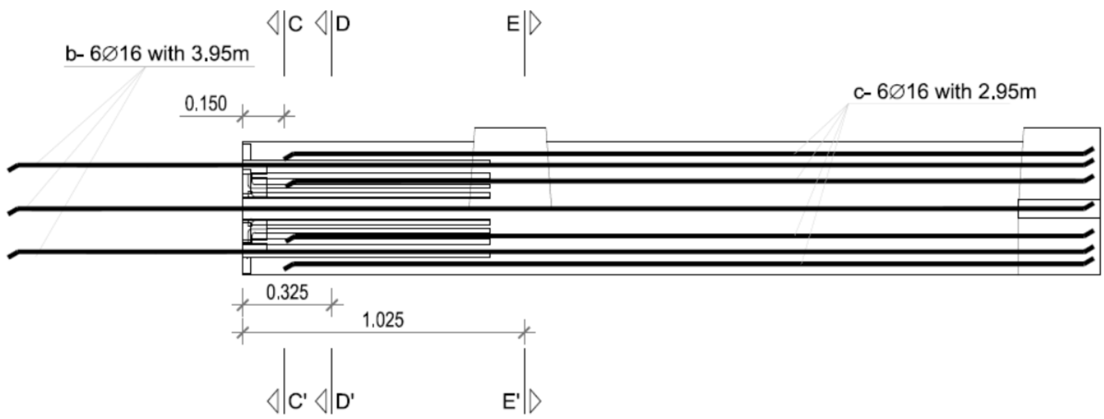

Figure 3.25: Column B of specimens S1 and S2, lateral view.

The sections C-C', D-D' and E-E', indicated in Figure 3.26, show the distribution and identification of strain gauges placed at 150 mm, 325 mm and at 1025 mm, respectively, from the connection surface of column B of specimens S1 and S2. The section C-C' shows the strain gauges used on connection longitudinal reinforcement (Ext.7/8; Ext.9/10 and Ext.11/12) while section D-D' and E-

E’ indicate the strain gauges used on ordinary longitudinal reinforcement (Ext.13/14 and Ext.15/16, respectively).

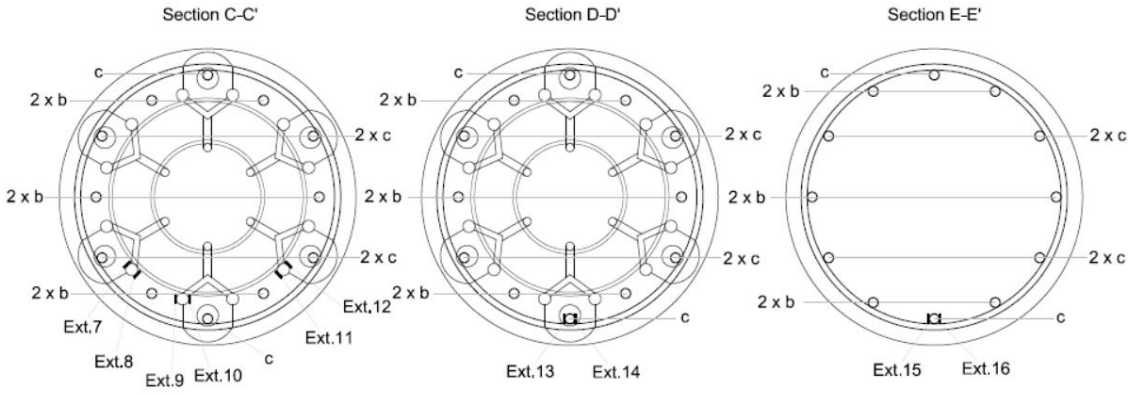

Figure 3.26: Column B of specimens S1 and S2 - Positioning and identification of strain gauges placed in longitudinal reinforcement.

To allow results comparison, the strain gauges positioning adopted in specimen S3 was the same as in specimens S1 and S2. However, there are slight differences in strain gauges positioning, since the connection longitudinal reinforcement adopted in specimen S3 is different from previous specimens. The location of strain gauges used in column A of specimen S3 is specified in following Figures 3.27 and 3.28.

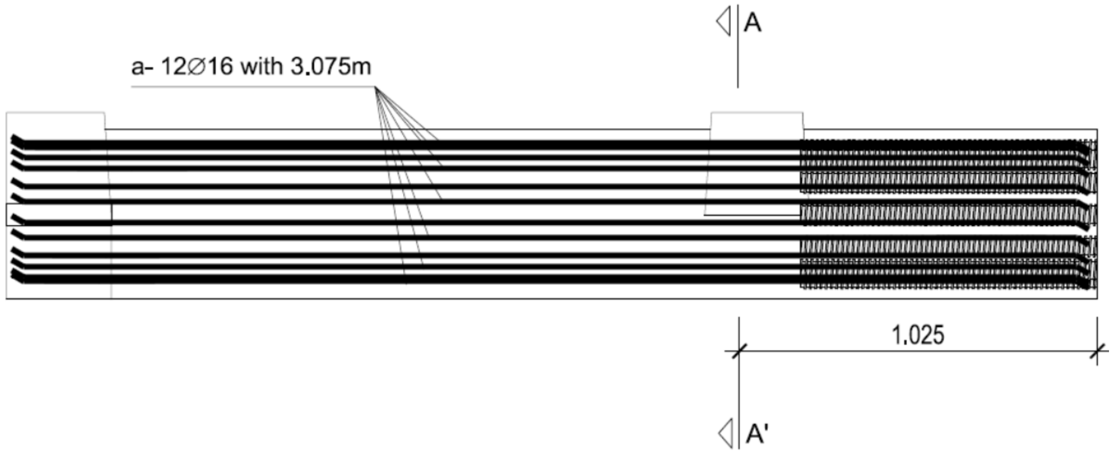

Figure 3.27: Column A of specimen S3, lateral view.

The section A-A’, defined in Figure 3.28, shows the distribution and identification of strain gauges placed to 1025 mm from the connection surface of column A of specimen S3 (Ext.1/2).

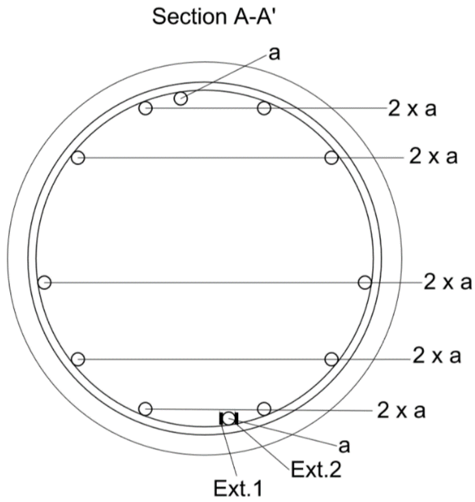

Figure 3.28: Column A of specimen S3 - Positioning and identification of strain gauges placed in longitudinal reinforcement.

The location of strain gauges used in column B of specimen S3 is specified in Figures 3.29 and 3.30.

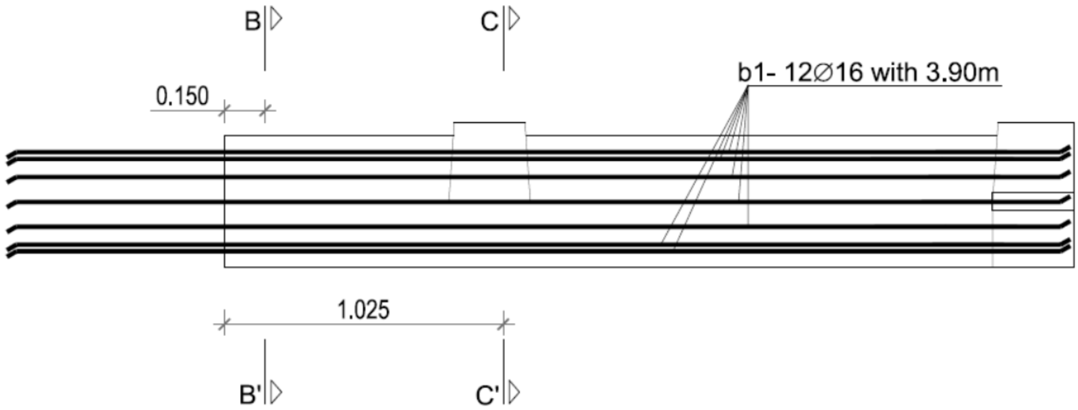

Figure 3.29: Column B of specimen S3, lateral view.

The sections B-B 'and C-C', defined in Figure 3.30, show the distribution and identification of strain gages placed at a distance of 150 mm (Ext.3/4; Ext.5/6 and Ext.9/10) and at 1025 mm (Ext.7/8) from the face of the column B, respectively.

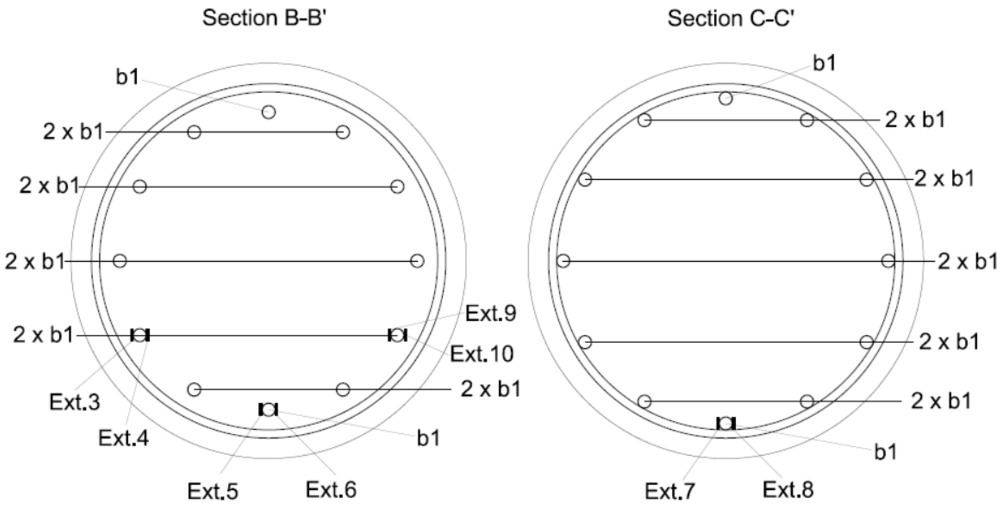

Figure 3.30: Column B of specimen S3 - Positioning and identification of strain gauges placed in longitudinal reinforcement.

The only differences between connection reinforcement adopted in specimen S4 and specimens S1 and S2 are the absence of corrugated steel ducts and protruding longitudinal bars in columns A and B, respectively, but these changes did not have any influence on instrumentation of specimens S1 and S2. So, in specimen S4 the same distribution of strain gauges considered in columns A and B of specimens S1 and S2 was adopted. See Figures 3.23, 3.24, 3.25 and 3.26.

Displacement transducers

To analyse the deformation (vertical displacement) of the specimens during the tests, seven displacement transducers were installed. The displacement transducers D1 to D6 were placed in the lower surface of each specimen. The displacement transducers D1 and D6, D2 and D5, D3 and D4 measured the displacements at 1.00 m, 2.00 m and 2.75 m from the column's support, respectively. Displacement transducer D7 was positioned at middle span of the experimental specimen to measure the maximum displacement. Figures 3.31 and 3.32, show the location of displacement transducers, in lateral view and top view respectively.

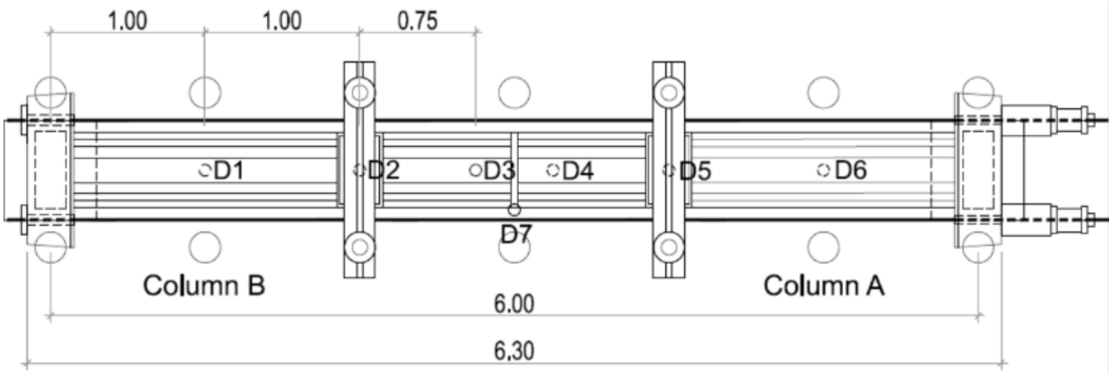

Figure 3.31: Location and identification of the displacement transducers used in specimen S1, top view.

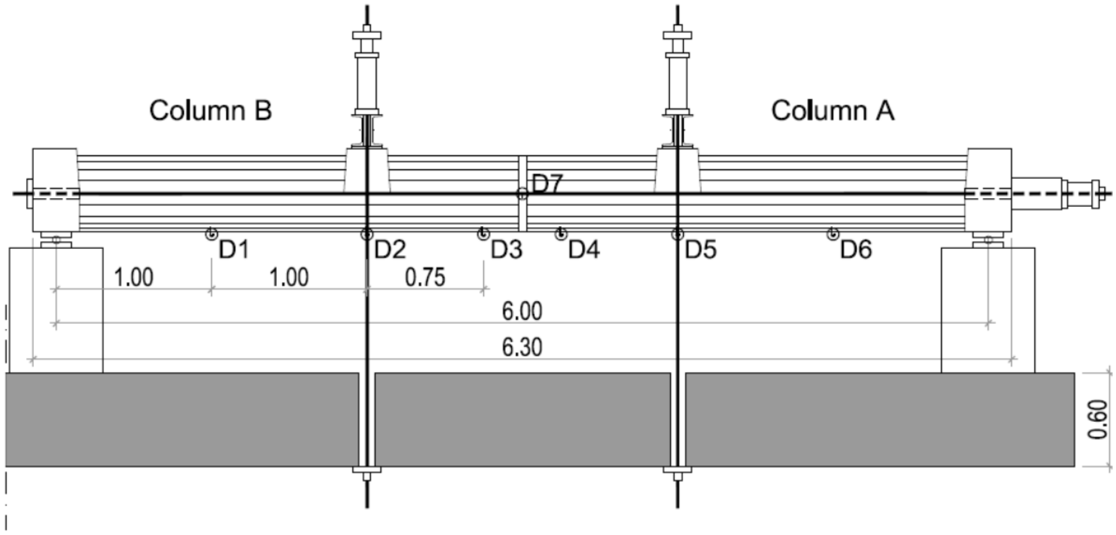

Figure 3.32: Location and identification of the displacement transducers used in specimen S1, lateral view.

Positioning of the displacement transducers adopted in experimental specimens S2, S3 and S4 was the same as in specimen S1 with exception of displacement transducer D7, which, in remaining specimens, was placement in opposite side to allow a better view of crack openings throughout the tests.

Relative displacement transducers (TML type PI)

Besides the vertical displacement transducers, four (4) relative displacement transducers were also used at middle span of each specimen. These elements allowed the measurement of crack openings that occurred in connection joint. The configuration of these devices as well as the instrumentation adopted in each experimental specimen, is shown in Figures 3.33 and 3.34, respectively.

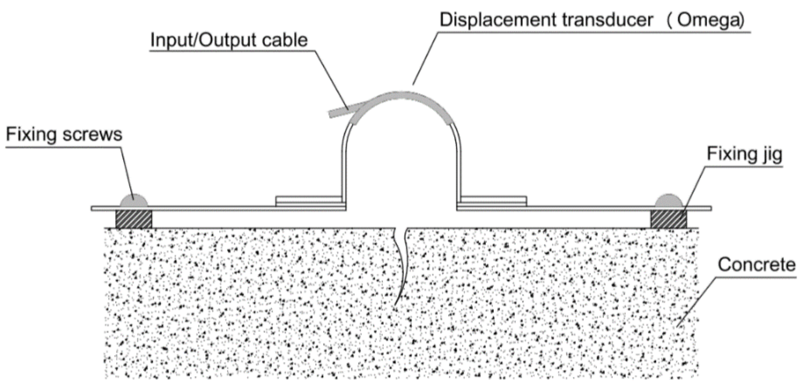

Figure 3.33: Configuration of displacement transducers used to measure the crack openings in concrete

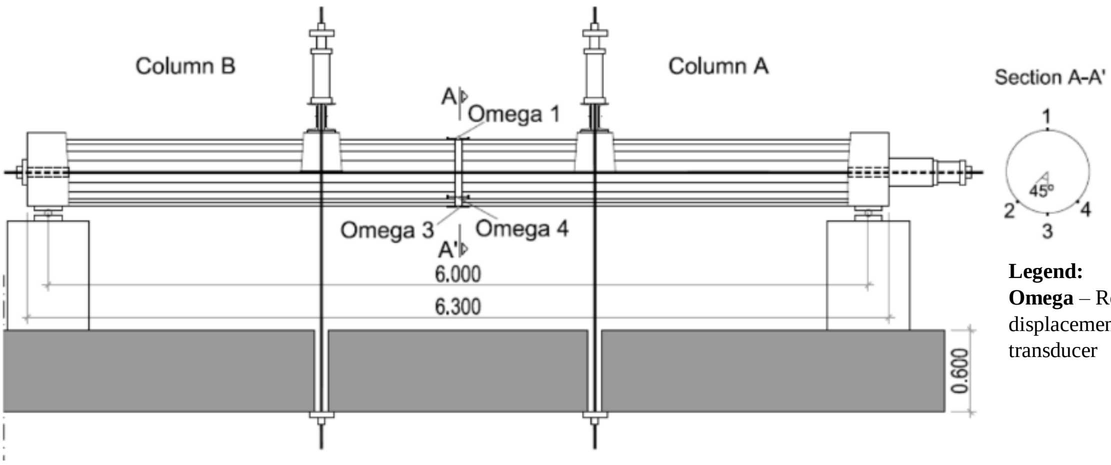

Legend:
Omega – Relative displacement transducer

Figure 3.34: Position of the relative displacement transducers used to monitor the crack openings, in specimens S1, S2, S3 and S4.

Load cells

The load cells adopted position in specimens S1, S2, S3 and S4, is shown in Figure 3.35. Load cells CC1 and CC2 were responsible for controlling axial force applied to the specimen while four load cells, CC3 to CC6, controlled the vertical load values. The load cells can also be reviewed, in lateral view, in Figure 3.17.

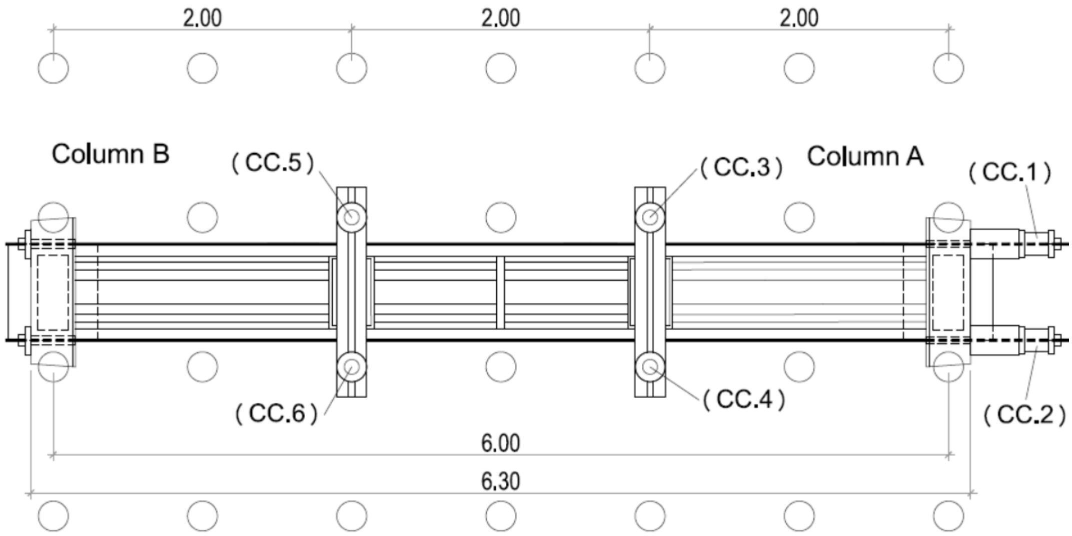

Figure 3.35: Specimens S1/S2/S3 and S4 - Test setup with position of the load cells (CC1 to CC.6), top view.

Chapter 4

Material properties

4.1 Steel

4.1.1 Ordinary reinforcement

In order to characterize the mechanical properties of steel reinforcement used in the design of specimens S1, S2, S4, and of connection reinforcement (protruding longitudinal bars) adopted in specimen S3, tensile tests were performed on 10 and 16 mm diameter steel bars. These tests were performed according to NP EN 10002-1 [33] in LNEC (Laboratório National de Engenharia Civil). Table 4.1 shows the test results, where $\boldsymbol{E_m}$ is mean Young's modulus, $\boldsymbol{f_y}$ is the tensile yield stress, $\boldsymbol{f_{ym}}$ is the mean tensile yield strength, $\boldsymbol{\varepsilon_y}$ is the yield strain and $\boldsymbol{\varepsilon_u}$ is the ultimate strain.

Table 4.1: Main mechanical characteristics of the ordinary reinforcement.

Spec. (N.º)	**Diameter** (mm)	**Class** (-)	E_m (GPa)	f_y (MPa)	f_{ym} (MPa)	f_u (MPa)	f_{um} (MPa)	ε_y (%)	ε_{ym} (%)	ε_u (%)	ε_{um} (%)
1	10	A500NRSD	200	546	550.3	641	641	0.27	0.27	12.7	11.9
2	10			549		639		0.27		10.6	
3	10			556		643		0.28		12.3	
1	16			547	546.3	657	656.7	0.27	0.27	13.4	12.9
2	16			548		658		0.27		13.3	
3	16			544		655		0.27		11.9	

The yield strain of each tested specimen tested was obtained through expression (4.1), where $\boldsymbol{E}$ = 200 GPa:

$$\varepsilon_y = \frac{f_y}{E} \tag{4.1}$$

4.1.2 Reinforcement of the connection

The mechanical characteristics of the anchor bolt connections Trejor-TEP27 used in the connection of specimens S1, S2 and S4, were obtained through tensile strength tests on 12.5 mm and 16 mm diameter steel bars. These tests were performed according to NP EN 10002-1 [33] at IST (Instituto Superior Técnico) and are shown in Figure 4.1. The tensile test results obtained for steel bars are shown in Table 4.2 and shown in graphs form in Figure 4.2 and 4.3.

(b) Positioning of mechanical strain gauge

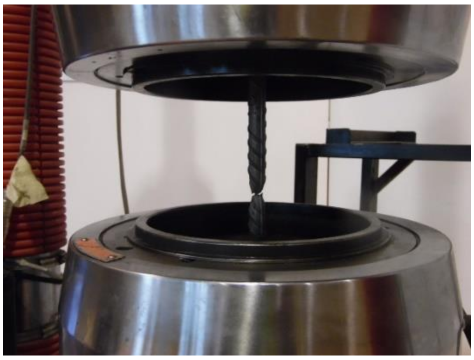

(a) Equipment used in tensile tests

(c) Steel's failure

Figure 4.1: Steel laboratory tests at IST

Table 4.2: Main mechanical characteristics of the anchor bolt connection.

<table>
<tr><th>Spec.
(N.º)</th><th>Diameter
(mm)</th><th>Class
(-)</th><th>E_m
(GPa)</th><th>f_y
(MPa)</th><th>f_{ym}
(MPa)</th><th>f_u
(MPa)</th><th>f_{um}
(MPa)</th><th>ε_y
(%)</th><th>ε_{ym}
(%)</th><th>ε_u
(%)</th><th>ε_{um}
(%)</th></tr>
<tr><td>1</td><td>12.5</td><td rowspan="6">Trejor-TEP27</td><td rowspan="3">198.1</td><td>540</td><td rowspan="3">565.3</td><td>625.3</td><td rowspan="3">649.6</td><td>0.30</td><td rowspan="3">0.32</td><td>9.87</td><td rowspan="3">8.93</td></tr>
<tr><td>2</td><td>12.5</td><td>580</td><td>662.0</td><td>0.32</td><td>8.37</td></tr>
<tr><td>3</td><td>12.5</td><td>576</td><td>661.3</td><td>0.35</td><td>8.56</td></tr>
<tr><td>1</td><td>16</td><td rowspan="3">205.3</td><td>557</td><td rowspan="3">560.7</td><td>663.7</td><td rowspan="3">666.4</td><td>0.29</td><td rowspan="3">0.30</td><td>9.48</td><td rowspan="3">9.37</td></tr>
<tr><td>2</td><td>16</td><td>559</td><td>665.7</td><td>0.27</td><td>9.50</td></tr>
<tr><td>3</td><td>16</td><td>566</td><td>669.7</td><td>0.34</td><td>9.14</td></tr>
</table>

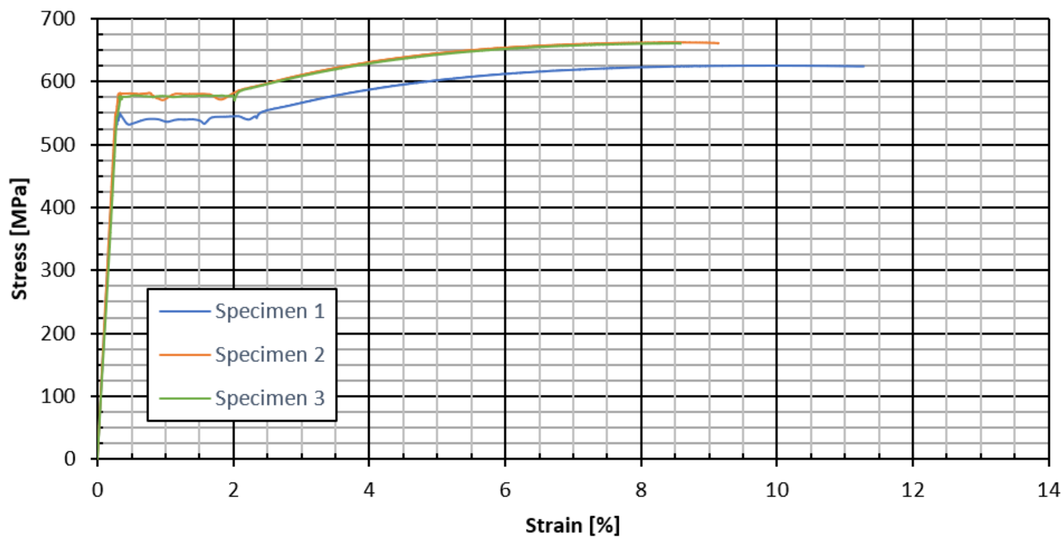

Figure 4.2: Stress-strain relation for steel bars with 12.5 mm diameter.

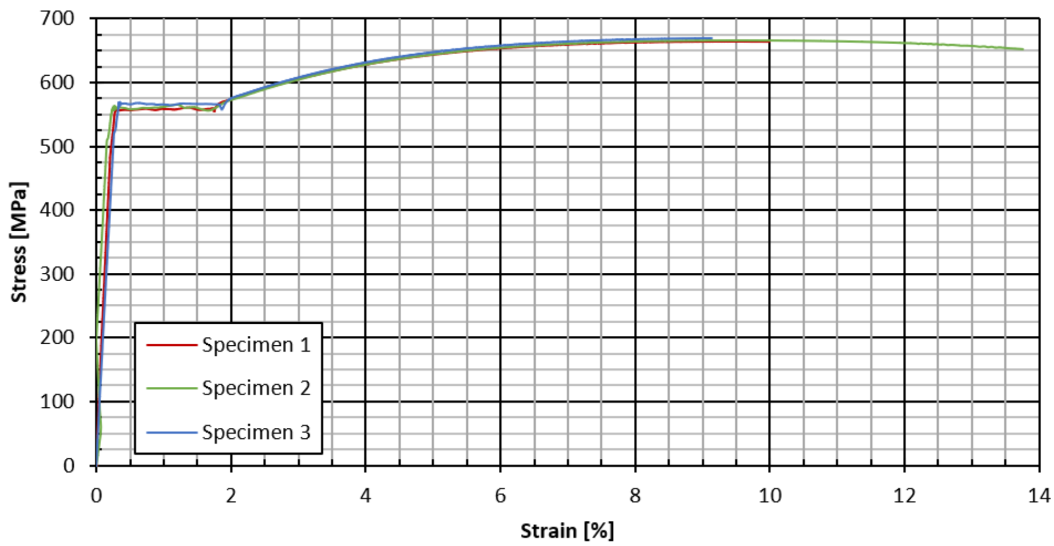

Figure 4.3: Stress-strain relation for steel bars with 16 mm diameter.

4.2 Concrete

Compressive strength tests were performed on the cubic and cylinder specimens collected during the casting of the models to determine the mechanical characteristics of concrete used in the construction of the precast specimens S1, S2, S3 and S4. The compressive tests were done according to NP EN 12390-3 [34] and the tensile splitting were performed according to NP EN 12390-6. The characterization of concrete was defined according to NP EN 206-1 [35]. Figure 4.4 represents the dimensions of specimens tested, and in Figure 4.5 the compressive strength tests carried out in the Civil Engineering Department of the Faculty of Science and Technology – UNL can be seen.

(a) Cylinder

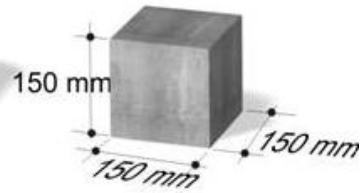

(b) Cubic specimen

Figure 4.4: Dimensions of the specimens tested under compression.

(a) Compressive strength tests on cubes

(b) Compressive strength tests on cylinders

(c) Cylinder spliting tests

Figure 4.5: Concrete laboratory tests

Table 4.3 shows the mean secant modulus of elasticity (***E_{cm})***, the mean compression strength on cylinder specimens (***f_{cm})***, the mean tensile strength (***$f_{ctm,sp}$)*** and the mean compression strength on cube specimens (***$f_{cm,cube}$***). The mean secant modulus of elasticity was determined according to Eurocode 2 [30].

Table 4.3: Concrete mechanical characteristics

Specimen	Column	N.º Spec. on compression		N.º Spec. on Splitting	$f_{ctm,sp}$ (MPa)	$f_{cm,cube}$ (MPa)	f_{cm} (MPa)	E_{cm} (GPa)
		Cubic	Cylinder	Cubic				
S1	A	3	0	3	4.6	56.4	-	-
	B	3	3	3	3.8	53.9	58.5	37.4
S2	A	6	3	3	3.7	52.9	53.6	36.4
	B	3	0	3	3.7	46.0	-	-
S3	A	3	3	3	3.6	50.0	49.4	35.5
	B	6	0	3	3.8	46.0	-	-
S4	A	3	3	3	4.3	49.1	52.4	39.5
	B	3	0	3	4.2	58.0	-	-

4.3 Grout

MASTERFLOW 765 grout was used to fill the corrugated steel ducts of each experimental specimen. The filling process was gravity aided, as seen in Figure 4.6.

Figure 4.6: Filling process of corrugated steel ducts by gravity.

In case of specimen S1, a 50 mm thick connection joint allowed a simple and easy filling process. However, in experimental specimens S2 and S3, the small space between the column surfaces (dry joint), led to difficulties in the filling process of the corrugated steel ducts. This filling was done before inserting the protruded bars and the contact between the column surfaces. For this reason, the filling process of the corrugated steel ducts was done rapidly to avoid the grout starting to cure before the connection between the columns was completed.

Due to the adverse environmental conditions (temperatures close to 30ºC) and the reasons mentioned above, a fluid grout was used in the filling process. As can be observed in Figure 4.7, notwithstanding the filling difficulties in specimens S2 and S3, the corrugated steel ducts were completely filled.

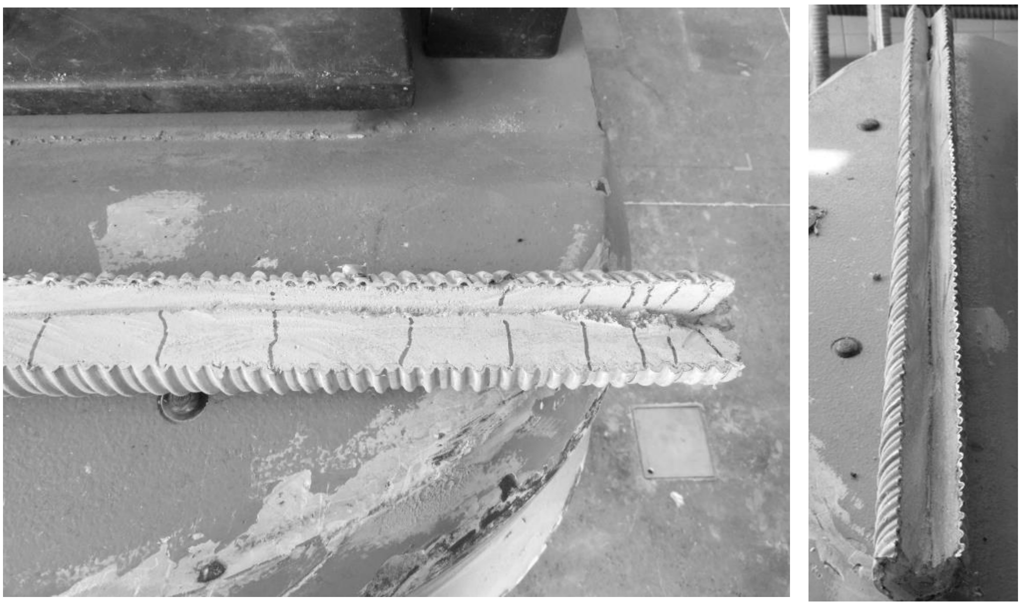

Figure 4.7: Corrugated steel ducts cut after experimental tests of specimens S2 and S3.

In order to define the mechanical properties of the grout used to fill the corrugated steel ducts of specimens S1, S2 and S3, 18 prismatic specimens (160x40x40 mm) were tested in laboratory according to the NP EN 196-1 [36]. These tests are illustrated in Figure 4.8.

From the bending test, it is possible to compute the maximum tensile stress present at mid-span of the specimen, with the equation (4.2):

$$f_{ct,b} = \frac{3\, N.\ell}{2\, b.h^3} \tag{4.2}$$

where $f_{ct,b}$ is the tension due to bending, N is the applied force, **h** is the specimen's height (40 mm), **b** is the specimen's width (40 mm) and ℓ is the distance between supports (100mm). From by tensile tests were used the specimens halves (40x40x40mm) to performed the compression tests.

$$f_c = \frac{N_c}{A} \tag{4.3}$$

in which N_C is the applied compression force and **A** is the specimen's area (40x40 mm^2). Through the previous equations (4.2 and 4.3), the mean tensile strength from bending test ($f_{ctm,b}$) and mean compression strength (f_{cm}) were calculated and these results are depicted in Table 4.4.

(a) Bending test (b) Compression test

Figure 4.8: Grout laboratory tests.

Table 4.4: Grout's mechanical properties obtained from test results

Specimen	*Column*	*Age* (days)	f_{cm} (MPa)	$f_{ctm,b}$ (MPa)
S1	A	25	68.9	10.0
S2	A	45	63.1	8.0
S3	A	47	66.0	8.9

These results agree with the compression resistance of the MASTERFLOW 765, presented in Table 4.5. However, the same did not happen to the bending tests results as the tensile strengths of specimens S2 and S3 are slightly lower than to be expected.

Table 4.5: MASTERFLOW 765 mechanical strengths, according to manufacturer data [37].

MASTERFLOW 765

Age	**Temperature**	**Mixture consistency**	f_{cm}	$f_{ctm,b}$
(days)	(ºC)		(MPa)	(MPa)
1			approx. 30	approx. 5.8
7	+20	fluid	approx. 45	approx. 8.7
28			approx. 62	approx. 9.9

4.4 Unidirectional Fibre Reinforced Grout (UFRG)

The 50 mm thickn connection joints (specimens S1 and S4) and column B holes of specimens S1, S2 and S4, were filled with a fibre reinforced grout whose composition was studied and developed by Gião [38]. This fibre reinforced grout has a high mechanical resistance and controlled shrinkage and, therefore, is a good material to fill the joints [38].

The steel fibre mat used for this dissertation was provided by Favir [39] and was fabricated from 3.1 mm diameter steel wires. The production process consisted of a lamination procedure of the steel wire, resulting in a non-woven mat formed by filaments [38].

Gião [38] studied the properties of the grout with a steel fibre volume equal to 0, 1%, 2% and 3% of the total volume. However, in this study, the percentage of fibres used was 0.28% of the total volume of the mixture, because filling the joints and holes with a higher percentage of fibres would be very challenging. Table 4.6 presents the composition of the grout considered.

Table 4.6: Grout's composition

Matrix composition		
Portland Cement Type I Class 42.5R	-	1356 (kg/m^3)
Silica fume (%)	2 %	31 (kg/m^3)
Water-binder ratio	0.30	470 (kg/m^3)
Super-plasticizers: Sika Viscocrete 3005	0.5 %	8 (kg/m^3)
Steel fibres	0.28%	22 (kg/m^3)

Figure 4.9 shows the placement of steel fibres in the connection joint of specimens S1 and S4 and in the holes of column B of specimens S1, S2, and S4.

(a) Weighing the steel fibres

(a) Steel fibre placement

Figure 4.9: Steel fibres of UFRG

Figure 4.10 illustrates the connection joint of experimental specimens S1, S2 and S4, before and after the filling with UFRG.

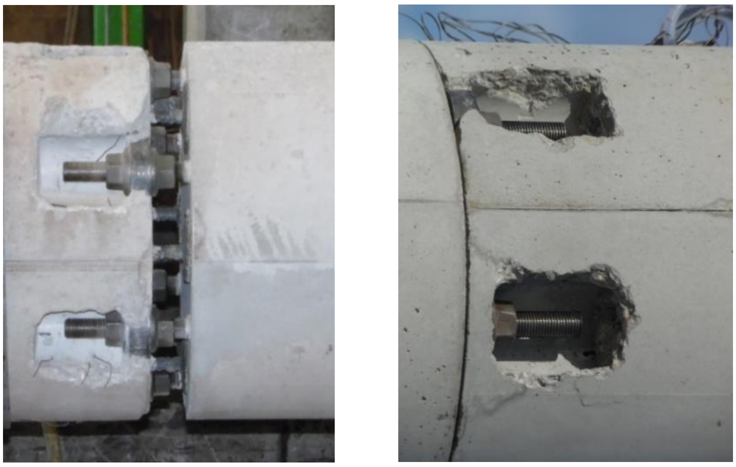

(a) Before the filling – specimen S1 and S4

(c) Before the filling – specimen S2

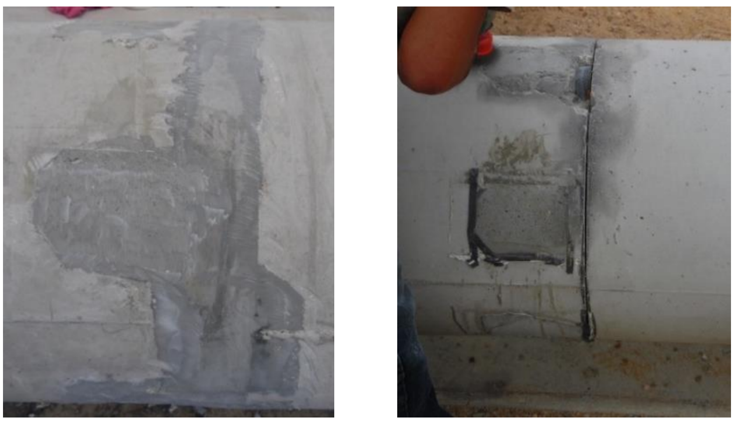

(b) After filling – specimen S1 and S4

(d) After filling – specimen S2

Figure 4.10: Connection joint of experimental specimens S1, S2 and S4, before and after filling with UFRC.

In order to determine the mechanical properties of the fibre reinforced grout (UFRC), 12 prismatic specimens (160x40x40 mm) with steel fibres and 9 prismatic specimens (160x40x40 mm) without steel fibres were tested in laboratory according to the NP EN 196-1 [36]. After bending tests of the prismatic specimens (160x40x40 mm), the specimen halves (40x40x40 mm) were reused for compression tests. These tests were done one the same day as the tests of specimens S1, S2 and S4, and are shown in Figure 4.8.

Using the previous equations (4.2) and (4.3) the average stresses $f_{ctm,b}$ and f_{cm} were determined for grout reinforced with steel fibres and for grout without steel fibres. These results are shown in Tables 4.7 and 4.8, respectively.

Table 4.7: Grout without steel fibres, tests' results.

Specimen	*Filled element*	*Age* (days)	f_{cm} (MPa)	$f_{ctm,b}$ (MPa)
S1	Holes	18	62.5	4.0
S2	Holes	31	87.4	8.8
S4	Holes	25	84.7	7.7

Table 4.8: Grout reinforced with steel fibres, tests' results.

Specimen	*Filled element*	*Age* (days)	f_{cm} (MPa)	$f_{ctm,b}$ (MPa)
S1	Joint	18	67.2	6.2
S2	Holes	31	83.1	6.1
S4	Joint	25	84.4	8.5

Analysing the test results from bending and compression, it can be concluded that the mechanical resistance of the grout is nearly the same, independently whether it is reinforced with steel fibres or not. However, according to [38], when fibre volume is superior to 1% of total volume, the decrease in strength of the grout is significant when compared with grout without steel fibres and the main reason is that the void volumes increases significantly. So, in case of specimens S1, S2 and S4, during the filling process of holes and joints with UFRG appropriate precautions were taken (external vibration) to reduce the presence of voids. Consequently, with the use of UFRG, the segregation phenomena have less impact.

4.5 Epoxy resin

The joints of specimens S2 and S3 were filled with low viscosity epoxy resin - *Sikadur-52 Injection* – as it was not possible to use fibre reinforced grout to fill the 3mm dry joint gap. The filling procedure is described below:

i. To avoid resin leaks, the edges of the joint were sealed with mortar and nozzles were placed along the joint perimeter, to allow resin injection and control the filling process (Figure 4.11);

ii. After 24 hours, the injection with resin was performed from bottom up in order to allow the air in the joint to be expelled from nozzles located in higher positions. Whenever the resin was expelled from a nozzle, this was immediately blocked to maintain the pressure and force the rising of resin trough the joint (Figure 4.12).

(a) sealing the joint– specimen S2 (b) Nozzles positioning – specimen S3

Figure 4.11: Sealing process around the joints of specimens S2 and S3.

(a) Resin expelled through a nozzle (b) Blocking of nozzle

Figure 4.12: Filling of joints of specimens S2 and S3 with epoxy resin.

Unlike the other materials, it was not necessary to carry out experimental tests to define the mechanical properties of the epoxy resin because. The mechanical properties of the epoxy resin (*Sikadur-52 Injection*) used to inject dry joints of specimens S2 and S3, were defined according the manufacturer data [32]. These characteristics are depicted in Table 4.9**.**

When specimens S2 and S3 were tested, the epoxy resin was 13 and 8 days old respectively.

Table 4.9: *Sikadur-52 Injection* mechanical strengths, according [32].

Age	***Temperature***	f_{cm}	f_{ctm}	$f_{ctm,b}$
(days)	(ºC)	(MPa)	(MPa)	(MPa)
After 7	+23	approx. 52	approx. 37	approx. 61

Chapter 5

Analysis of the experimental results

5.1 Introduction

In this chapter the results obtained from experimental tests performed on specimens S1, S2, S3 and S4 are analysed. The following will be analysed: vertical displacements; the strains along the column span; the reinforcing steel strain at the middle span and below loading points; the diagrams of the internal forces and the cracking and failure mechanism of each experimental specimen.

5.2 Vertical displacements

5.2.1 Specimen S1

Figure 5.1 presents the evolution of the vertical displacements versus total vertical load applied on specimen S1. Based on expression (5.1), the theoretical value of cracking bending moment (**M_{cr}**) was determined.

$$M_{CR} = W\left[0.7\, f_{ctm} + \frac{P}{A}\right] \tag{5.1}$$

Where fctm is the mean tensile strength of concrete, corresponding to 90% of mean tensile strength obtained in splitting tests, N is the axial load applied on test specimens (prestressing load), A is the area of the circular cross section of the column, and W corresponds to bending modulus of circular cross section.

So, according to the expression (5.1), until there is a vertical load of 87.4 kN, the column has an elastic behaviour. Above this load, some cracks began to appear, and the structure model began to lose stiffness, i.e. the increase of displacements is no longer proportional to the increase in vertical load. For a vertical load of 289.7 kN, the specimen reached the yielding level and specimen failure occurred when vertical load achieved approximately 315.7 kN.

Table 5.1 shows the values of vertical displacements corresponding to different vertical load levels applied to specimen S1. Displacement transducers D1 to D6 were removed at yielding level to avoid damage. Figure 5.2 shows the deformed shapes of S1 during experimental test.

Figure 5.1: Load-displacement relation of specimen S1.

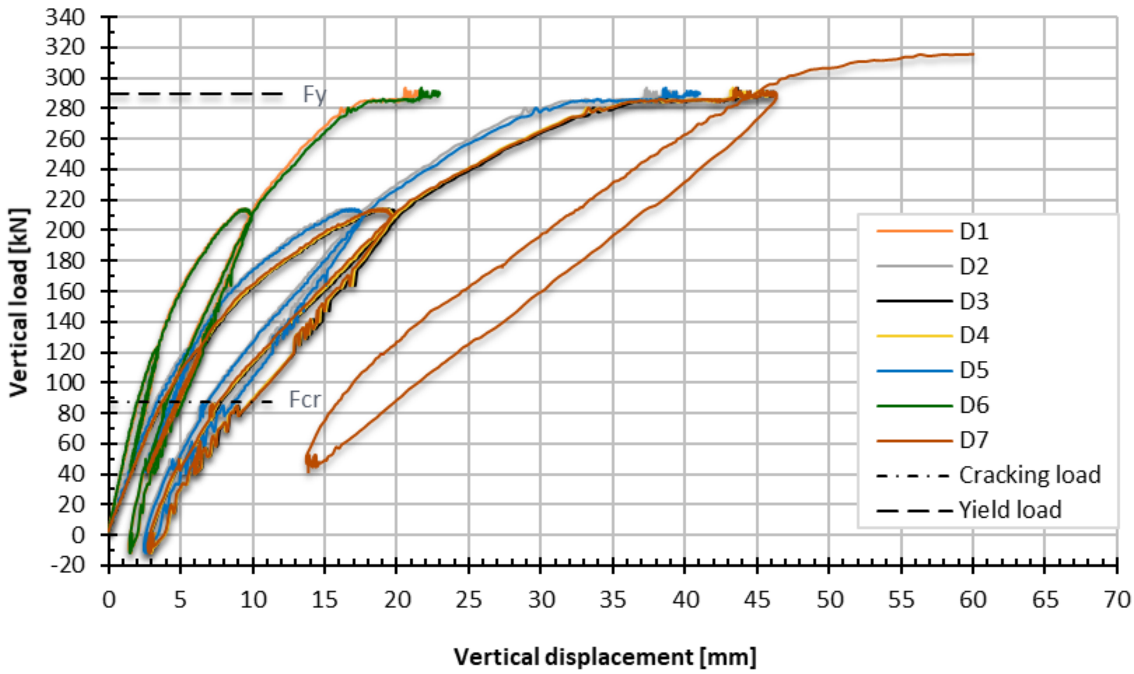

Table 5.1: Vertical displacement values to different load levels applied on specimen S1.

Specimen S1										
Displacement transducer		-	**D1**	**D2**	**D3**	**D7**	**D4**	**D5**	**D6**	-
dist. from left support	(m)	0	1	2	2.75	3	3.25	4	5	6
cracking F_{CR}=87.4kN	(mm)	0	2.10	3.36	3.97	3.89	3.93	3.52	2.10	0
vertical load F=120kN	(mm)	0	3.30	5.41	6.27	6.17	6.18	5.67	3.31	0
vertical load F=200kN	(mm)	0	9.12	16.07	18.73	18.36	18.48	16.45	9.23	0
93% of failure/ yield level F=293.7kN	(mm)	0	20.60	37.34	43.65	43.56	43.32	38.69	21.72	0
Failure F=315.7kN	(mm)	0	-	-	-	60.02	-	-	-	0

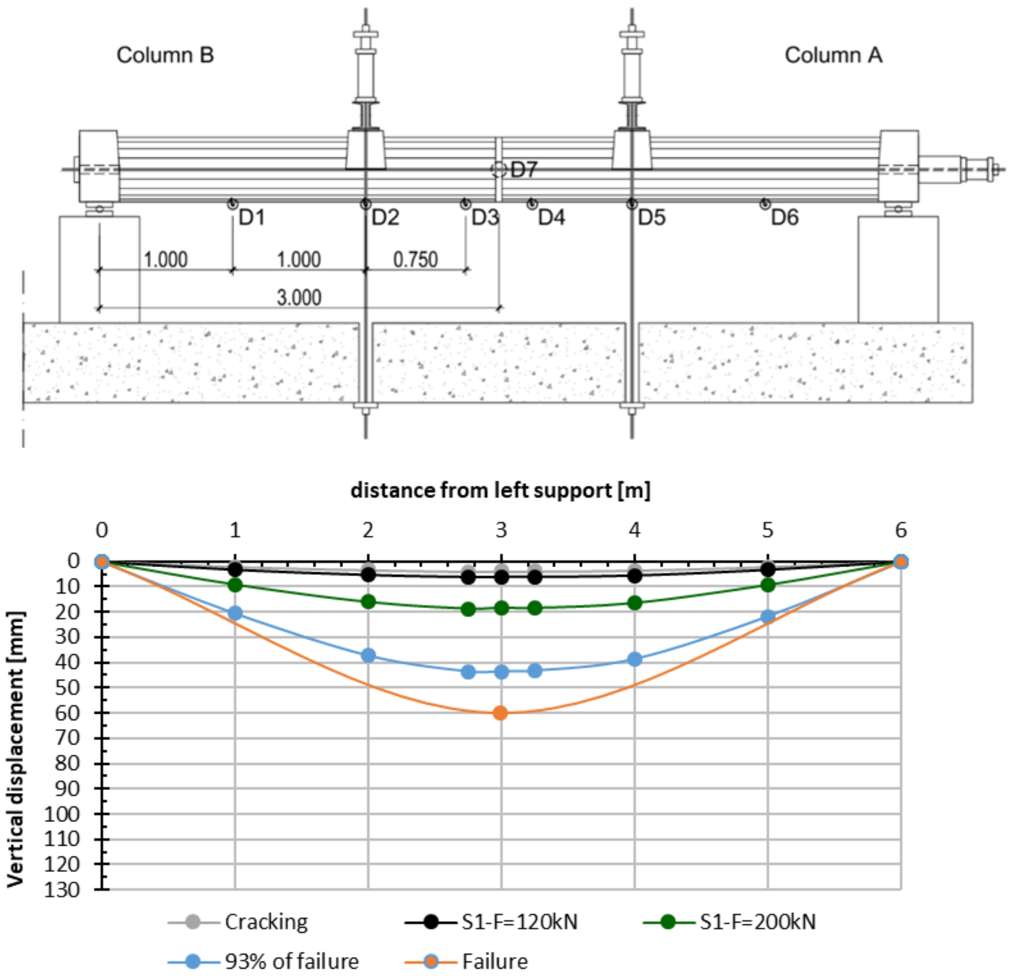

Figure 5.2: Deformed shapes of specimen S1 to different load levels

5.2.2 Specimen S2

Figure 5.3 shows the evolution of vertical displacements of the vertical load applied to specimen S2. According to the previous expression (5.1), the first cracks appear at a vertical load of 86.7 kN (**F_{CR}**). The ultimate vertical load reached 315.3 kN. This value is similar to the ultimate vertical load supported by specimen S1.

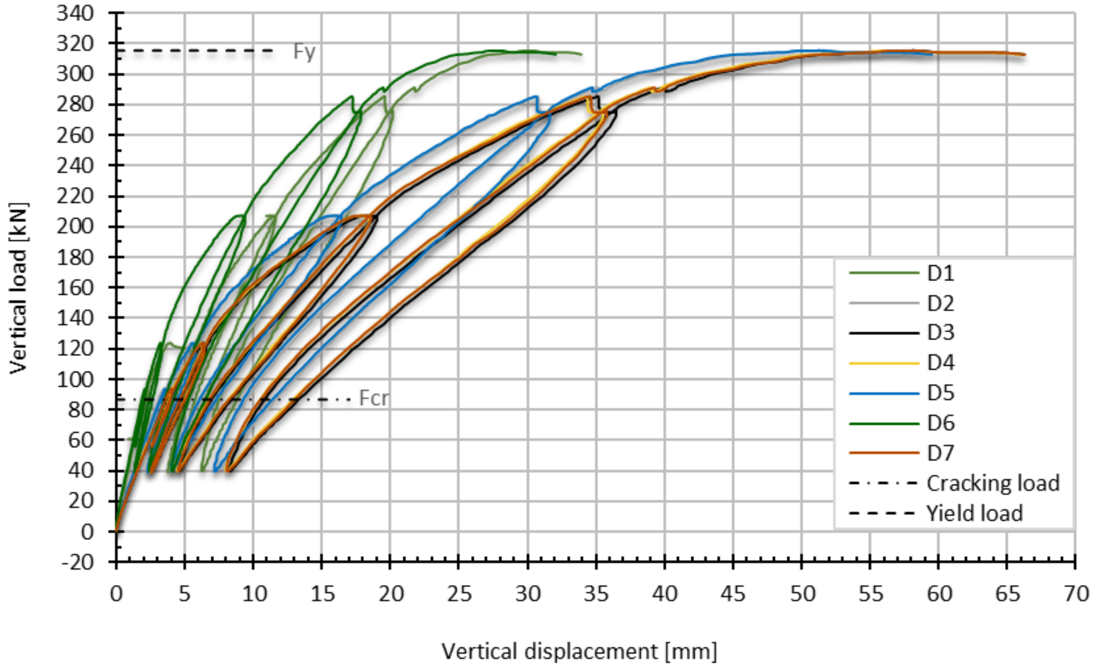

Figure 5.3: Load-displacement relation of specimen S2.

As may be observed in Figure 5.4, the behaviour of deformed shape after failure phase, below the load application zone, is different to the remaining experimental specimens. This happens because the failure of specimen S2 occurred precisely below the load application zone.

Table 5.2 depicts the values of vertical displacements corresponding to the different vertical load levels applied to specimen S2. In this experimental test, the displacements D1 to D6 were not removed during failure phase, which made it possible to study the deformed post-failure shape of column.

Table 5.2: Vertical displacement values to different load levels applied on specimen S2.

Specimen S2										
Displacement transducer		-	**D1**	**D2**	**D3**	**D7**	**D4**	**D5**	**D6**	-
dist. from left support	(m)	0	1	2	2.75	2.98	3.20	3.95	4.95	5.95
cracking F_{CR}=86.7 kN	(mm)	0	2.15	3.20	3.79	3.72	3.72	3.35	1.94	0
vertical load F=120kN	(mm)	0	4.25	5.57	6.41	6.34	6.28	5.70	3.25	0
vertical load F=200kN	(mm)	0	11.01	15.92	18.19	17.71	17.70	15.69	8.97	0
93% of failure F=293.2 kN	(mm)	0	22.43	36.42	41.40	40.66	40.38	35.94	20.09	0
failure/yield level F=315.3 kN	(mm)	0	30.29	51.51	58.03	58.01	57.30	51.16	27.91	0
Maximum displacement F=298.98 kN	(mm)	0	45.35	81.64	95.15	96.53	97.23	92.52	48.22	0

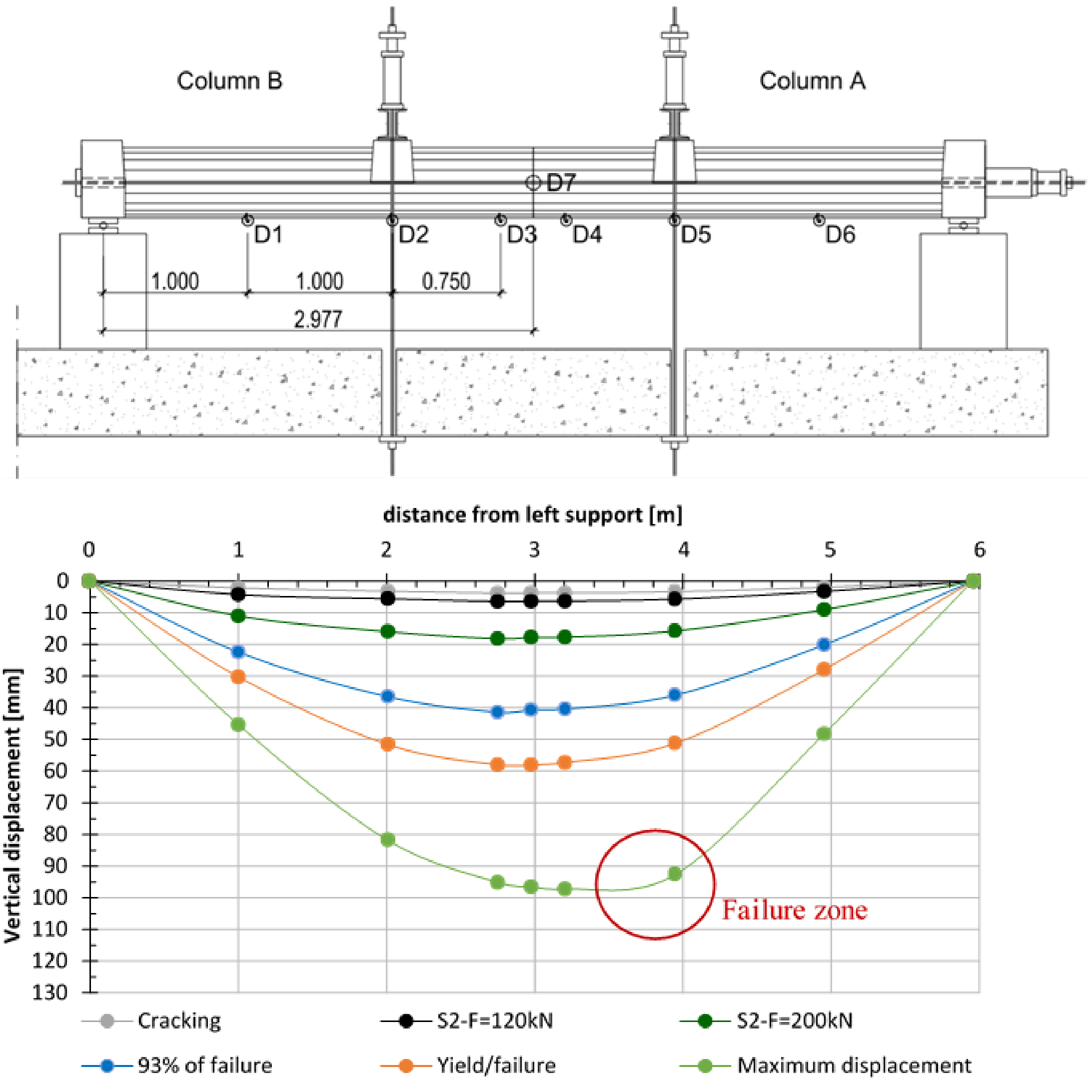

Figure 5.4: Deformed shapes of specimen S2 to different load levels.

5.2.3 Specimen S3

Figure 5.5 shows the evolution of vertical displacements with the vertical load applied to specimen S3. According to the previous expression (5.1), the first cracks appear for a vertical load of 86.0 kN ($\mathbf{F_{CR}}$). The ultimate vertical load was reached by specimen S3 at 266.90 kN.

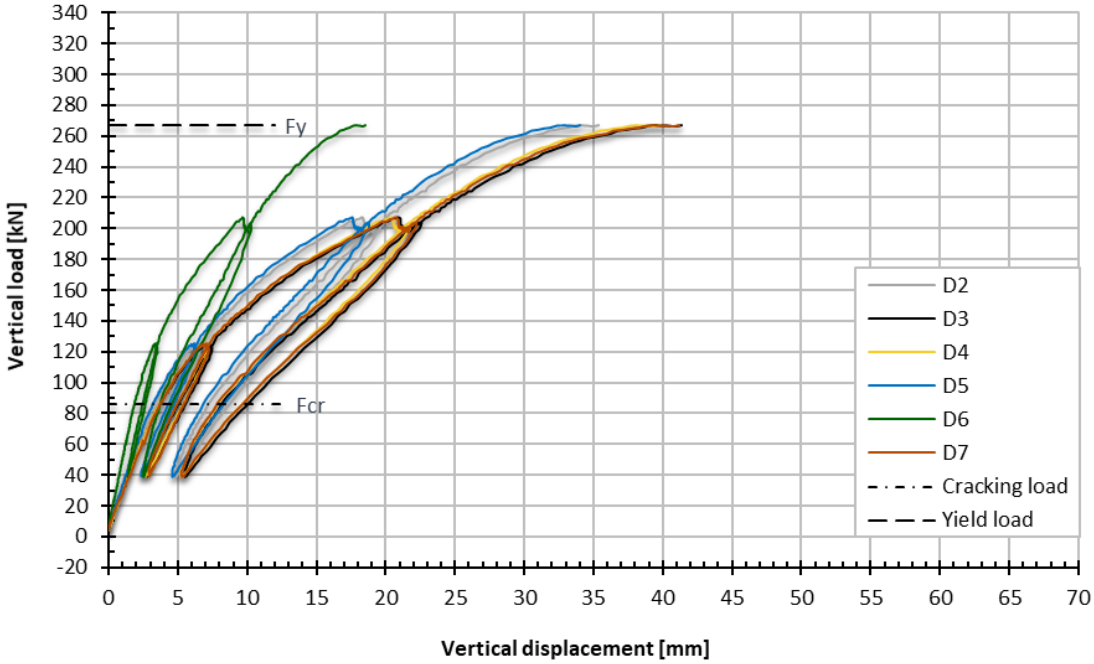

Figure 5.5: Load-displacement relation of specimen S3.

Table 5.3 shows the vertical displacements for different vertical load levels. The maximum displacement obtained (after failure phase) was in the mid-span, as expected since the failure also occurred at the mid-span (Figure 5.6).

Table 5.3: Vertical displacement values to different load levels applied on specimen S3.

Specimen S3										
Displacement transducer		**-**	**D1**	**D2**	**D3**	**D7**	**D4**	**D5**	**D6**	**-**
dist. from left support	(m)	0	1	2	2.75	2.98	3.20	3.95	4.95	5.95
Cracking F_{CR}=86.0 kN	(mm)	0	-	3.31	3.73	3.74	3.66	3.19	1.89	0
vertical load F=120kN	(mm)	0	-	6.57	7.41	7.13	7.12	6.22	3.46	0
vertical load F=200kN	(mm)	0	-	18.96	21.77	21.43	21.05	18.05	9.98	0
93% of failure F=248.3kN	(mm)	0	-	27.15	31.37	30.82	30.31	26.13	14.45	0
failure/yield level F=266.9kN	(mm)	0	-	35.40	41.39	41.18	39.88	34.00	18.55	0
Max. displacement F=220.9kN	(mm)	0	-	80.03	101.57	102.17	96.91	76.13	39.31	0

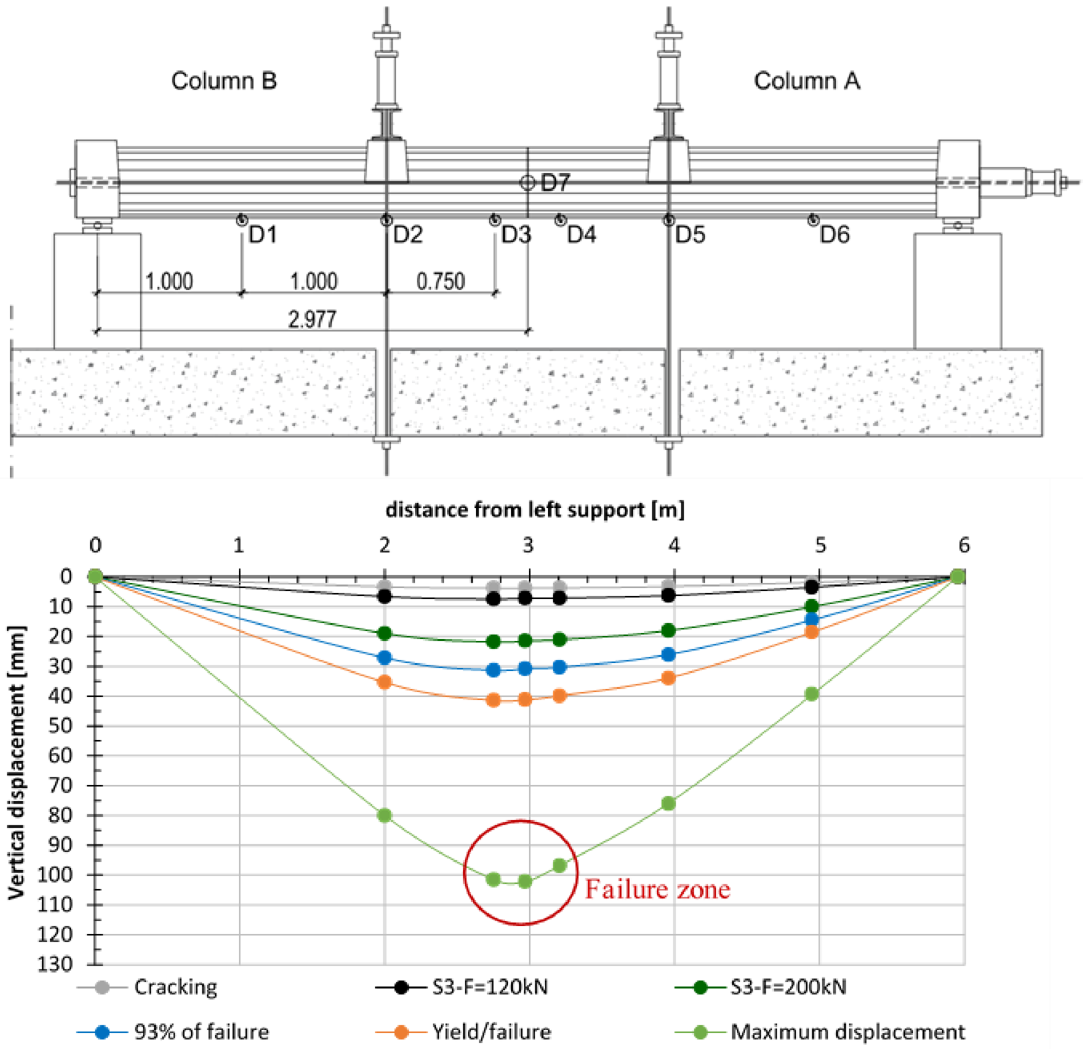

Figure 5.6: Deformed shapes of specimen S3 for different load levels

5.2.4 Specimen S4

Figure 5.7 shows the evolution of vertical displacements with the vertical load applied to specimen S4. The first cracks appeared for a vertical load of 90.3 kN and for 275.2 kN the structural model reached yielding level and simultaneous failure occurred.

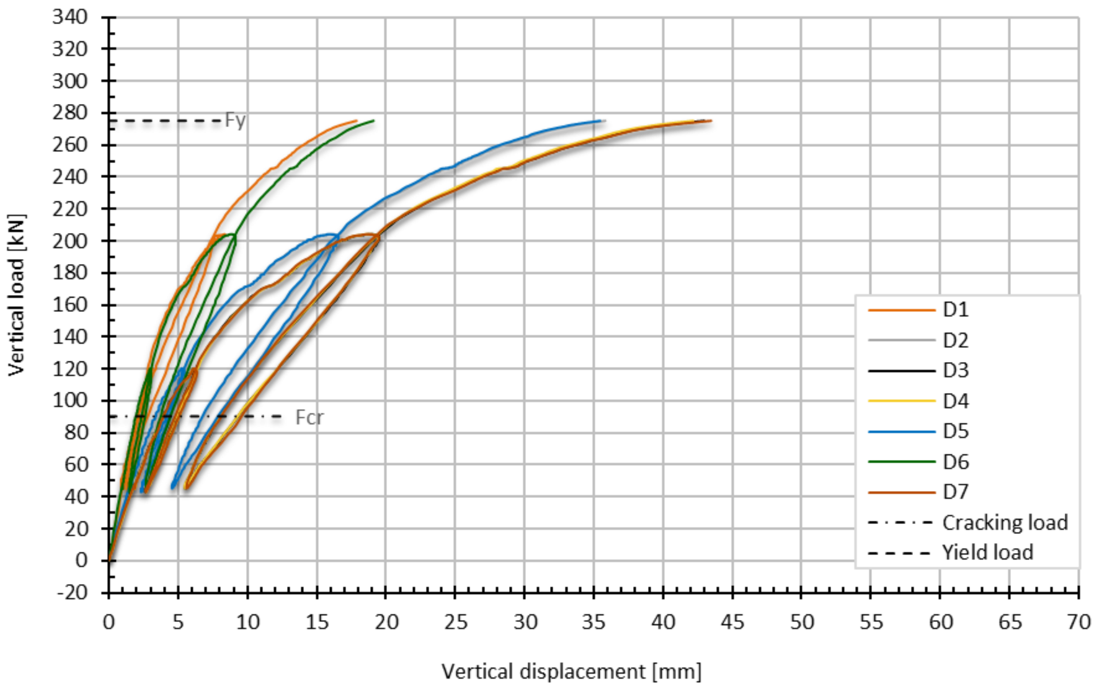

Figure 5.7: Load-displacement relation of specimen S4.

Table 5.4 shows the values of vertical displacements for different vertical load levels. As in specimen S3, for specimen S4 the failure occurred at mid-span (Figure 5.8).

Table 5.4: Vertical displacement values to different load levels applied on specimen S4.

Specimen S4										
Displacement transducer		-	**D1**	**D2**	**D3**	**D7**	**D4**	**D5**	**D6**	-
dist. from left support	(m)	0	1.0	2.0	2.75	3.0	3.25	4.0	5.0	6.0
Cracking F_{CR}=90.3kN	(mm)	0	2.10	3.40	3.89	3.96	3.91	3.40	1.94	0
vertical load F=120kN	(mm)	0	3.14	5.33	6.10	6.14	6.15	5.23	2.99	0
vertical load F=200kN	(mm)	0	8.33	16.02	18.72	18.58	18.60	15.93	8.76	0
93% of failure F=256.0kN	(mm)	0	13.47	27.52	32.39	32.38	31.95	27.26	14.85	0
failure/yield level F=275.2kN	(mm)	0	17.87	35.82	42.95	43.46	42.16	35.45	19.10	0
Max. displacement F=64.8kN	(mm)	0	41.95	84.85	114.25	119.28	111.11	83.99	42.71	0

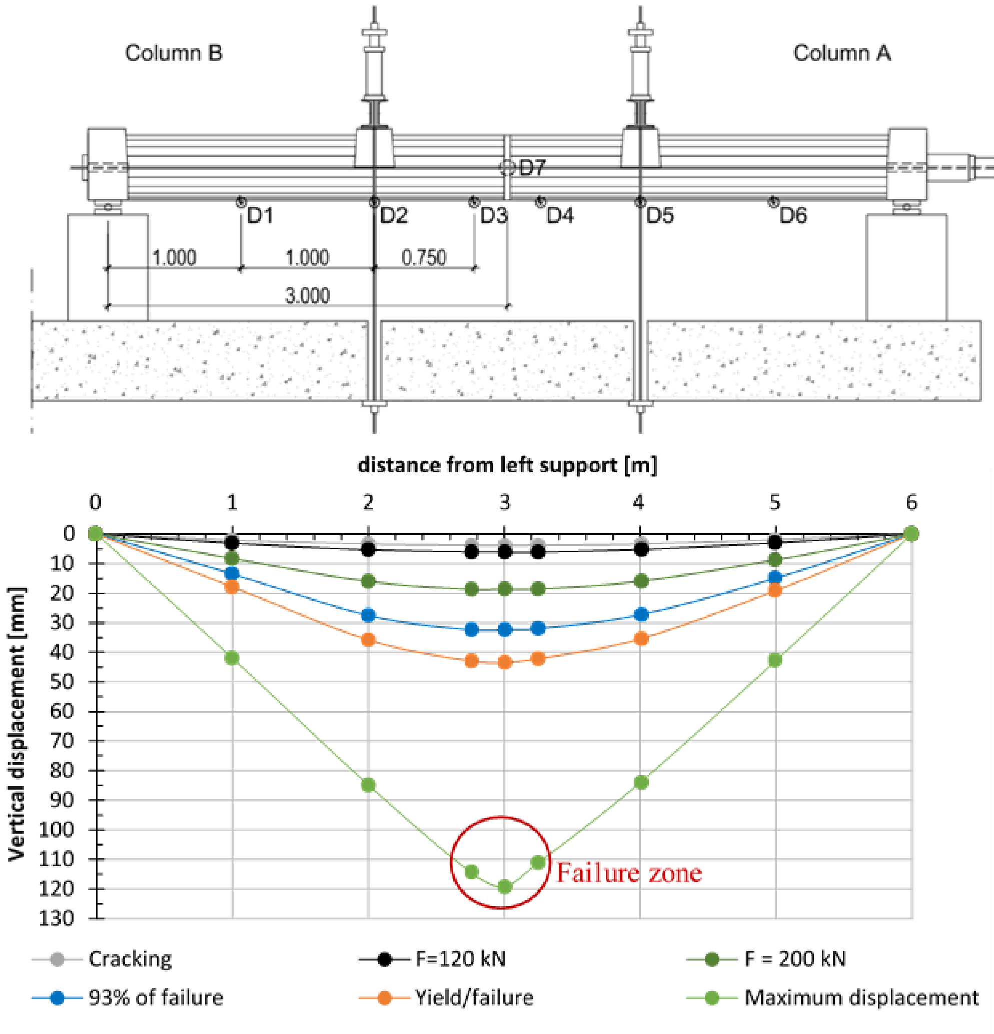

Figure 5.8: Deformed shapes of specimen S4 to different load levels

5.2.5 Comments

Based on figures 5.1, 5.3, 5.5 and 5.7 one can conclude that the beginning of specimen cracking occurred when a vertical load of 87.6 kN (mean value of four tested specimens) was reached, until then the behaviour of the specimens is elastic, i.e. the relation vertical load-displacement is linear.

Comparing the results depicted in Tables 5.5 and 5.6 it may be concluded that specimens S1 and S2 have higher resistance (nearly 17% higher) and higher ductility (40% higher) than specimens S3 and S4. These conclusions make sense since the amount of reinforcement considered in connection S1 and S2 is the same and also larger than in specimens S3 and S4.

The reduction of connection joint thickness "dry joint" of the specimen S2 does not have any influence on stiffness/ductility (Figure 5.9).

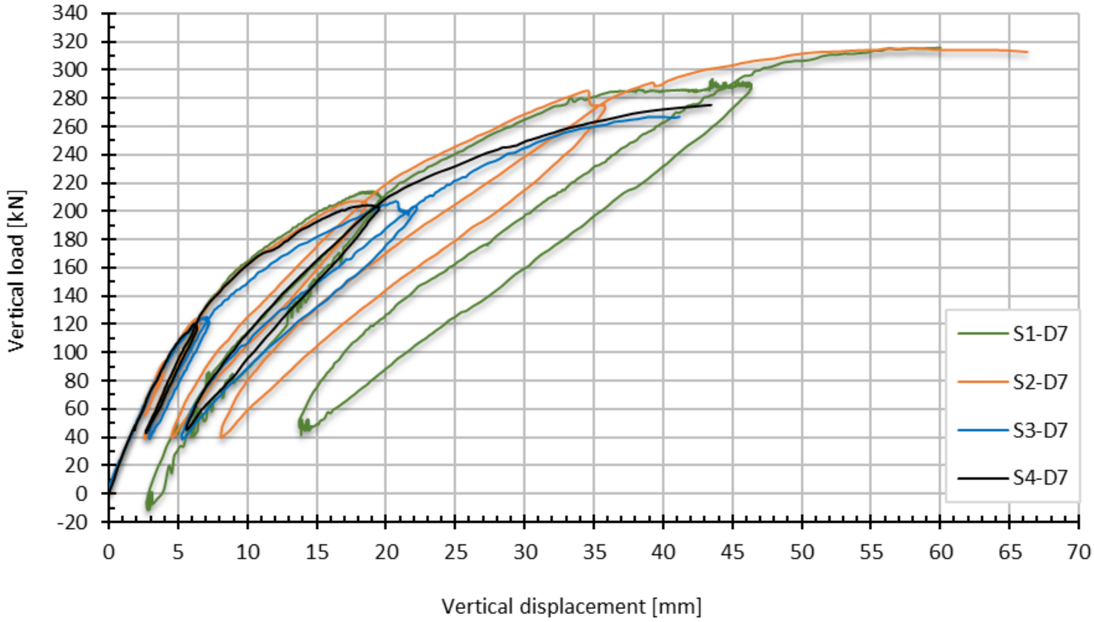

Figure 5.9: Load-displacement relation at mid-span for each experimental specimen.

Table 5.5: Vertical load values in cracking, 93% failure, and failure for each experimental specimen.

Experimental specimen		**S1**	**S2**	**S3**	**S4**
In cracking	(kN)	87.4	86.7	86.0	90.3
To 93% of failure	(kN)	293.7	293.4	248.6	256.6
In failure	(kN)	315.7	315.3	266.9	275.2

Table 5.6: Displacement at mid-span in specimens failure phase.

Displacement transducer	**D7 [mm]**
Specimen S1	60.02
Specimen S2	58.01
Specimen S3	41.18
Specimen S4	43.46

5.3 Steel strains

The following table presents, for each experimental specimen, the strain gauges used for the strains measurement of longitudinal reinforcement subjected to tensile forces. The positioning of strain gauges was defined in order to allow the direct comparison of strains between all experimental specimens, this can be also reviewed in more detailing in Section 3.3.3.

Table 5.7: Strain gauges' identification

Specimen	Column	Connection zone				Below of load application zone
-	-	Trejor reinf.			Ordinary reinf.	Ordinary reinf.
S1	A	Ext 1-2	Ext 3-4	Ext 5-6	-	Ext 17-18
	B	Ext 7-8	Ext 9-10	Ext 11-12(*)	Ext 13-14(*)	Ext 15-16
S2	A	Ext 1-2	Ext 3-4	Ext 5-6	-	Ext 17-18
	B	Ext 7-8	Ext 9-10	Ext 11-12	Ext 13-14	Ext 15-16(*)
S3	A	-	-	-	-	Ext 1-2
	B	-	-	-	Ext 3-4; Ext 5-6; Ext 9-10	Ext 7(*)-8(*)
S4	A	Ext 1-2	Ext 3-4	Ext 5-6	-	Ext 17-18
	B	Ext 7-8	Ext 9-10	Ext 11-12	Ext 13-14(*)	Ext 15-16

(*) – Strain gauges damaged

The strain development during tests are presented in the following graphs. The strain values are the average of the readings from each pair of strain-gauges placed in each bar cross section. The yielding strain obtained in steel characterization tests were also plotted in theses graphs.

Figure 5.10 show that female Trejor elements reached the yielding stage (Ext7/8 e Ext9/10). However, the male Trejor connections remained in the elastic range (Ext 1/2, 3/4 and 5/6). The ordinary reinforcement, below the load application zone, also reached yielding, as would be expected as the maximum bending moment extends from the connection joint to this zone.

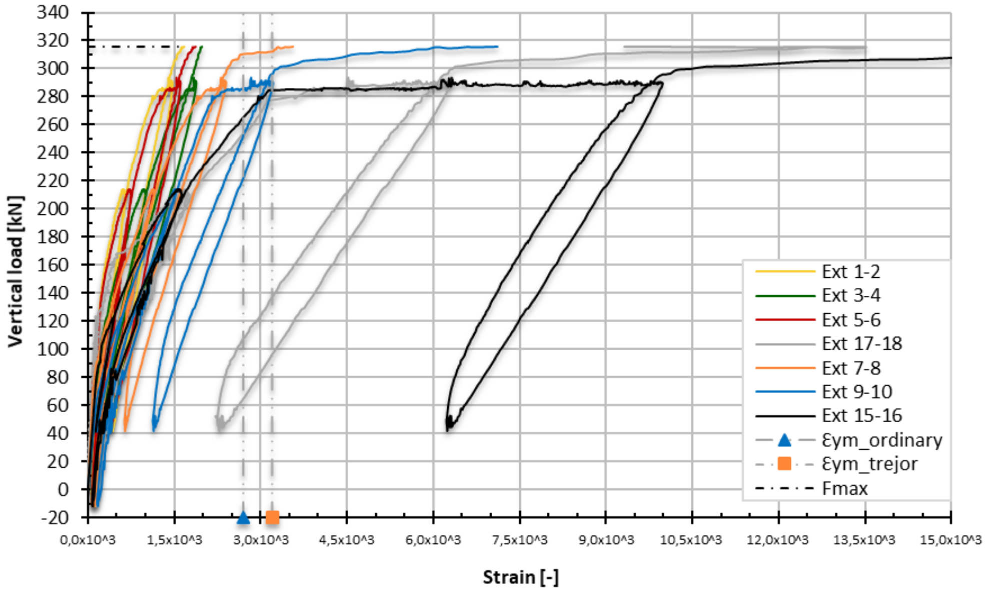

Figure 5.10: Load-strain relation of longitudinal reinforcement on the specimen S1

From Figure 5.11 it may be concluded that the ordinary reinforcement below the load application zone, was the only one that reached yielding (Ext15 and Ext 17/18). The reinforcement of the connection (Trejor elements) remained in the elastic stage, corresponding to a failure of specimen S2 below the application zone. In specimen S3, all longitudinal ordinary reinforcement instrumented reached yielding (Figure 5.12).

Figure 5.11: Load-strain relation of longitudinal reinforcement on the specimen S2

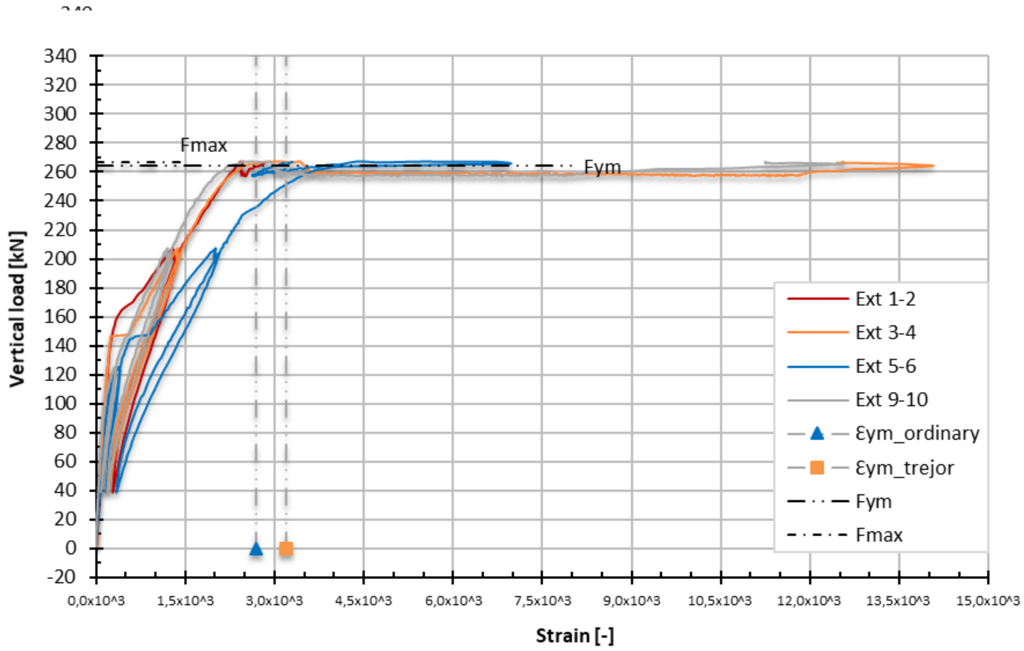

Figure 5.12: Load-strain relation of longitudinal reinforcement on the specimen S3.

Figure 5.13 shows that, at failure stage of specimen S4, only female Trejor elements reached yielding. The remaining steel bars maintained their elastic stage.

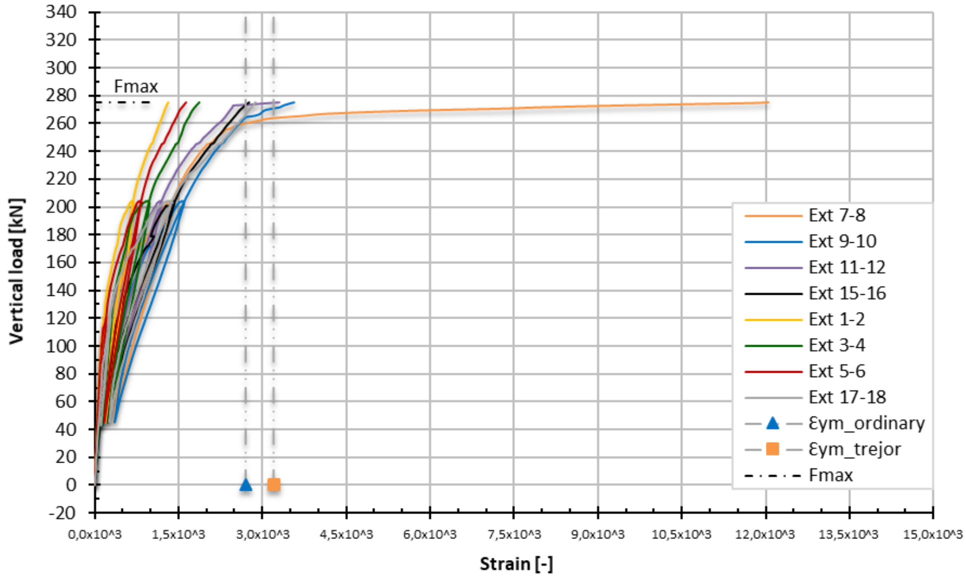

Figure 5.13: Load-strain relation of longitudinal reinforcement on the specimen S4.

The Trejor male connection, with larger effective depth (d), showed similar evolution of strains (Figure 5.14), as was expected since this comparison is made between bars with the same properties and placed at the same effective depth. It was expected that the strains developed on the Trejor female connection would be similar, however that did not happen (Figure 5.15). When comparing the strains developed in all the Trejor connection elements (Figure 5.16), it can be concluded that female Trejor connection in the connection zone, reached higher strains than male the Trejor connections (Figure 5.16).

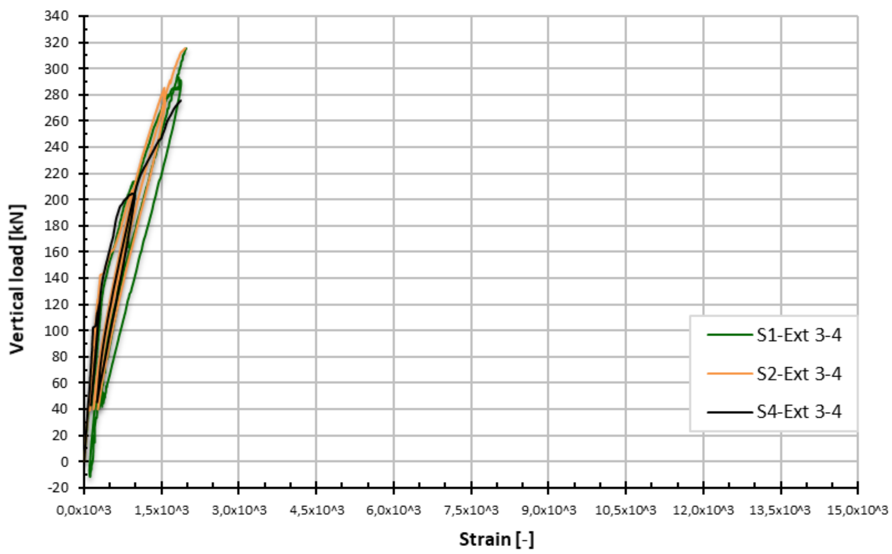

Figure 5.14: Load-strain relation for male Trejor elements, of specimens S1, S2 and S4.

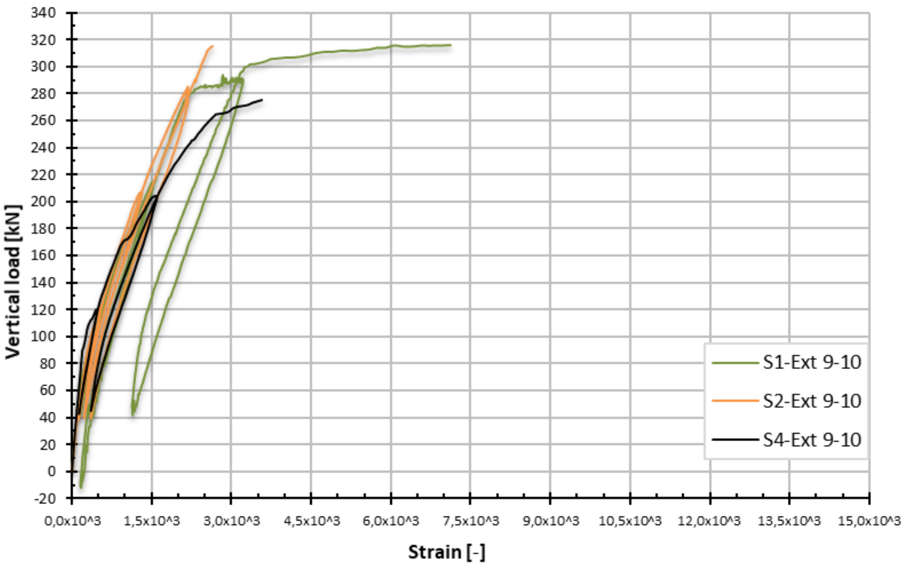

Figure 5.15: Load-strain relation for female Trejor elements, of specimens S1, S2 and S4.

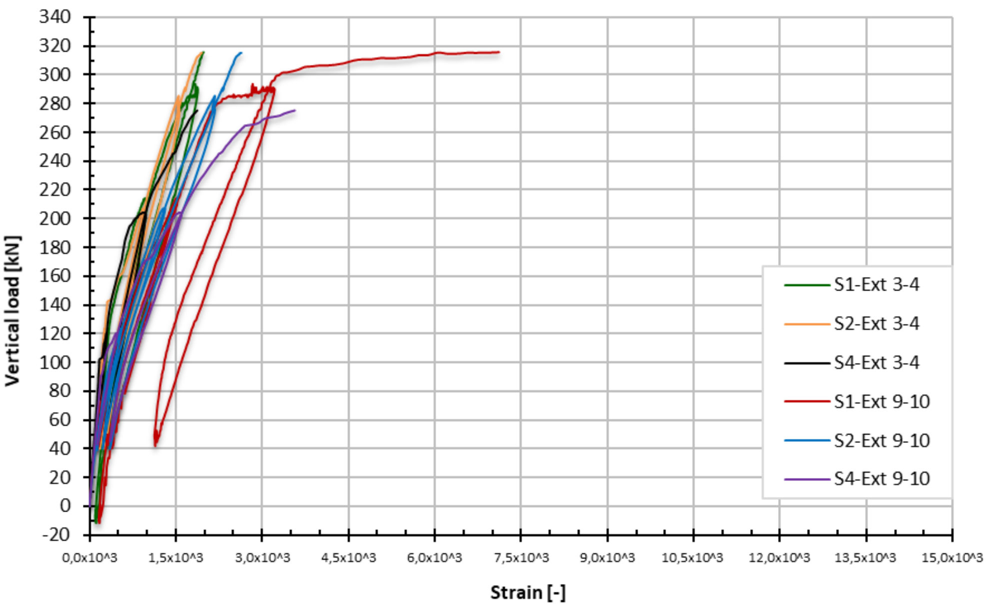

Figure 5.16: Comparison load-strain relation between male and female Trejor elements, of specimens S1, S2 and S4.

Figure 5.17 shows the strains of the ordinary reinforcement in each experimental test. In this case, the comparison is made between bars with larger effective depth, placed in the zone of vertical load application. As may be seen, the strains are very similar in both columns (A and B), nevertheless, the maximum strains occurred in bars placed below of loaded zone of column B of the experimental tests S1, S2 and S4.

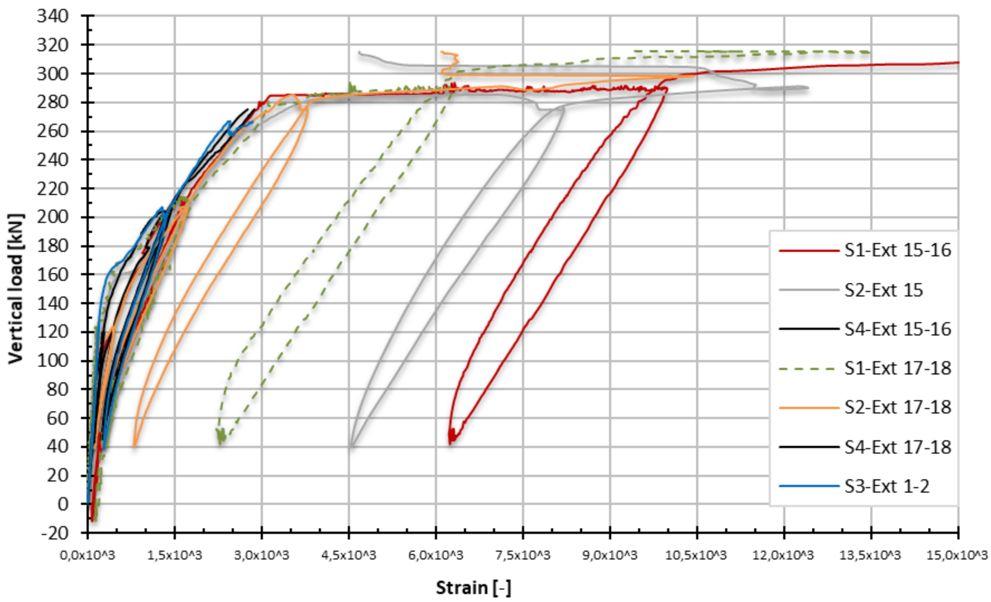

Figure 5.17: Load-strain of the ordinary reinforcement with larger effective depth (**d**) and placed at middle span.

5.4 Relative displacements in concrete

The relative displacement evolution at mid-span in the concrete may be analysed in following graphs. The positioning of omega transducers (relative displacement transducers) along middle span was made as follows: Omega 1 and Omega 3 were placed, respectively, on the upper and underside face of the column, in the connection joint. While Omega 2 and Omega 4 were placed, at 45 degrees to the left and right of Omega 3 (see Figure 3.34). The measuring maximum capacity of the relative displacement transducers is to 2 mm and the distance between the fixing points of device is 150 mm. So, to preserve the equipment it was removed before the relative displacements reached more than 1.85 mm.

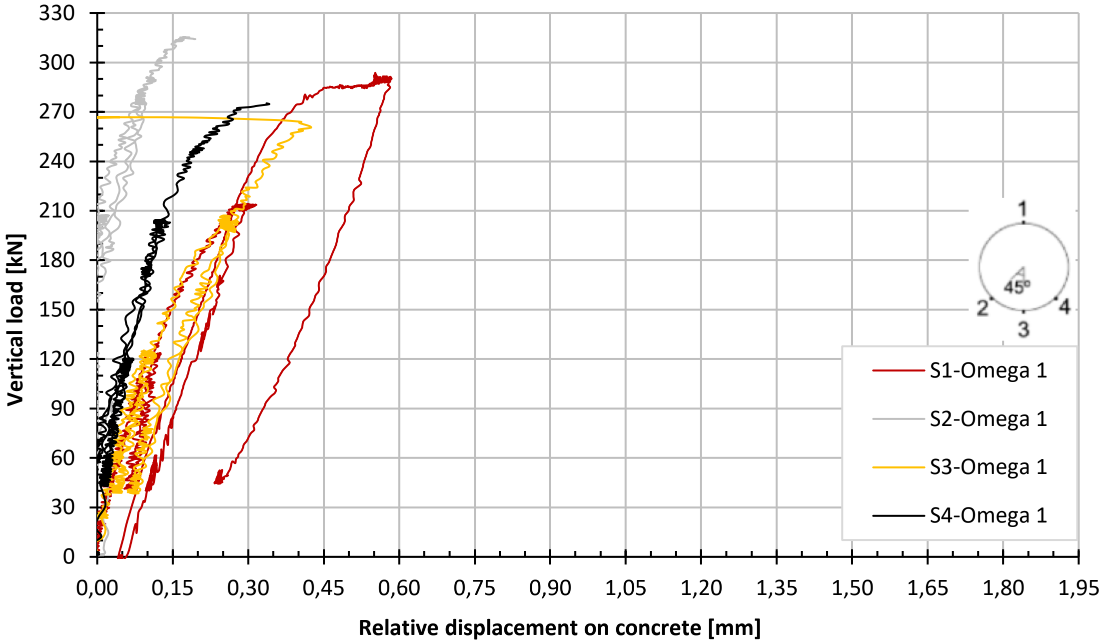

Figure 5.18: Load-relative displacement, for each experimental specimen, on the column top face in the connection joint.

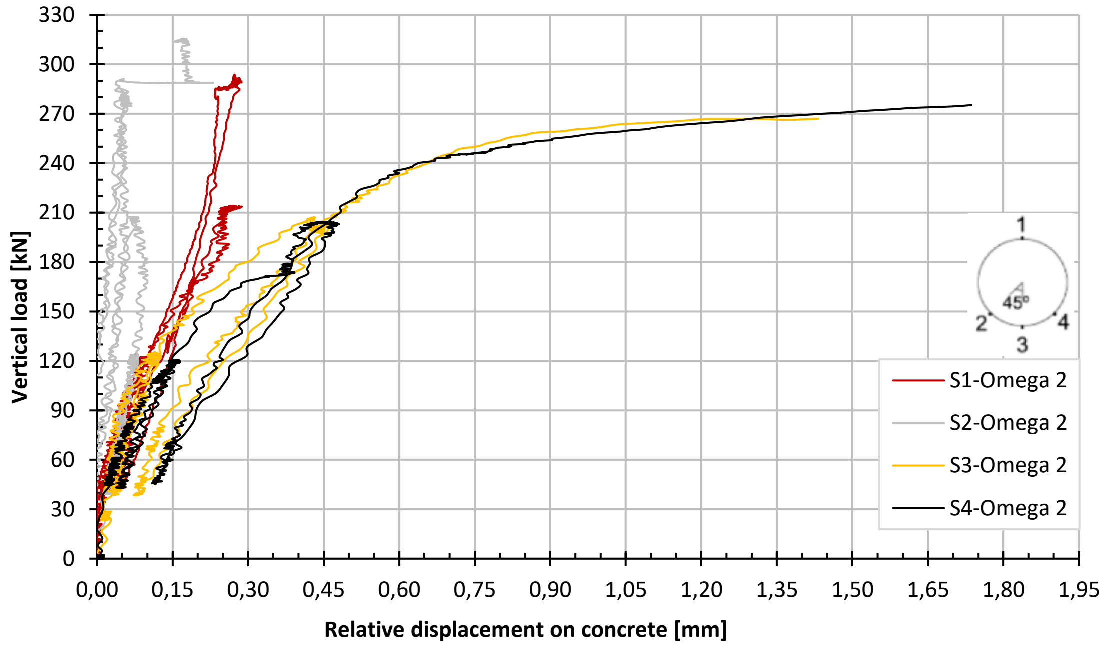

Figure 5.19: Load-relative displacement at 45 degrees, for each experimental specimen, from underside of column in the connection joint.

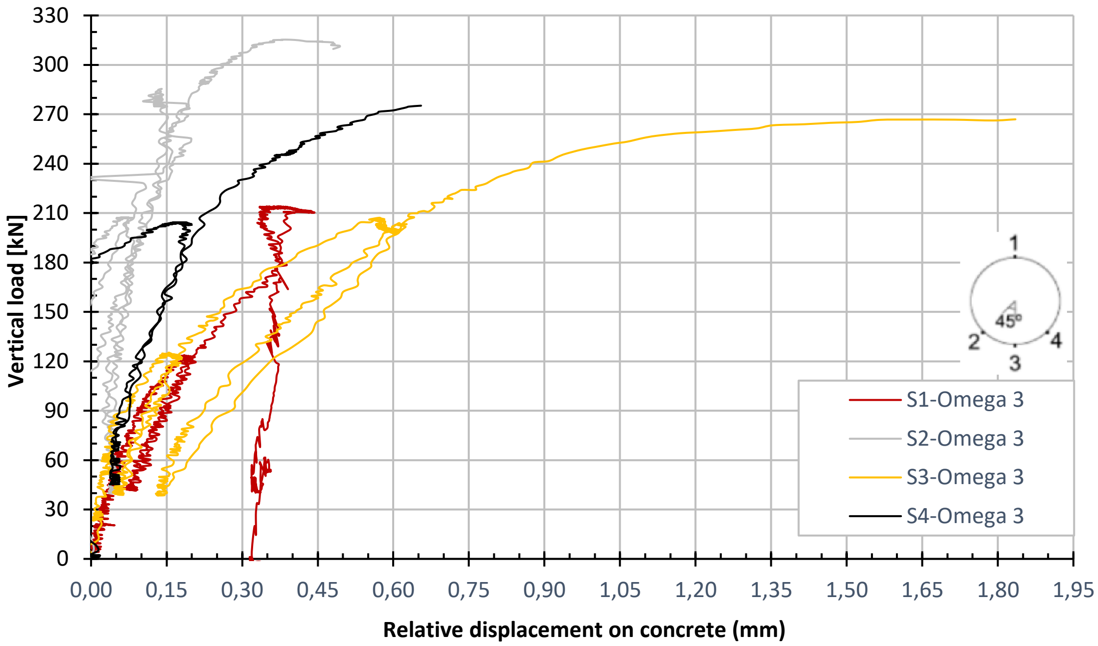

Figure 5.20: Load-relative displacement, for each experimental specimen, on the underside of column in connection joint.

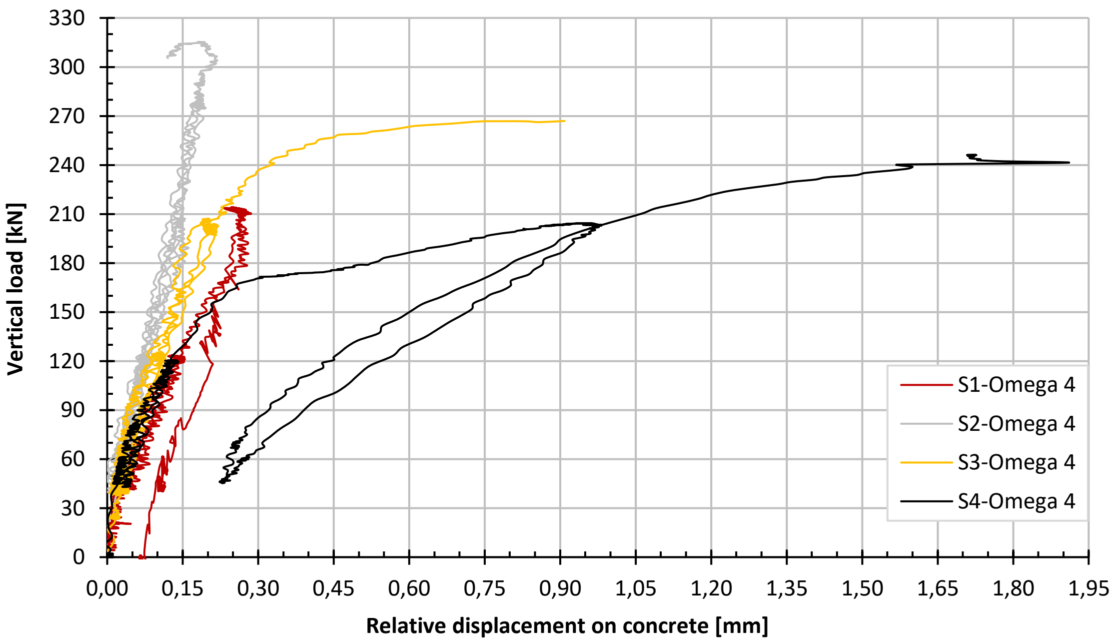

Figure 5.21: Load-relative displacement at 45 degrees, for each experimental specimen, from the underside at column face in the connection joint.

Comparing the specimens with a 50 mm joint (S1 and S4), the crack widths on concrete were higher in specimen S4. This is may be justified because model S4 has less reinforcement in the connection joint than specimen S1.

Comparing the specimens with a 3 mm joint (zero joint), the crack widths were significantly higher in specimen S3. This difference may be justified also by the difference of reinforcement that exists between the specimens with dry joint, since specimen S3 has less reinforcement in the connection than specimen S2.

To sum up, due to the lesser amount of reinforcement in specimen S3 in comparison with other specimens, the greatest crack widths occurred in experimental specimen S3 just as would be expected (See Table 5.8). On the lower surface of connection joint, the relative displacements measured was 0.97 mm at 93% of failure in specimen S3. In the remaining specimens the measured crack widths varied between 0.25 to 0.45 mm.

Table 5.8: Crack widths in the connection joint, for each experimental specimen.

Specimens	*"Omegas"*	*Relative displacements on concrete for:*		
		F=120 kN	*F=200 kN*	*93% of failure*
		[mm]	*[mm]*	*[mm]*
S1	1	0.10	0.29	0.55
	2	0.09	0.27	0.27
	3	0.19	0.34	0.40
	4	0.15	0.26	0.10
S2	1	0.00	0.02	0.11
	2*	0.07	0.07	0.17
	3*	-	0.06	0.25
	4	0.07	0.14	0.19
S3	1	0.11	0.25	0.37
	2	0.12	0.44	0.72
	3	0.18	0.59	0.97
	4	0.10	0.21	0.36
S4	1	0.07	0.13	0.24
	2	0.16	0.46	0.96
	3*	-	0.17	0.45
	4	0.14	0.94	1.72

(*) – relative displacement transducers damaged

5.5 Bending force diagrams

Figure 5.22 shows the bending and shear force diagrams caused by the applied vertical loading system.

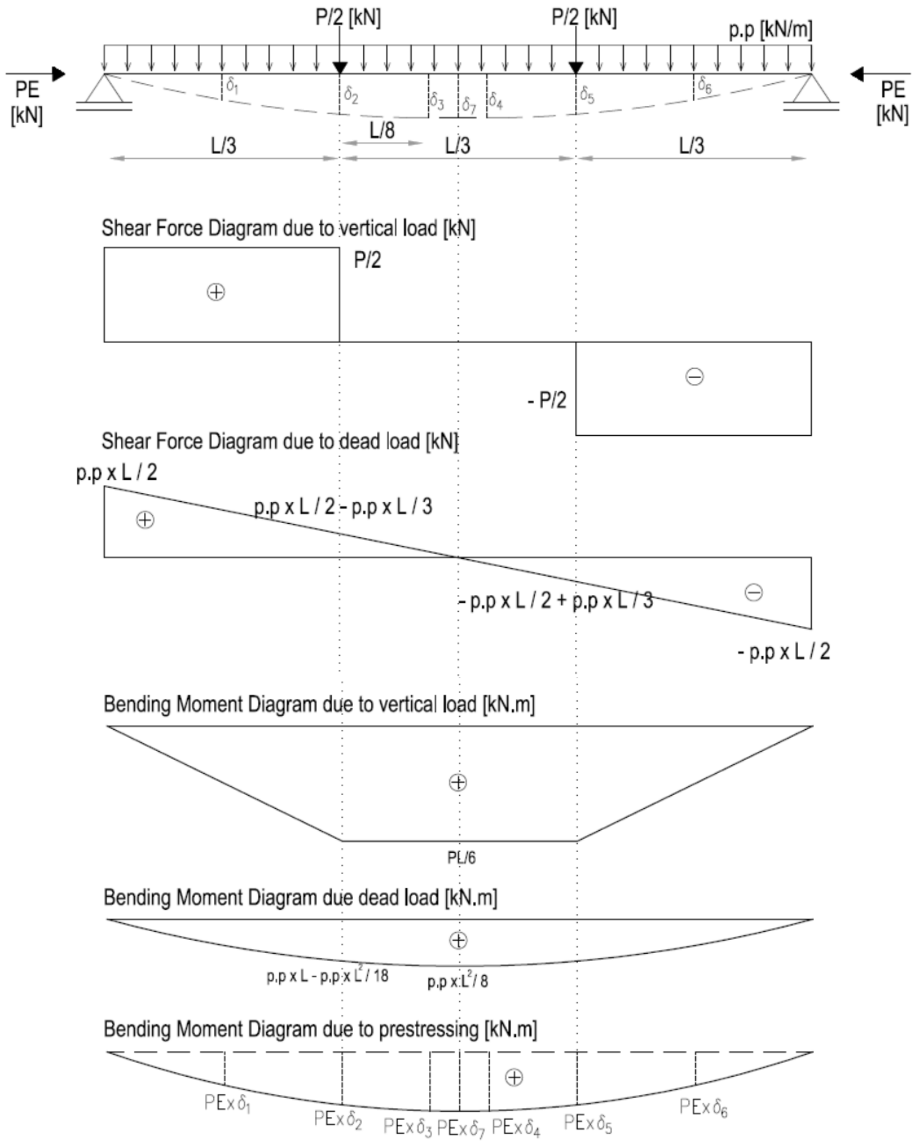

Figure 5.22: Shear force and bending moment diagrams of experimental specimens.

According to the scheme in Figure 5.22, the bending moment due to pre-stress was calculated through expression (5.2).

$$M_{PE} = \delta \times PE \tag{5.2}$$

Where: δ, is the eccentricity defined by distance between the pre-stressing strands axis and the column axis (vertical displacements, see section 5.2.1, Chapter 5) and PE is the axial load applied through pre-stressing.

Figures 5.23 and 5.24 show the bending moments due to pre-stress along the column span for stages with 93% of failure and at failure.

The final moment bending is obtained from the sum of bending moment caused by vertical load, by dead load and by pre-stressing (2nd order effects due column's deformation). The final values with 93% of failure and at failure are presented in graphs of Figures 5.25 and 5.26.

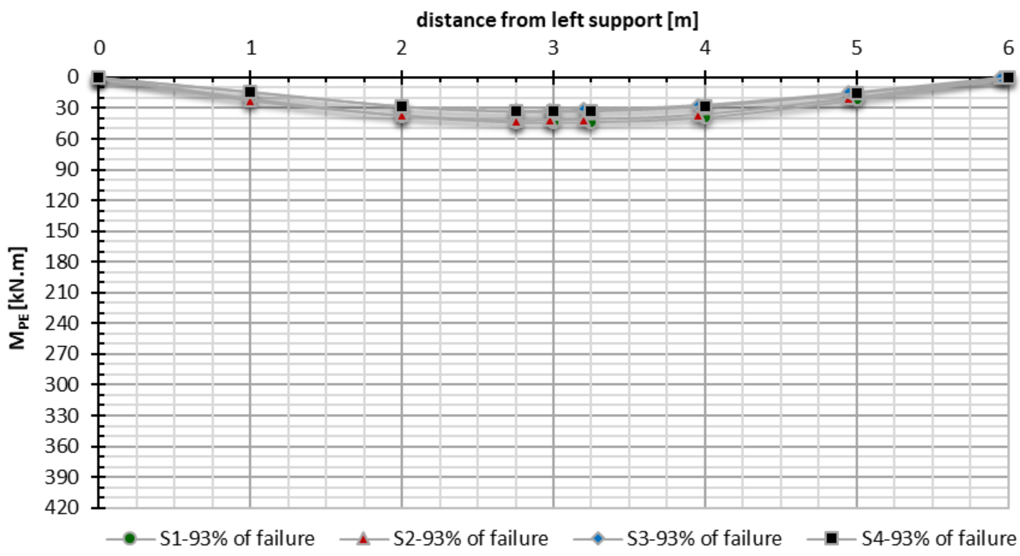

Figure 5.23: Diagrams of bending moment due to pre-stressing at 93% of failure.

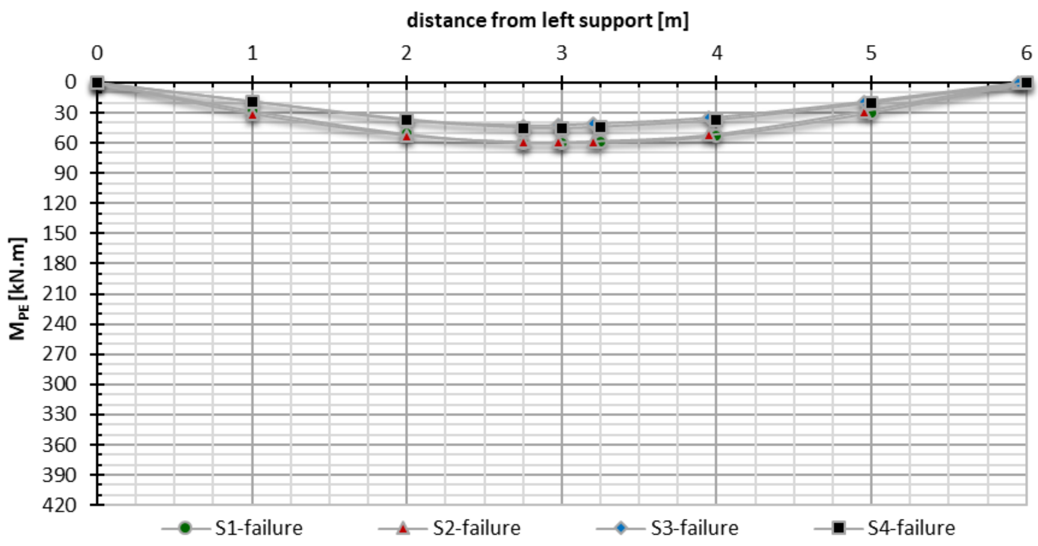

Figure 5.24: Diagrams of bending moment due to pre-stressing at failure.

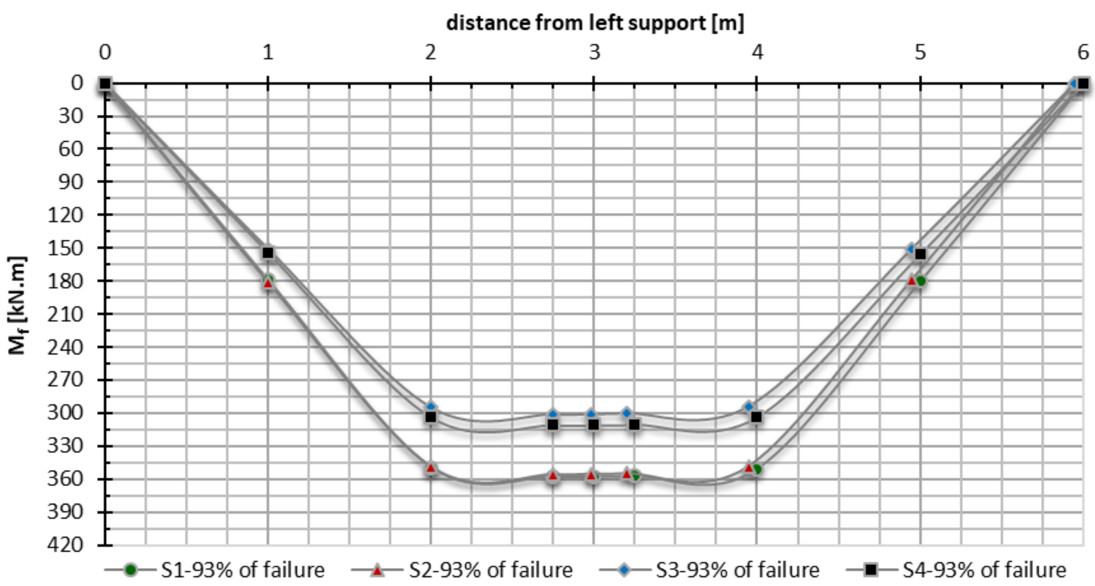

Figure 5.25: Diagrams of total bending moment at 93% of failure.

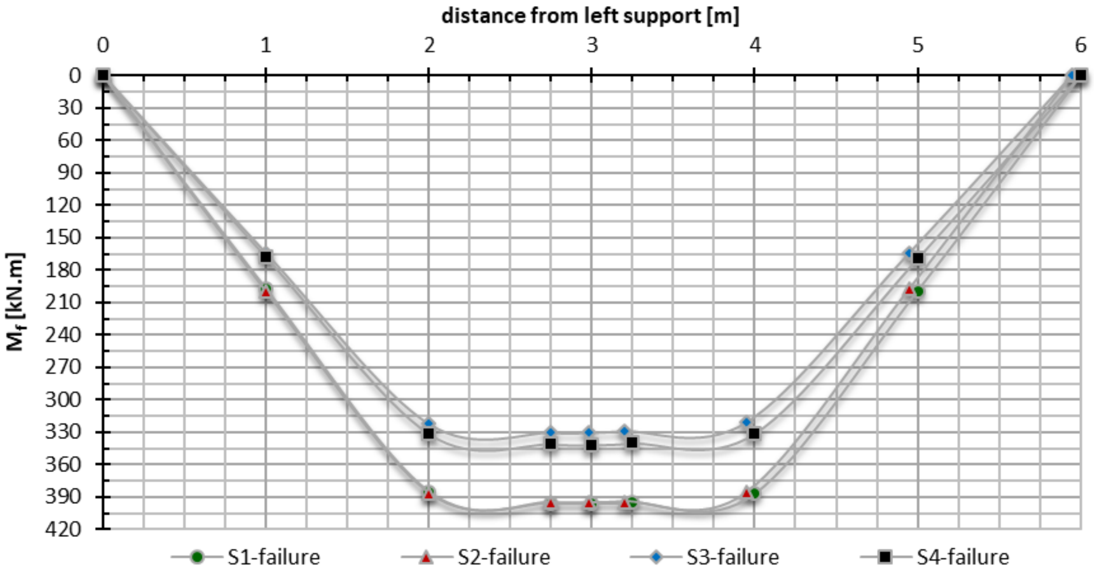

Figure 5.26: Diagrams of total bending moment at failure.

The cross section bending strength, M_{Rd}, was determined by the program "XD-CoSec". This program was created and developed by Civil Engineering Department of Aveiro University in Portugal [40]. Table 5.9 and 5.10 present the values of M_{Rd} for the circular cross section in the connection joint and below the load application zone (see Figures 5.27 to 5.34). It should be noted that during reinforcement assembly it is difficult to ensure that each bar is exactly as in the theoretical position. Table 5.11 presents the yielding shear force ($V_{Rd,s}$) and the maximum shear resistance ($V_{Rd,max}$), determined from the expressions (5.3) and (5.4) [30 and 41]. The maximum shear resistance obtained from the program "XD-CoSec" ($V_{Rd,XD}$) [40] are also presented in Table 5.11.

$$V_{Rd,s} = \frac{A_{sw}}{s} f_{ywd} \,.\, 0.9.\, d.\cot 30 \tag{5.3}$$

$$V_{Rd,max} = \frac{\alpha_{cw}\,.\, v.\, b_w\,.\, 0.9.\, d}{\cot\theta + \tan\theta} \tag{5.4}$$

Where,

$\frac{A_{sw}}{s}$, is the cross-sectional area of links;

f_{ywd}, is the theoretical steel yield strength.

d, is the effective depth

α_{cw}, is a coefficient that considers the state of the stress in the compression chord. The recommended values are as follow:

- α_{cw} = 1, for non-pre-stressed structures;
- $\alpha_{cw} = (1 + \sigma_{cp}/f_{cd})$, for $0 < \sigma_{cp} \leq 0.25 f_{cd}$
- α_{cw} = 1.25, for $0.25 f_{cd} < \sigma_{cp} \leq 0.5 f_{cd}$
- $\alpha_{cw} = 2.5(1 - \sigma_{cp}/f_{cd})$, for $0.5 f_{cd} < \sigma_{cp} \leq 1.0 f_{cd}$

v, is a strength reduction factor for concrete cracked in shear. The recommended value is as follows:

- $v = 0.6\left[1 - \frac{f_{ck}}{250}\right]$, f_{ck} in MPa

b_w, is the minimum width between tension and compression chords

f_{cd}, is the design value of the concrete compression force in the direction of the longitudinal member axis.

θ, is the angle between the concrete compression strut and the beam axis perpendicular to the shear force

σ_{cp}, is the mean compressive stress, measured positive, in the concrete due to the design axial force.

Table 5.9: M_{Rd} in the connection zone section of each experimental specimen, determined by XD-CoSec

Specimen	*Connection zone*	*M_{Final} (kN.m)*	*M_{Rd} (kN.m)*	*Error (%)*
S1	Column B – **failure's location**	395.90	372.36	-6.32
S2	Column B	395.20	373.96	----
S3	Column B – **failure's location**	330.18	272.76	-21.05
S4	Column B – **failure's location**	341.66	302.92	-12.79

Table 5.10: M_{Rd} of the cross section in below the load application zone of each experimental specimen, determined by XD-CoSec

Specimen	*Below the load application zone*	*M_{Final} (kN.m)*	*M_{Rd} (kN.m)*	*Error (%)*
S1	Column A	386.97	306.00	---
S2	Column A – **failure's location**	385.93	308.66	-25.03
S3	Column A	320.50	296.55	---
S4	Column A	330.95	307.02	---

Table 5.11: $V_{Rd,s}$ and $V_{Rd,max}$, for specimens S1, S2, S3, and S4.

Specimen	*Support zone*	*V_{Final} (kN)*	*$V_{Rd,S}$ (kN)*	*$V_{Rd, max}$ (kN)*	*$V_{Rd, XD}$ (kN)*
S1	X=0	171.3	618	1432	794
S2	X=0	171.40	618	1328	789
S3	X=0	147.22	618	1085	683
S4	X=0	151.48	618	1339	789

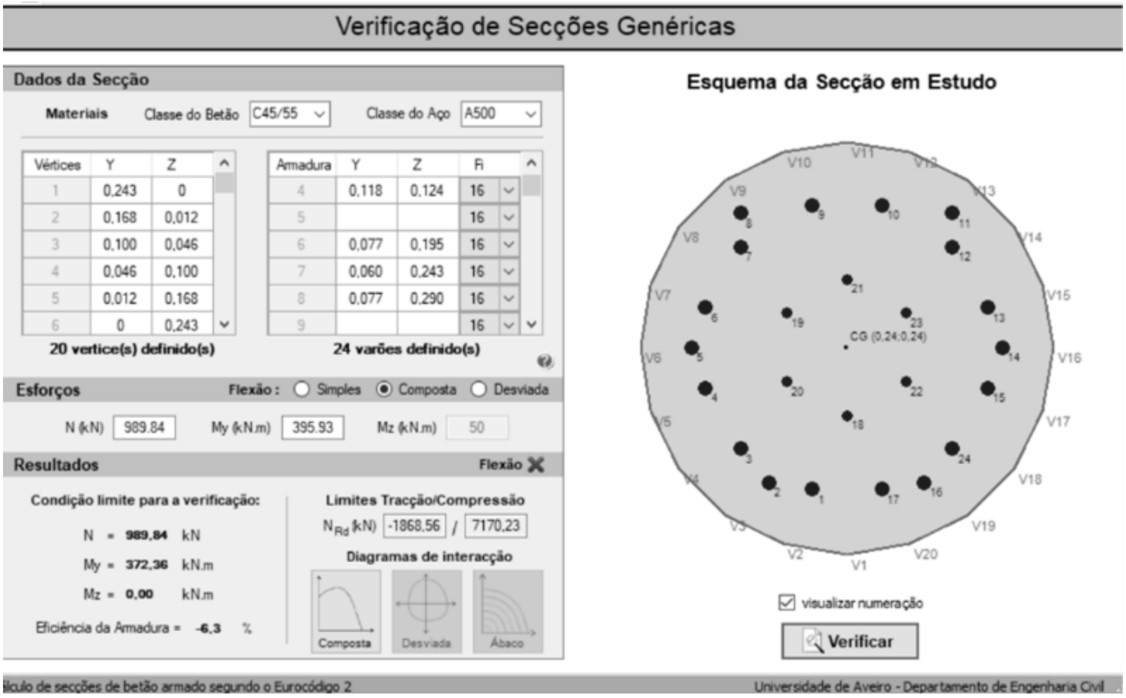

Figure 5.27: Specimen S1 – M_{Rd} and $V_{Rd,\,XD}$ in connection zone of column B, obtained by program XD-CoSec (in Portuguese).

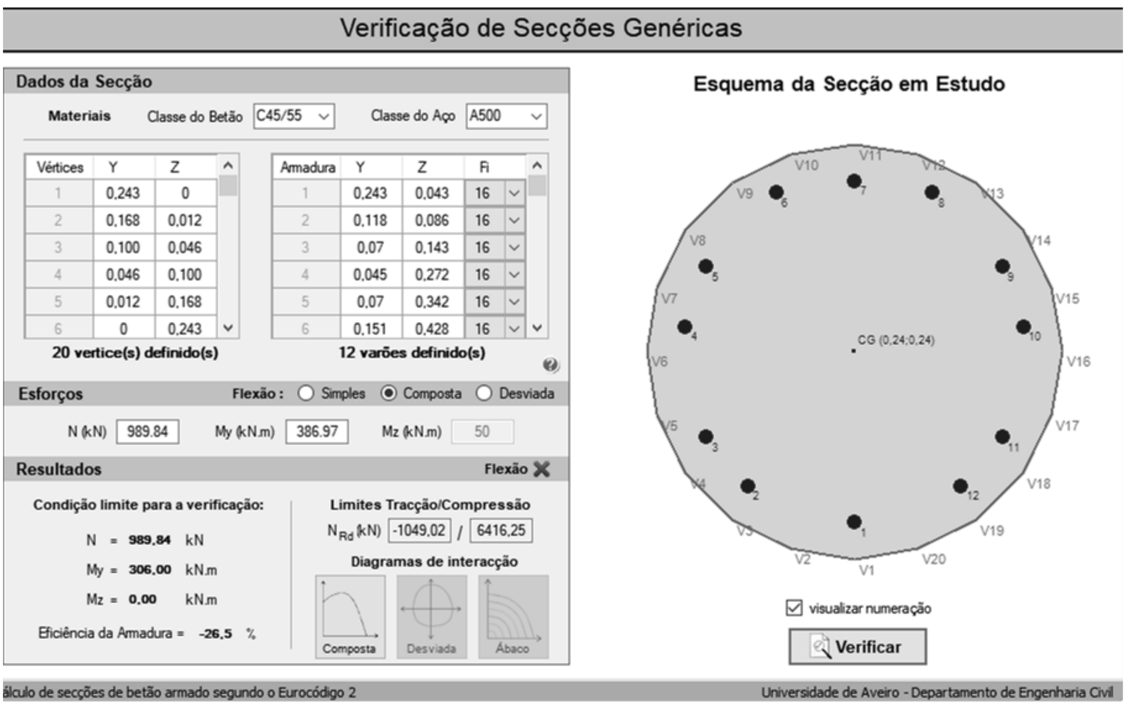

Figure 5.28: Specimen S1 – M_{Rd} and $V_{Rd,\,XD}$ in below the load application zone of column A, obtained by program XD-CoSec (in Portuguese).

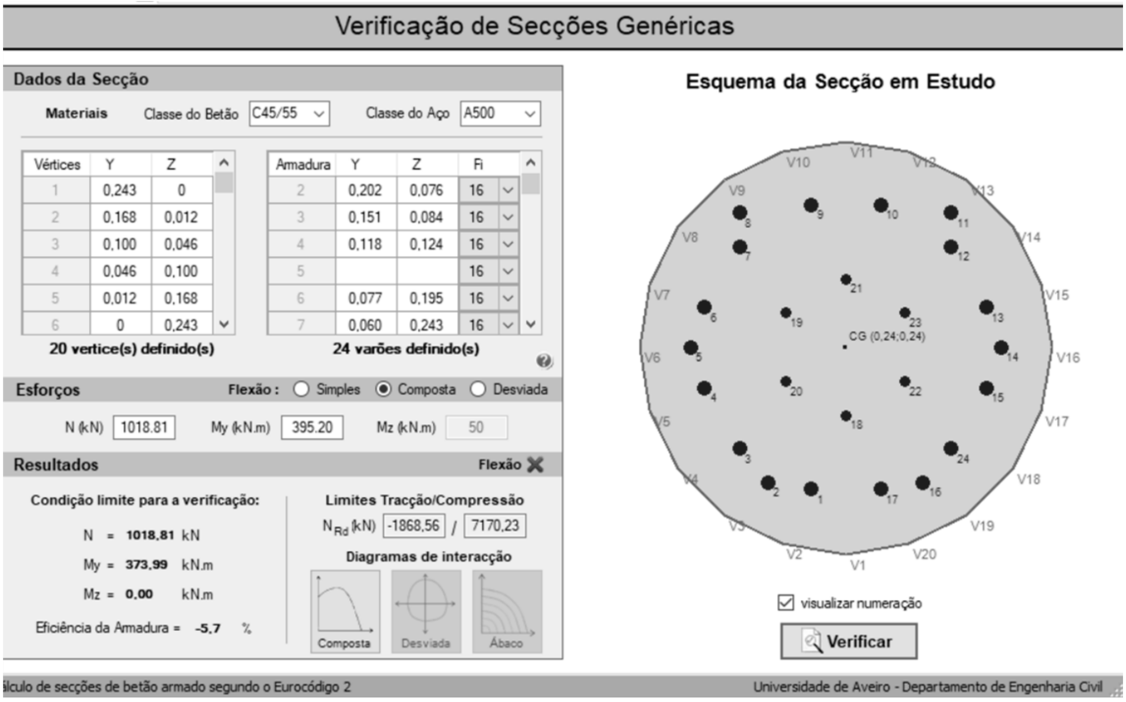

Figure 5.29: Specimen S2 – M_{Rd} and $V_{Rd,\,XD}$ in connection zone of column B, obtained by program XD-CoSec (in Portuguese).

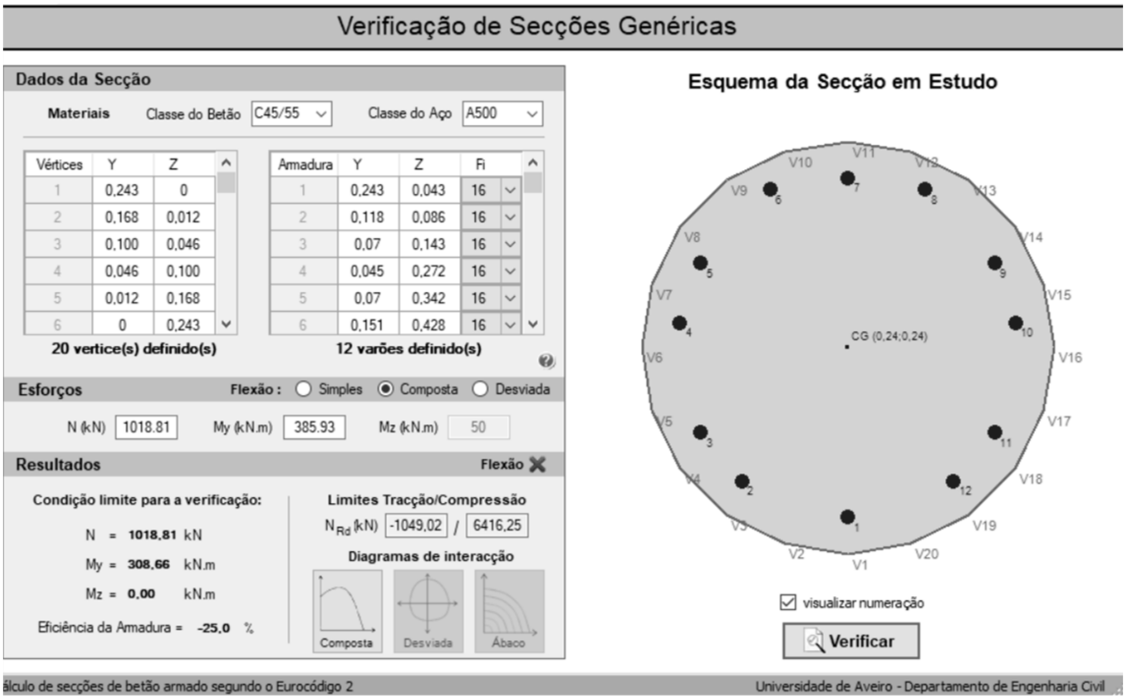

Figure 5.30: Specimen S2 – M_{Rd} and $V_{Rd,\,XD}$ in below the load application zone of column A, obtained by program XD-CoSec (in Portuguese).

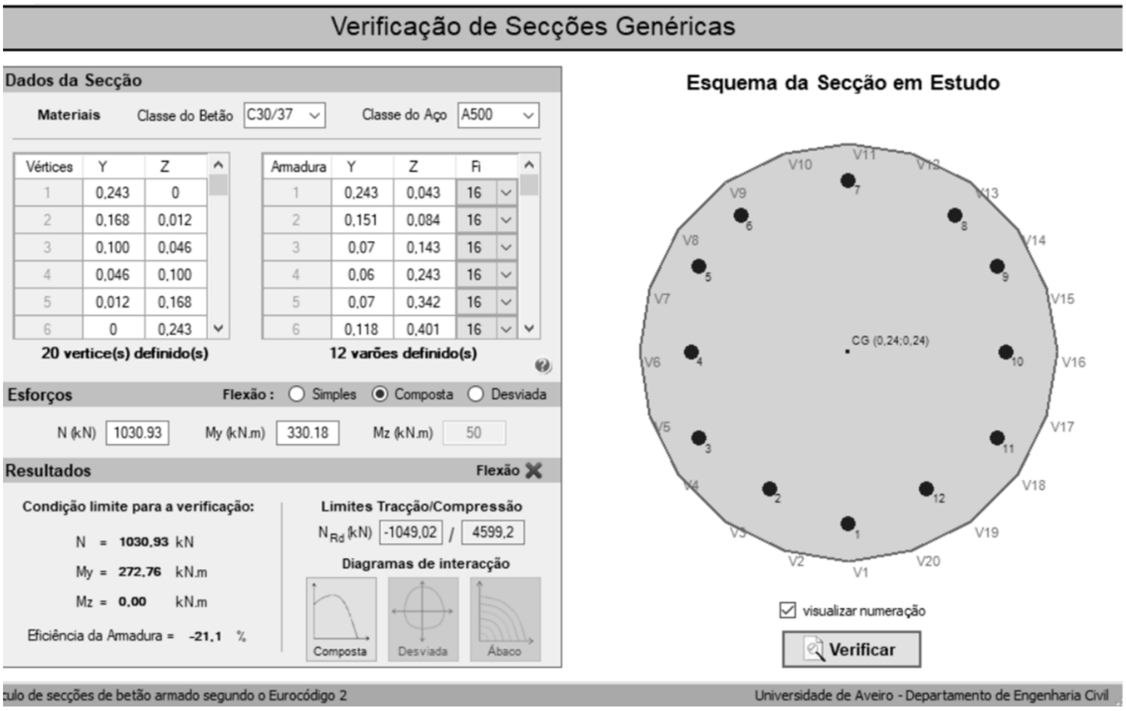

Figure 5.31: Specimen S3 – M_{Rd} and $V_{Rd,\,XD}$ in connection zone of column B, obtained by program XD-CoSec (in Portuguese).

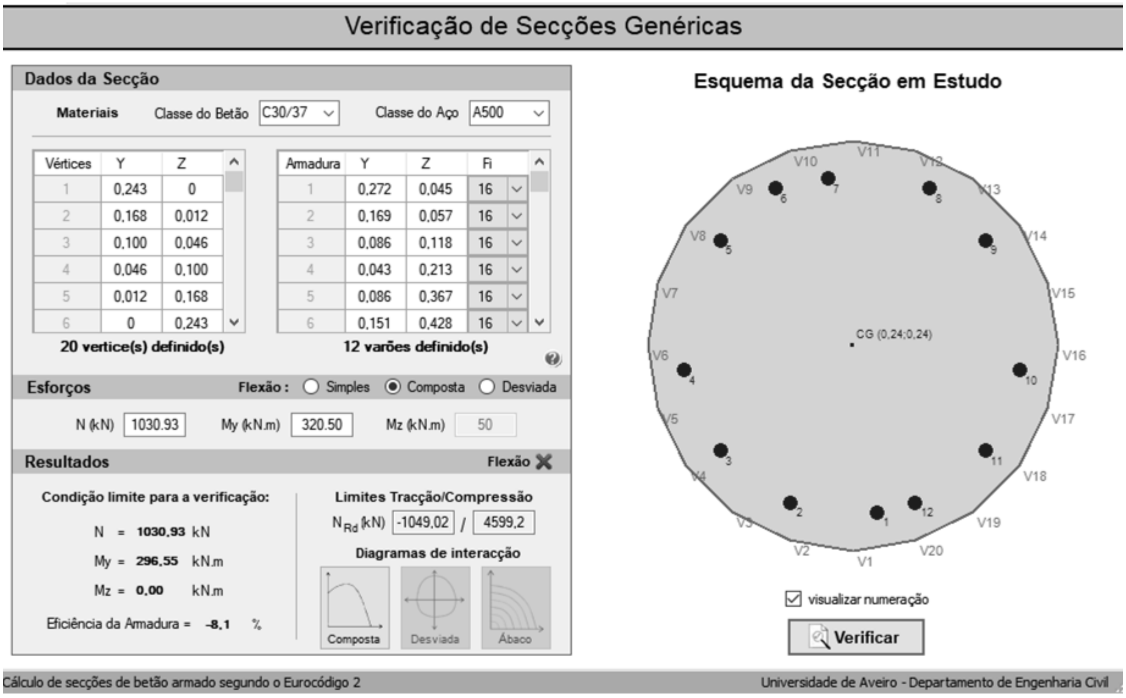

Figure 5.32: Specimen S3 – M_{Rd} and $V_{Rd,\,XD}$ in below the load application zone of column A, obtained by program XD-CoSec (in Portuguese).

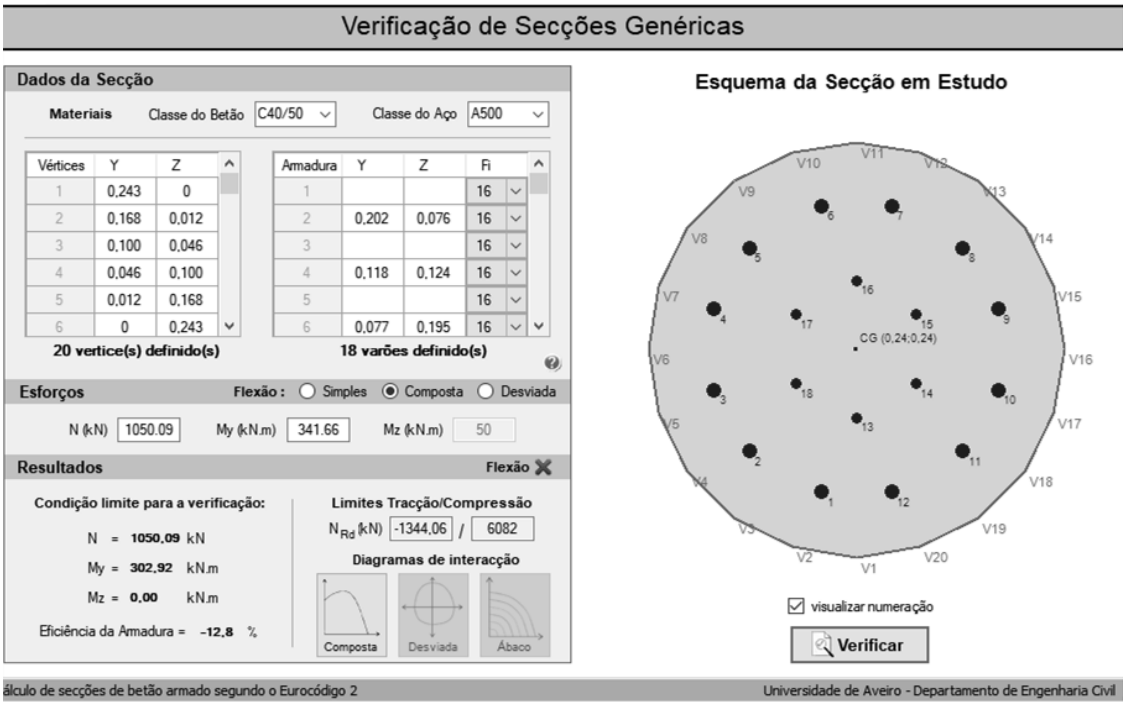

Figure 5.33: Specimen S4 – M_{Rd} and $V_{Rd,\,XD}$ in connection zone of column B, obtained by program XD-CoSec (in Portuguese).

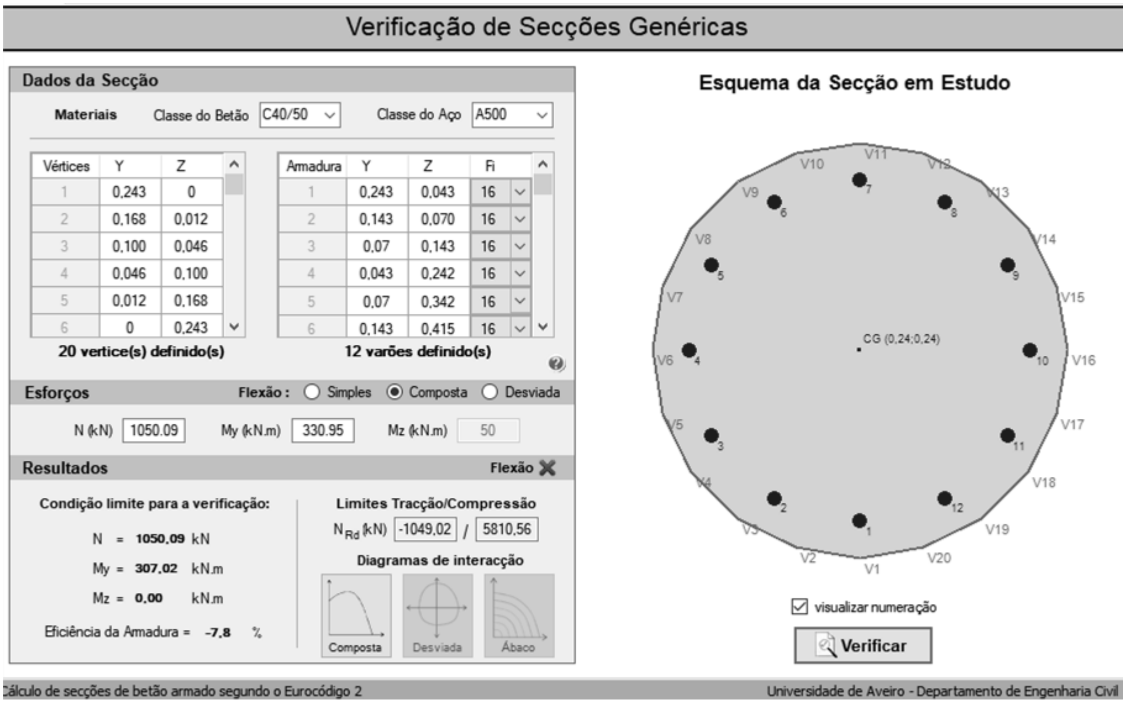

Figure 5.34: Specimen S4 – M_{Rd} and $V_{Rd,\,XD}$ in below the load application zone of column A, obtained by program XD-CoSec (in Portuguese).

The higher quantity of reinforcement in the S1 and S2 connection joints resulted in these two specimens being stronger in comparison to specimens S3 and S4 (see Figure 5.26). Also based on Figure 5.25 and 5.26, it may be concluded that S1 and S2 have the same strength, so the reduction of connection joint thickness in specimen S2 did not have any influence on the strength of the specimen.

The S3 and S4 have nearly the same resistance, which leads to the conclusion that with six 50 mm thick Trejor connection elements, the behaviour is similar to a connection with 12 steel protruding bars with a dry joint. On the other hand, the anchor bolts (connection type of specimen S4), make it possible to optimize time and resources in the assembly of precast concrete lattice tower making it more competitive.

Comparing the values of Tables 5.9 and 5.10, it can be conclude that specimen S2, below the vertical load application zone, has a similar bending resistance to specimens S3 and S4 in the connection zone.
It also important to conclude that (based on Tables 5.9 and 5.10) the bending strength (M_{Rd}) obtained from XD-CoSec is always lower than the final bending moment measured in each experimental specimen. So, the values obtained by program XD-CoSec are on the safe side, since if the bending moment of the XD-CoSec was applied to the experimental specimens, the failure stage would not be reached.

5.6 Failure modes

5.6.1 Specimen S1

The failure mode of specimen S1 happenned after a vertical load value of 315.73 kN and a bending moment of 395.90 kNm at the mid-span was attained.

Considering the difference in the reinforcement in column A and B (60.3 cm^2 and 48.24 cm^2 respectively) in the maximum bending moment zone, it would be expected that failure had occurred in column B, in the connection zone, or in column A, below of vertical load application zone, since in this zone there is a sharp transition of reinforcement in approximately 60% (see Figure 5.30). However, specimen S1 is one of the stronger specimens (see Table 5.11), the failure in connection joint was not avoided. The 50 mm joint with 50 mm did not make it possible to use shear reinforcement at least in 0.20 m at mid-span. This was one of the reasons that might have led to the failure of specimen S1, because the lack of links at mid-span allowed the buckling of the connection longitudinal bars (male Trejor elements) caused by compressive forces on the upper surface.

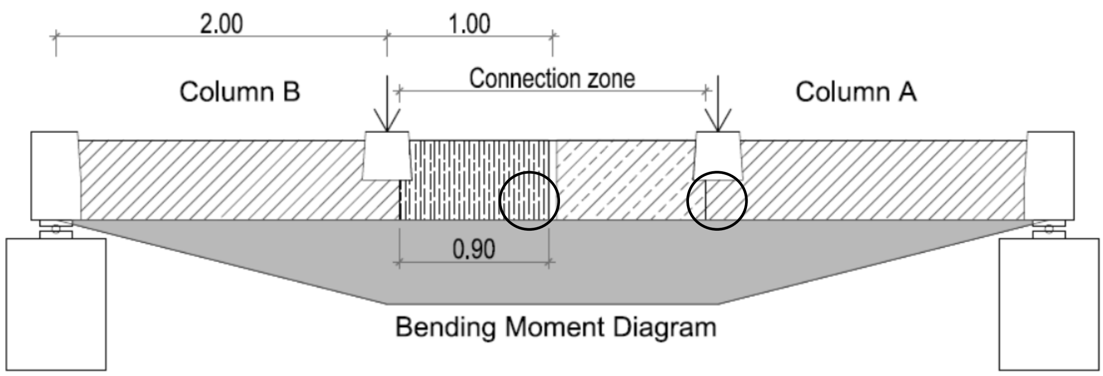

Legend:

Circular section with 12 longitudinal bars (Ø16);

Circular section with 18 ordinary bars (Ø16) and 12 Trejor bars (Ø16);

Circular section with 12 ordinary bars (Ø16), 12 Trejor bars (Ø16);

Expected failure zones;

Figure 5.35: Analysis of the behaviour of specimen S1.

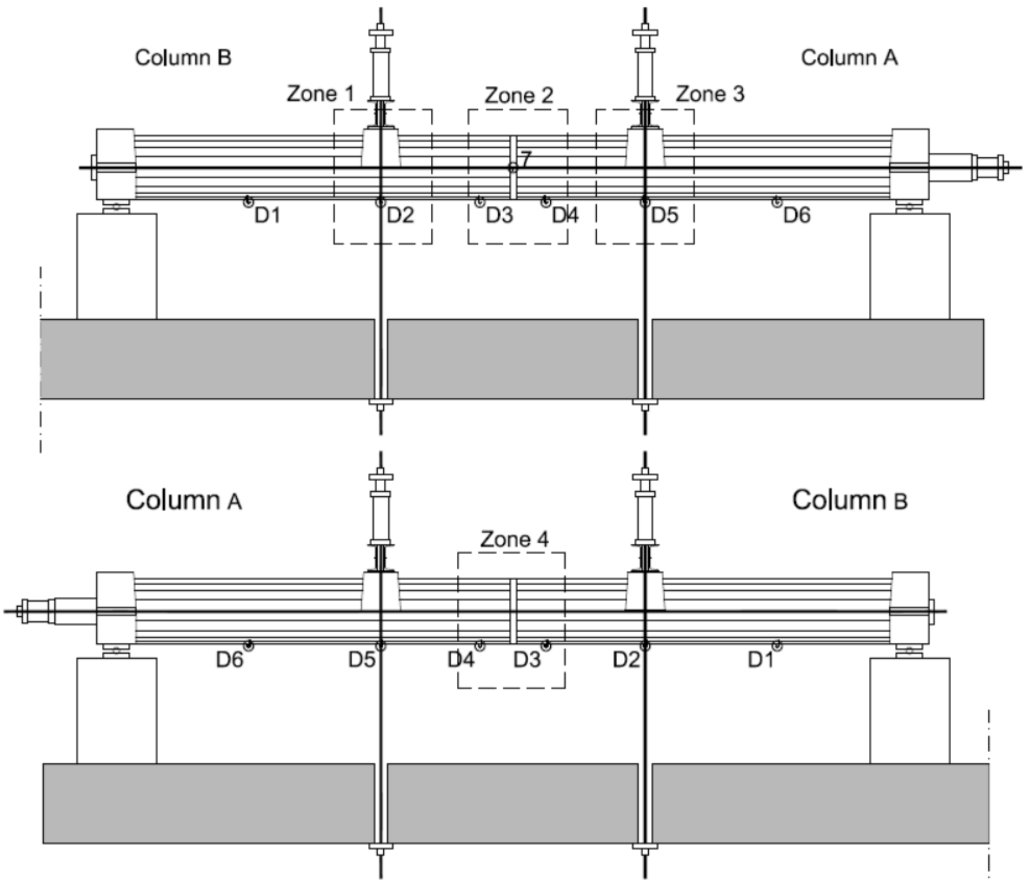

Figure 5.36: Identification of photographed zones of specimen S1 failure.

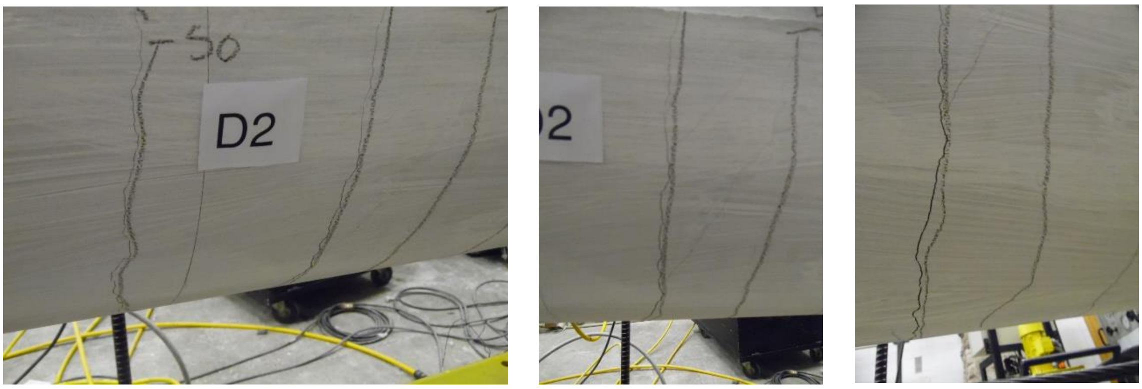

Figure 5.37: Overview of specimen S1 failure, in column B, below of vertical load application zone. (Zone 1)

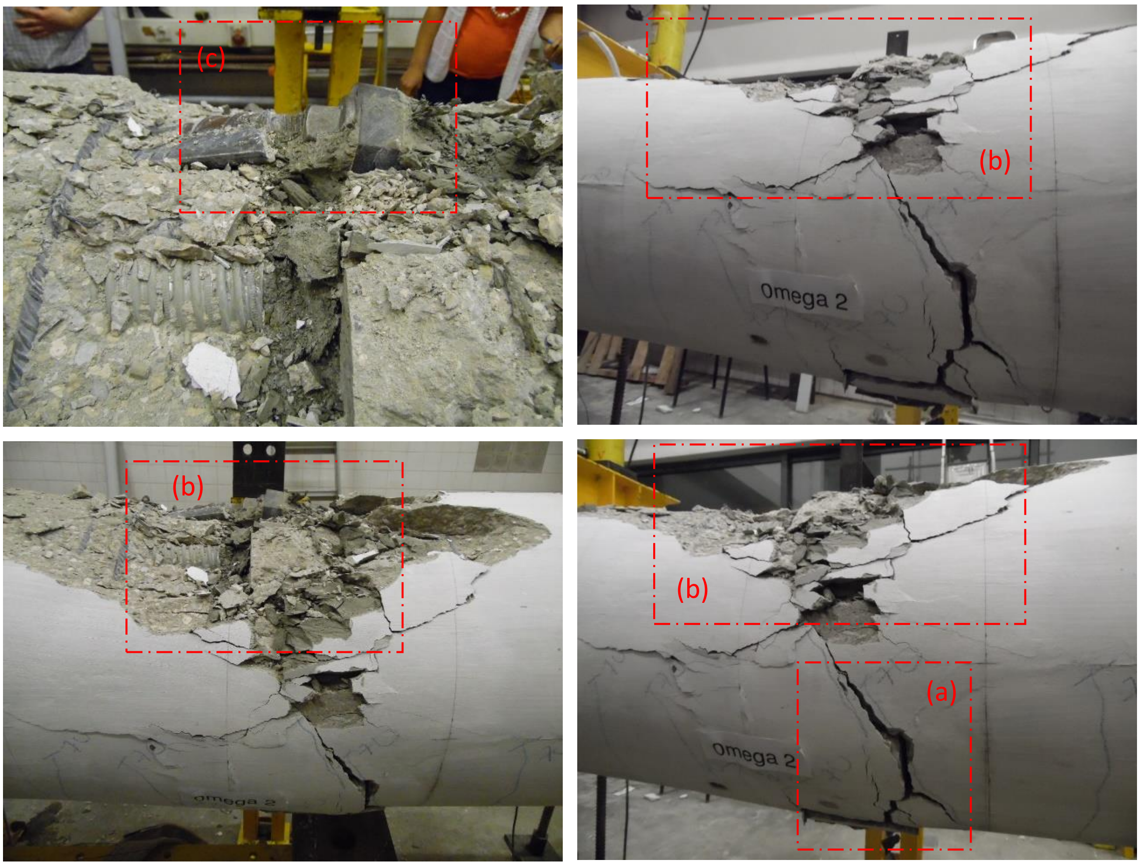

Legend: (a) detachment of concrete caused by deformation/rotation of Trejor female connection; **(b)** detachment followed by concrete crushing caused by buckling of Trejor male connection due to compressive forces on upper face; **(c)** buckling of Trejor male connection.

Figure 5.38: Overview of specimen S1 failure in connection joint. (Zone 4)

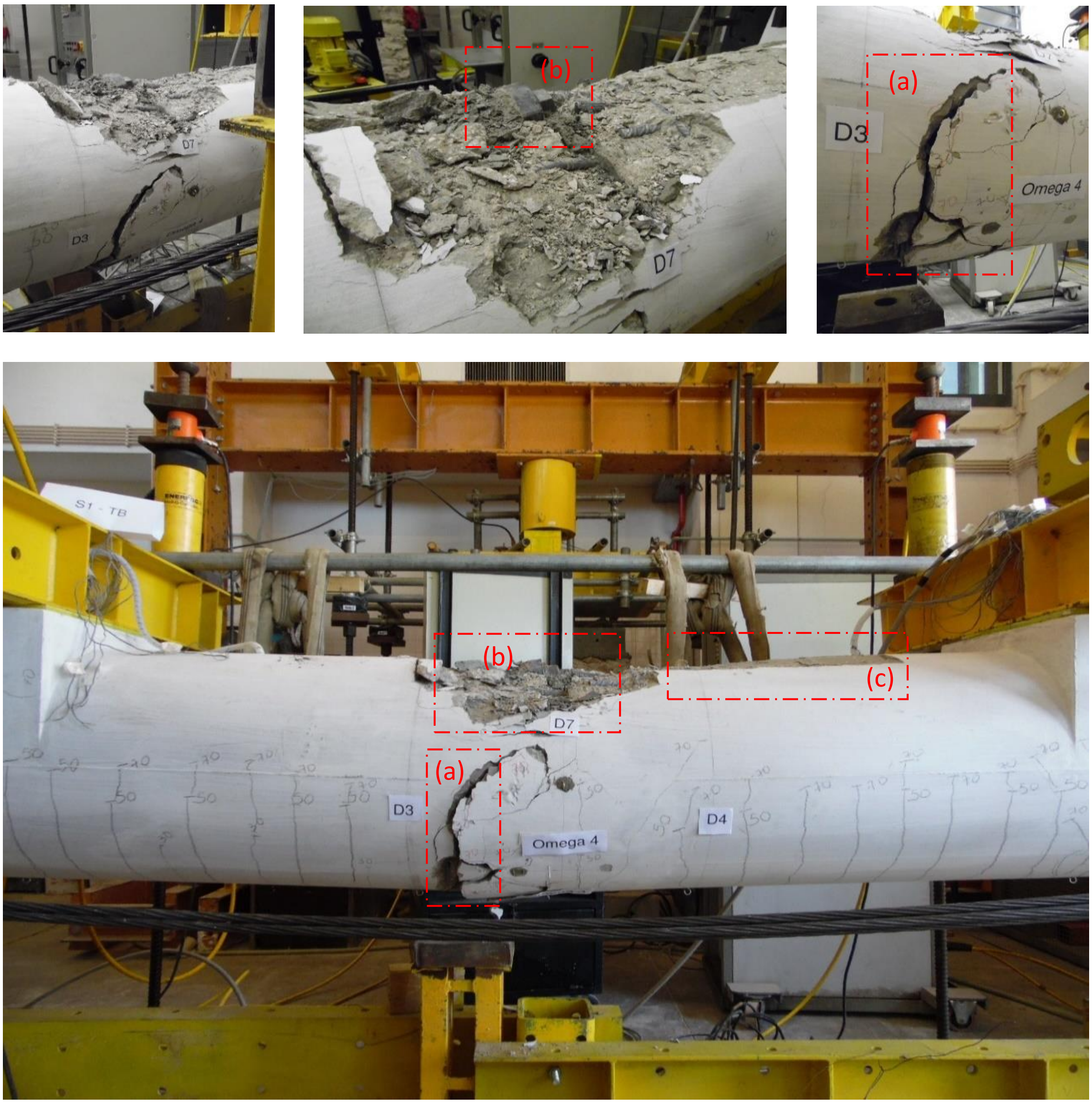

Legend: (a) detachment of concrete caused by deformation/rotation of Trejor female connection; **(b)/(c)** detachment followed by concrete crushing caused by buckling of Trejor male connection due to compression on upper face;

Figure 5.39: Overview of specimen S1 failure in the connection joint. (Zone 2)

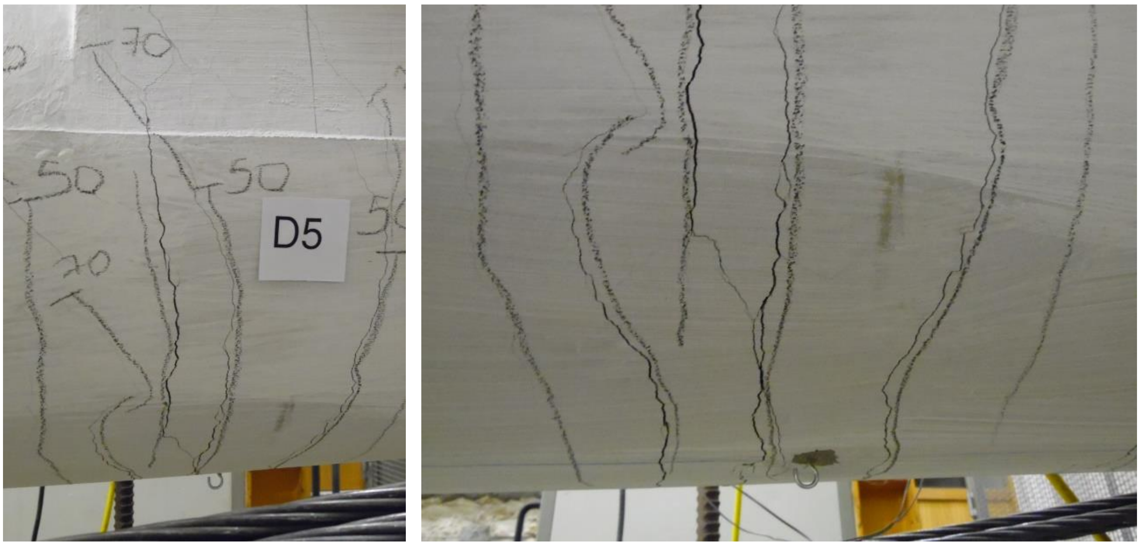

Figure 5.40: Overview of failure specimen S1, in column A, below of vertical load application zone. (Zone 3)

5.6.2 Specimen S2

The failure of the experimental specimen S2 happened after a total vertical load of 315.31 kN and a final bending moment of 395.20 kNm at mid-span was reached.

Specimen S2 has the same amount of reinforcement as specimen S1, therefore it would also be expected that specimen S1 failure had occurred in the connection zone of column B, or in column A, below the vertical load application zone (see Figure 5.36). Specimen S2 was as strong as specimen S1 (see Table 5.9 and 5.10). However, in specimen S2 the failure in the connection zone was avoided although it occurred in column A, below the vertical load application zone, and it can be analysed in detail in the figures below.

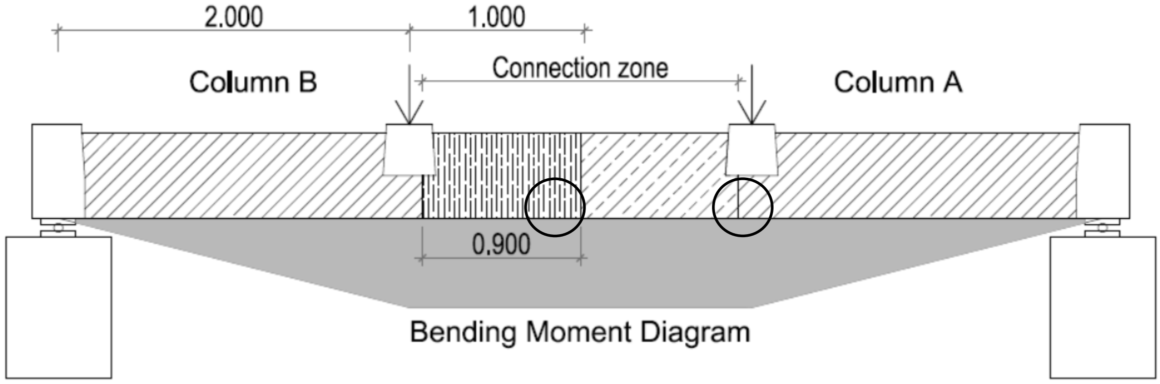

Legend:

Circular section with 12 longitudinal bars (Ø16);

Circular section with 18 ordinary bars (Ø16) and 12 Trejor bars (Ø16);

Circular section with 12 ordinary bars (Ø16), 12 Trejor bars (Ø16);

Expected failure zones;

Figure 5.41: Previous analysis to behaviour of specimen S2 along experimental test.

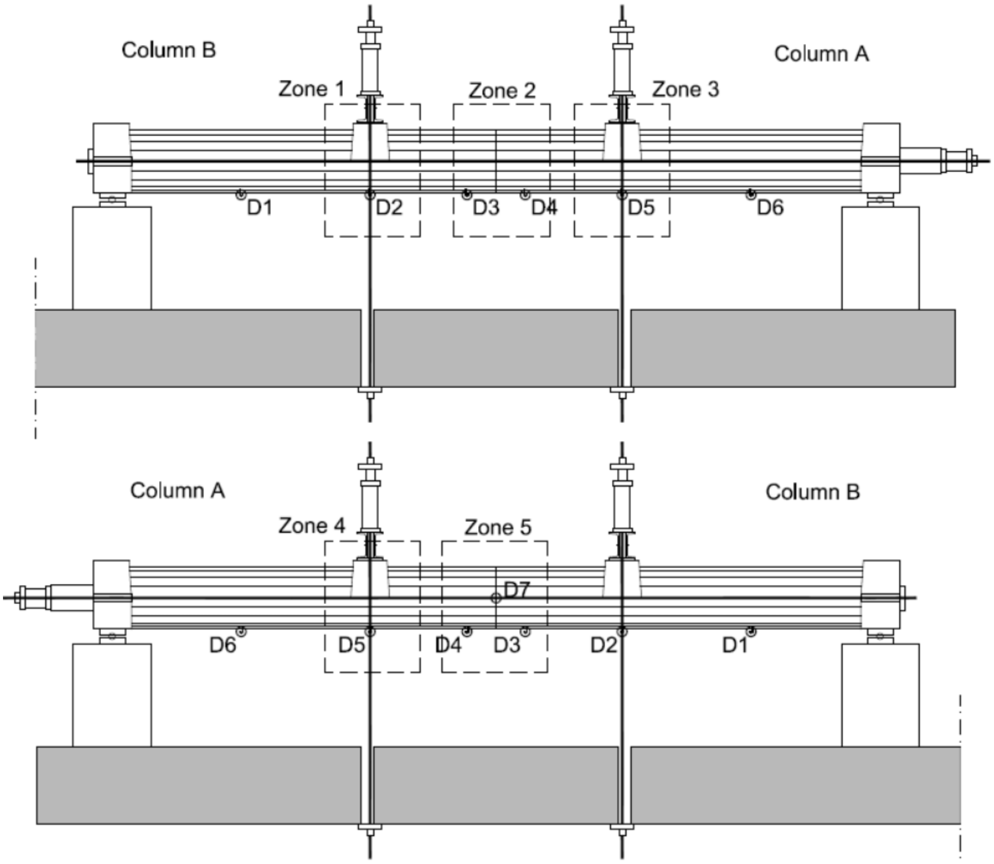

Figure 5.42: Identification of photographed zones of specimen S2 failure.

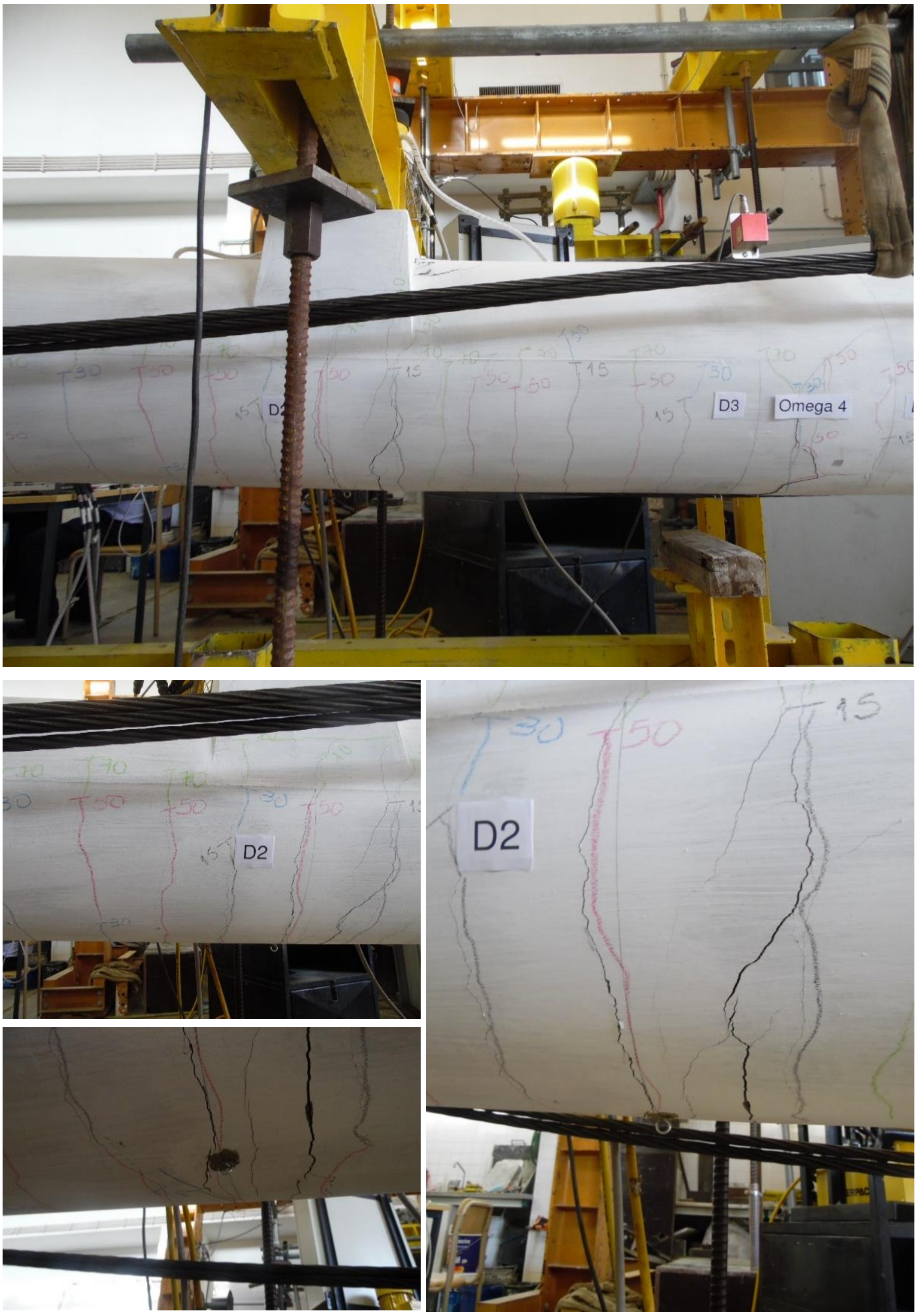

Figure 5.43: Overview of specimen S2 failure in column B, below the vertical load application zone. (Zone 1)

Figure 5.44: Overview of specimen S2 failure, in the connection joint. (Zone 2)

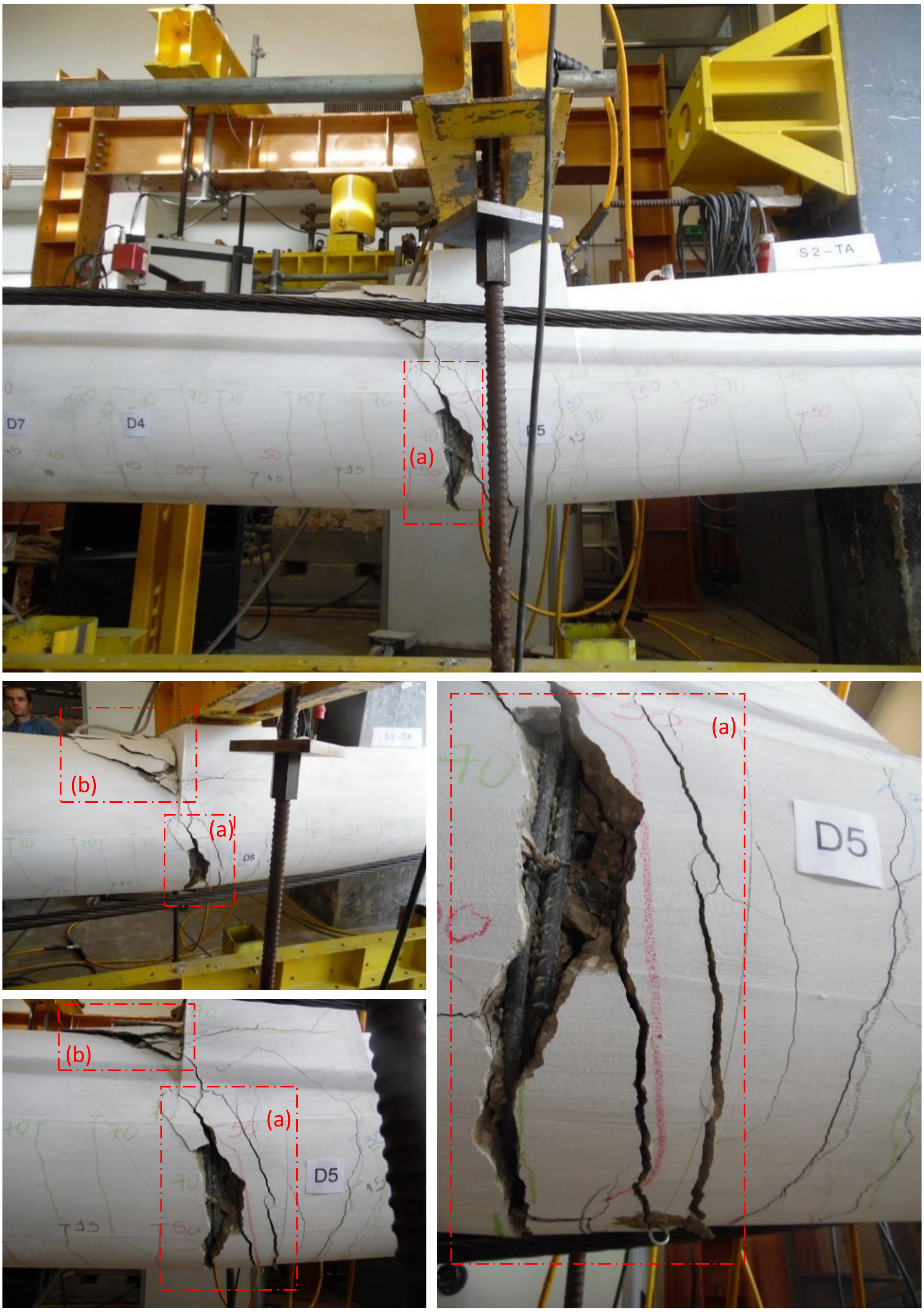

Legend: (a) Detachment of concrete caused by deformation of the longitudinal reinforcement; **(b)** concrete crushing caused by compression forces on upper face of column.

Figure 5.45: Overview of specimen S2 failure, in column A, below the vertical load application zone (Zone 3)

Legend: (a) Bending cracks; **(b)** concrete crushing caused by compression forces.

Figure 5.46: Overview of specimen S2 failure, in column A, below the vertical load application zone (Zone 4)

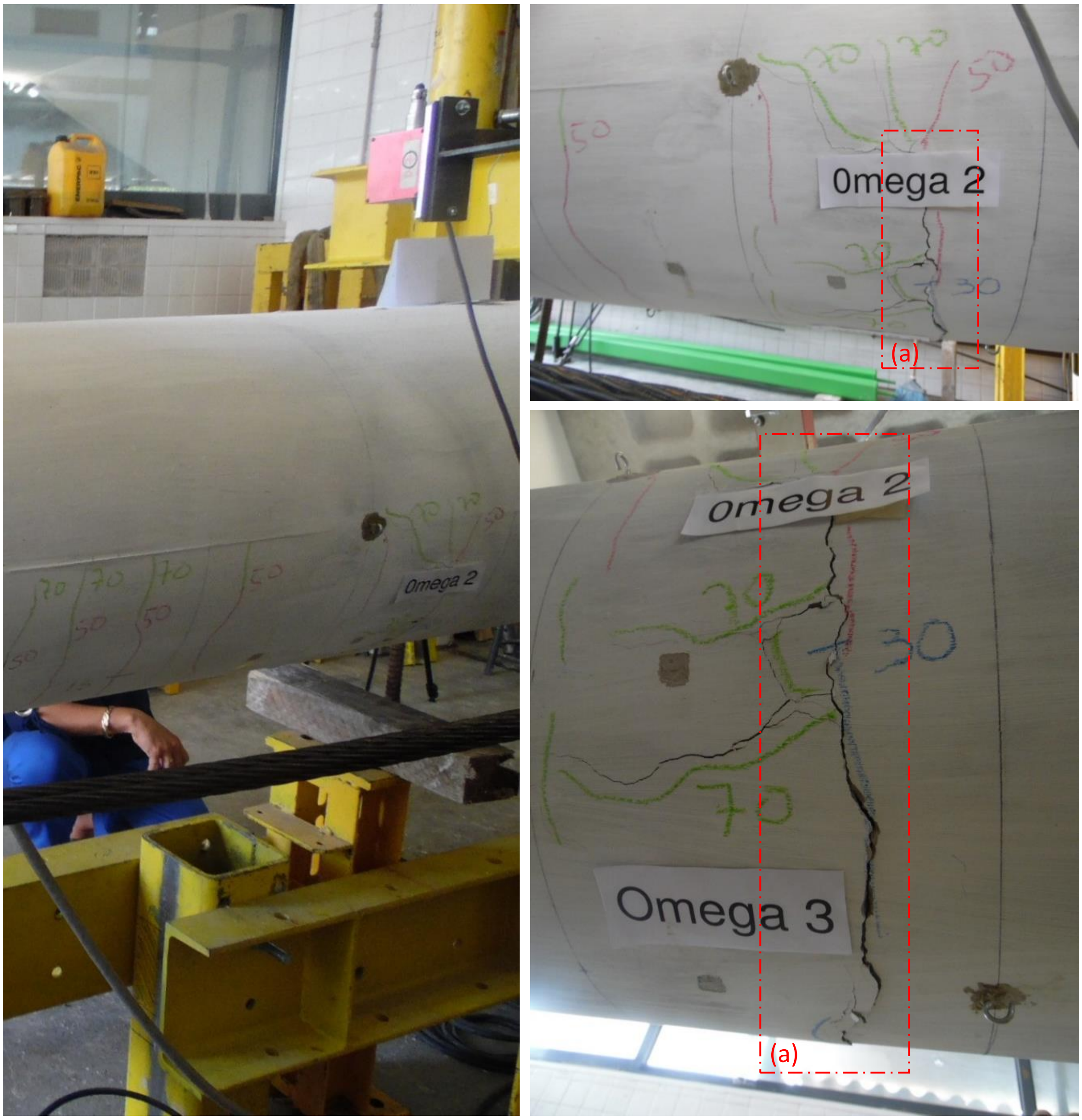

Legend: (a) Bending cracks.

Figure 5.47: Overview of specimen S2 failure, in the connection joint zone (Zone 5)

5.6.3 Specimen S3

Specimen S3 failure occurred after a vertical load of 266.94 kN and a final bending moment of 330.18 kNm at mid-span was reached.

With the type of connection adopted in specimen S3, it was possible to ensure the same amount of longitudinal reinforcement (A_s = 24.12 cm^2) throughout the column B length. However, the same did not happen in column A because column A was designed with 24 longitudinal bars in the area of maximum bending moment (A_s = 48.24 cm^2), twice the reinforcement of column B (see Figure 5.43).

Therefore, with less reinforcement in the connection zone of column B and with the sharp transition of reinforcement in column A below the vertical load application zone, it was expected that failure of specimen S3 had occurred in one of these zones.

During the experimental test, the failure occurred in the connection joint in the underside of column B. As seen in Figure 5.47, the absence of resin on the upper face of the connection joint, decreased the compression cross-section height leading to decrease of moment resistance (M_{Rd}). Moreover, the reduction of the compression area height also increased the deflection of the column in the mid-span and consequently the bending moment due to pre-stress application. Specimen S3 failure can be analysed in detail in the figures below.

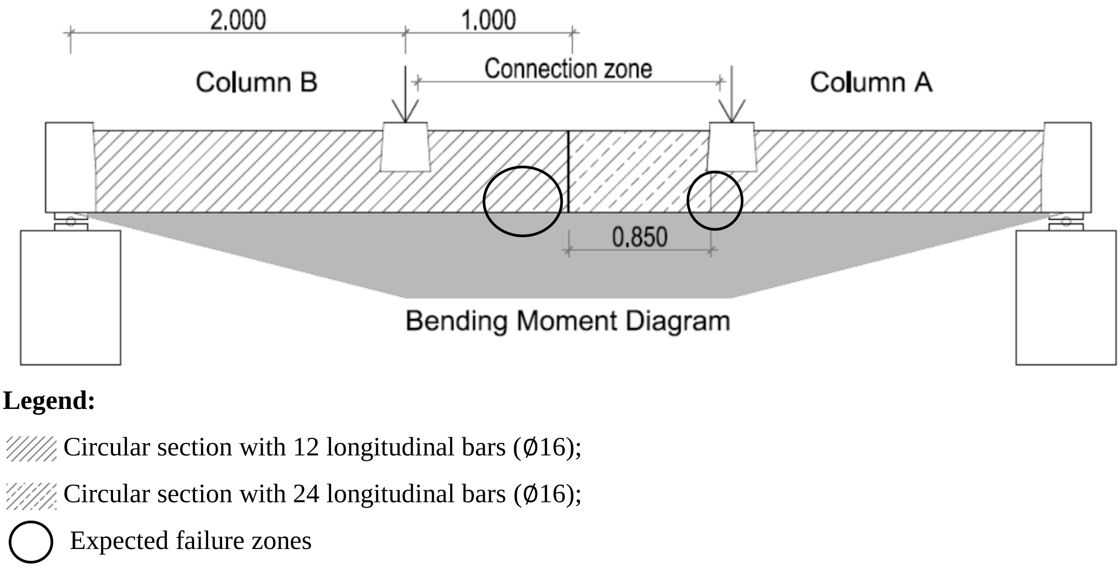

Figure 5.48: Analysis of the behaviour of specimen S3.

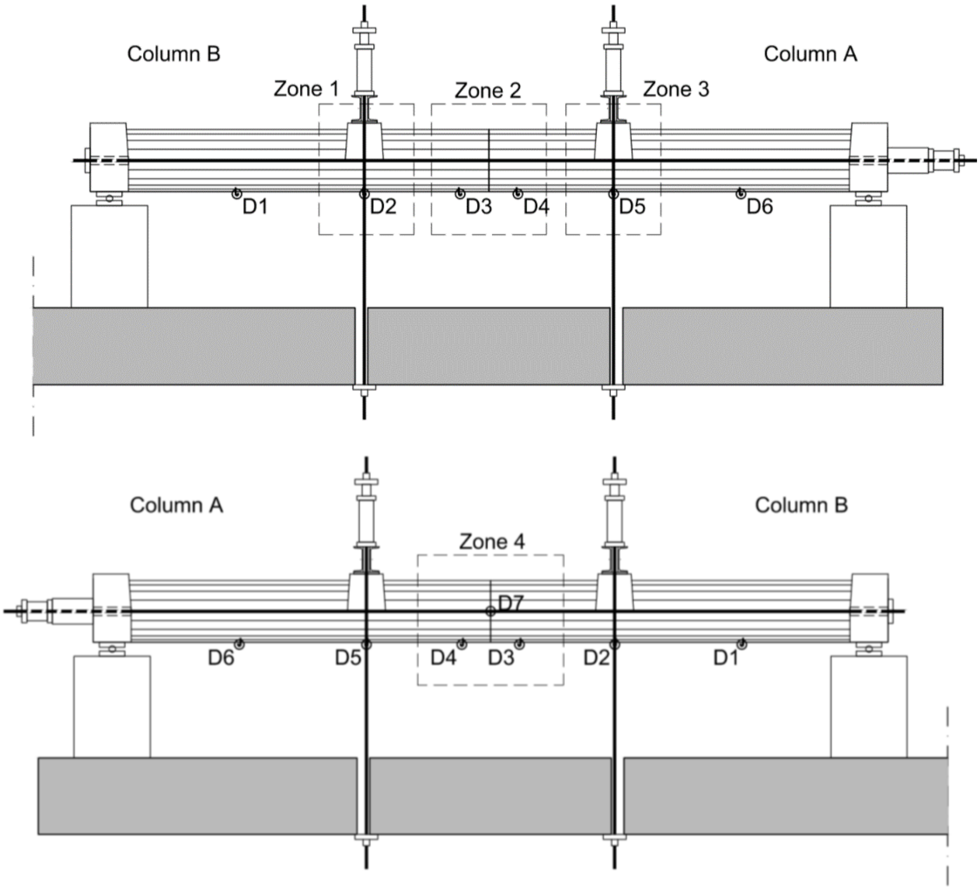

Figure 5.49: Identification of photographed zones of specimen S3 at failure.

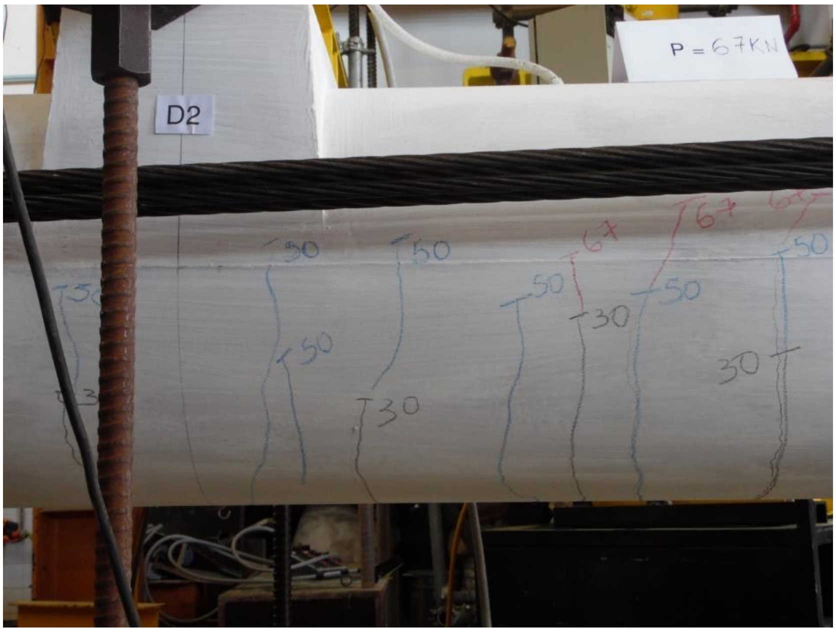

Figure 5.50: Overview of specimen S3 failure, in column B, below of vertical load application zone. (Zone 1).

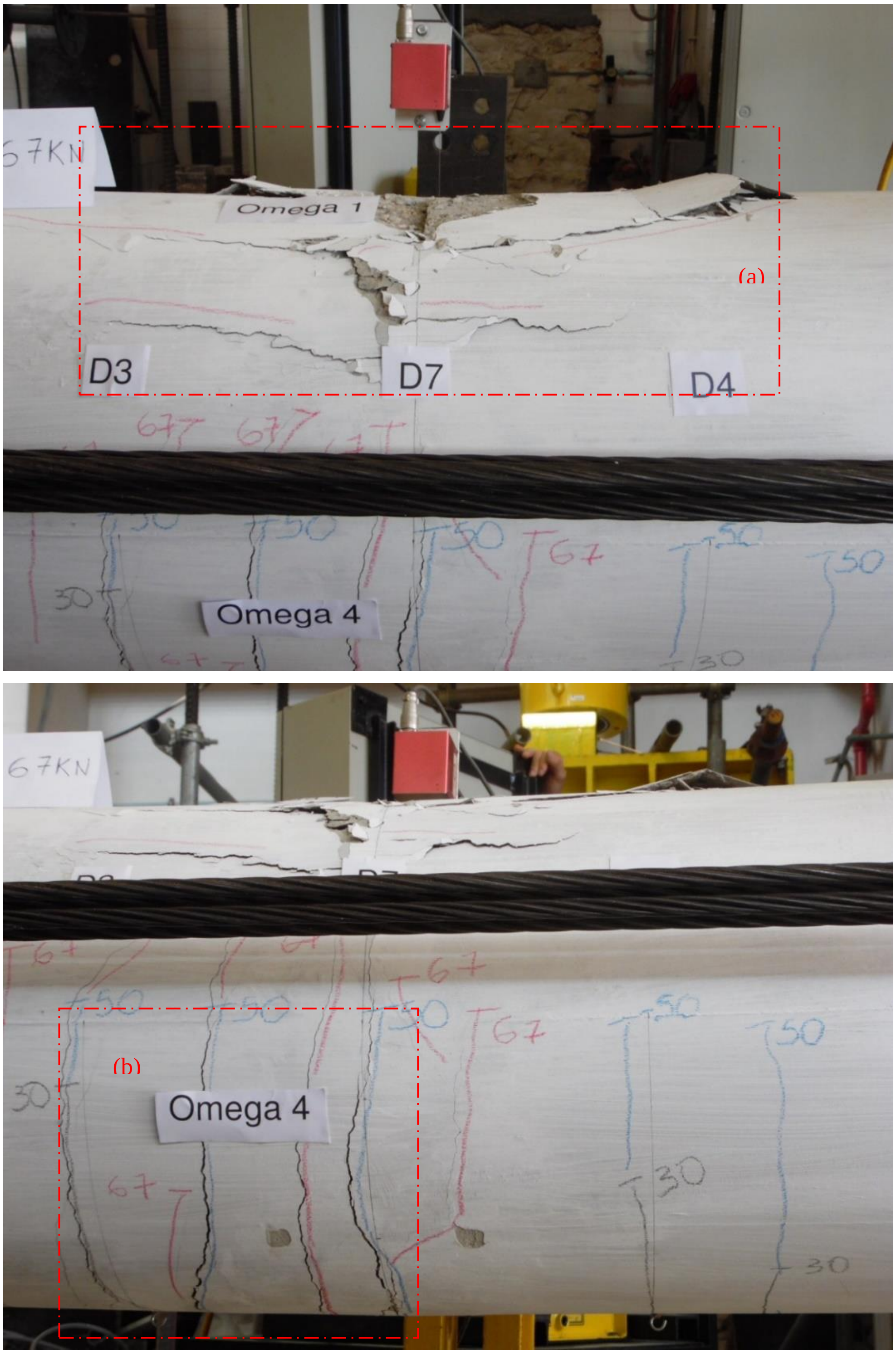

Legend: (**a**) Detachment and concrete crushing due to compression forces on the upper face; (**b**) crack openings on column underside.

Figure 5.51: Overview of specimen S3 failure, in connection zone (Zone 2)

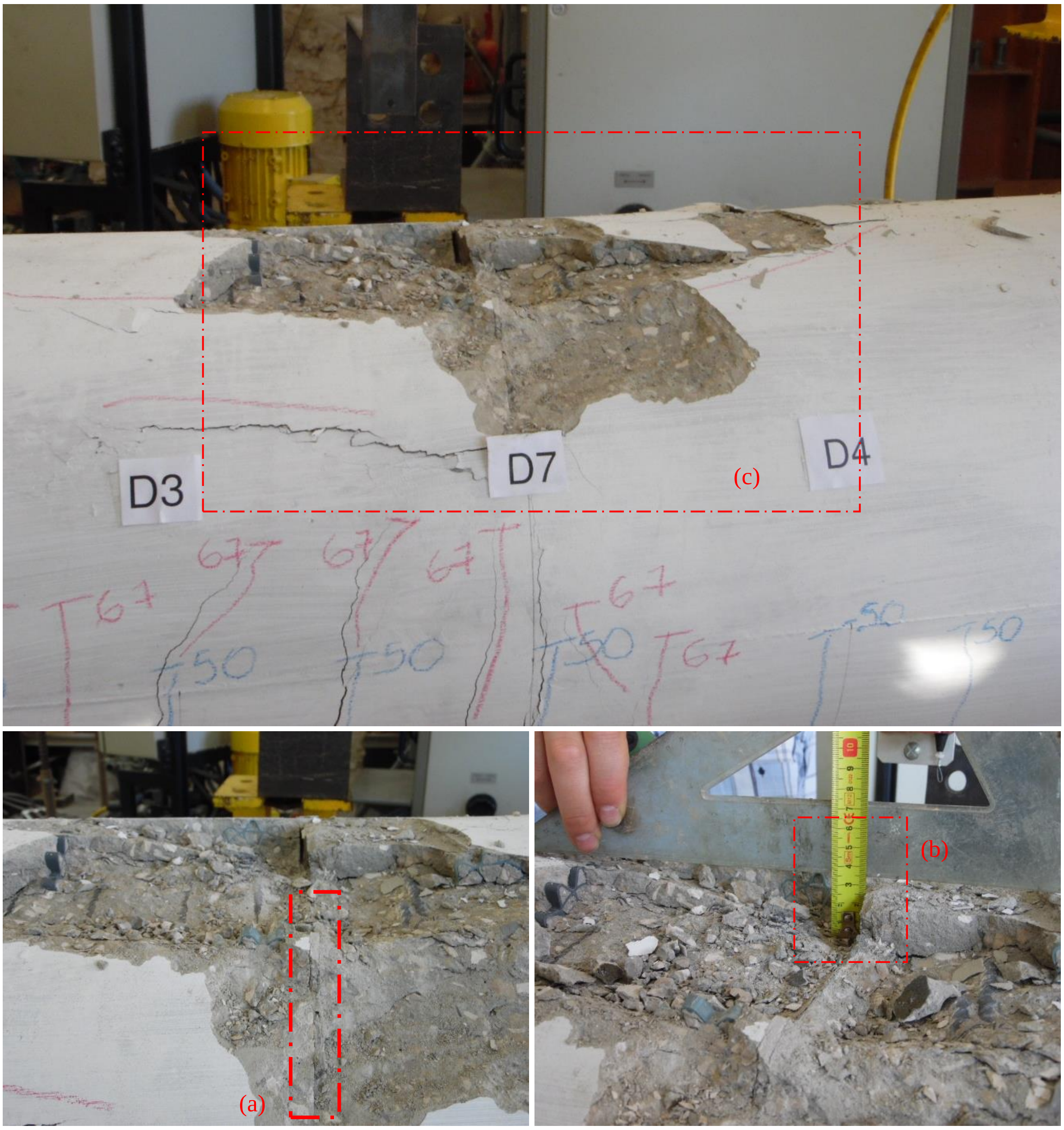

Legend: (**a**) Resin in connection joint; (**b**) absence of resin on the top of connection joint; (**c**): detachment and concrete crushing caused by compression forces in the column upper face.

Figure 5.52: Overview of specimen S3 failure, in upper part of connection zone (Zone 2)

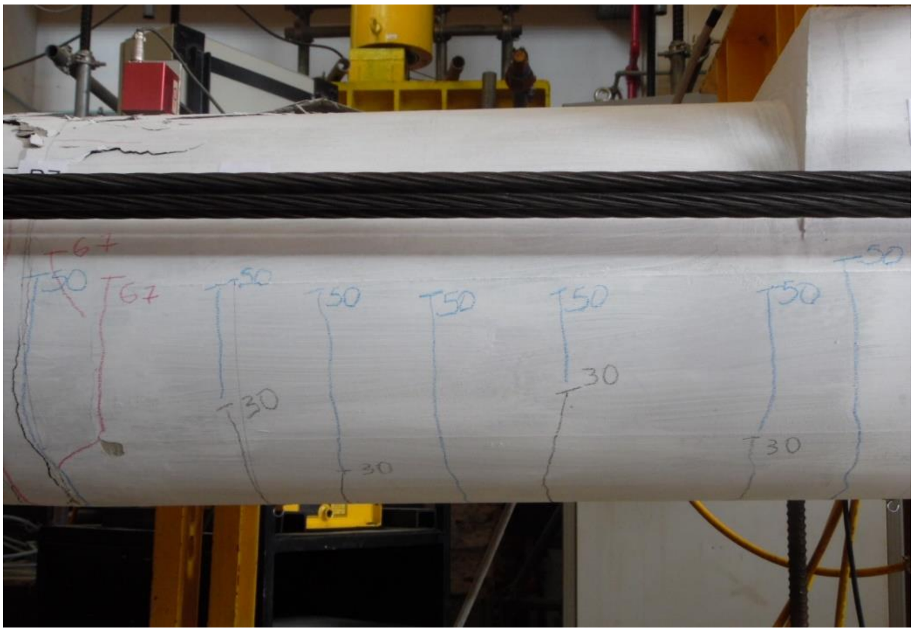

(a)

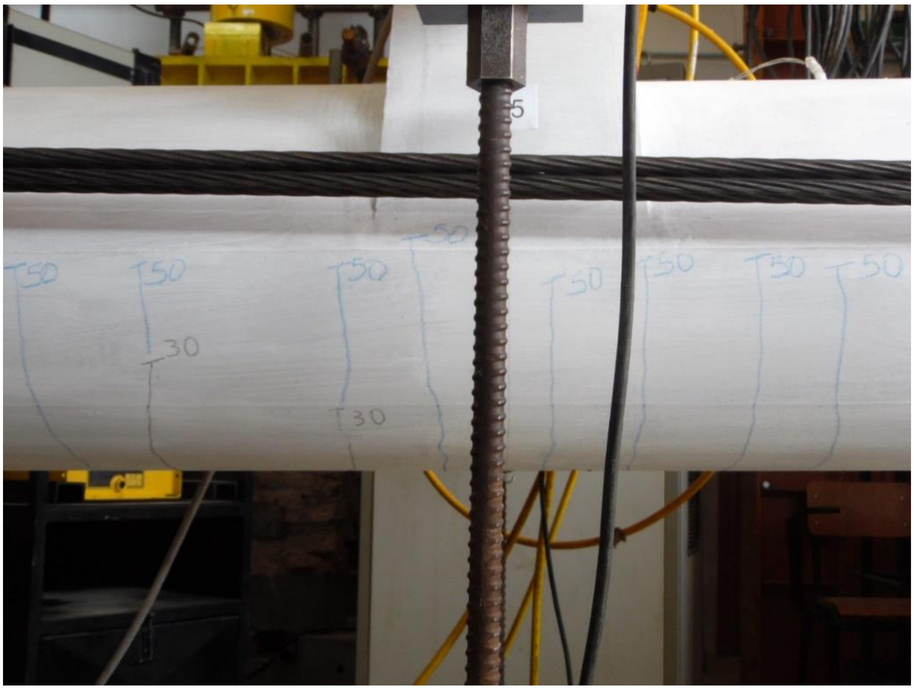

(b)

Legend: (**a**) In connection zone; (**b**) below vertical load application.

Figure 5.53: Overview of specimen S3 failure (Zone 3)

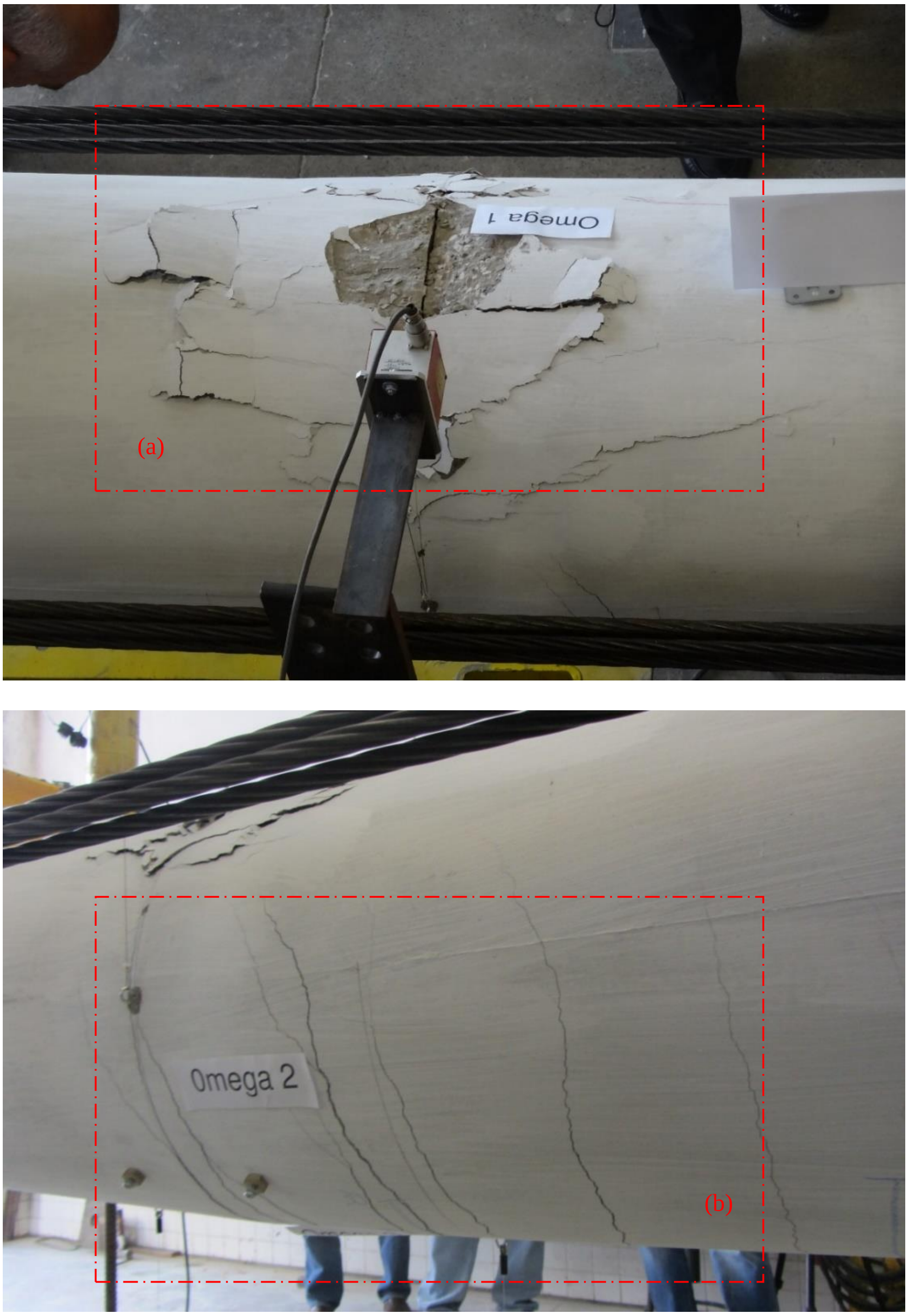

Legend: (**a**) detachment and concrete crushing on column upper face; (**b**) crack openings on column underside.

Figure 5.54: Overview of specimen S3 failure, in connection zone (Zone 4)

5.6.4 Specimen S4

Specimen S4 failure occurred after a vertical load of 275.23 kN and a final bending moment of 341.66 kNm at mid-span was reached.

With Trejor connection it was possible to ensure the same amount of reinforcement in connection zone of columns A and B. So, both columns (A and B), in connection zone, were designed with 24 longitudinal bars of 16 mm diameter ($A_s = 48.24$ cm^2). Outside the connection zone, both columns (A and B) were designed with 12 longitudinal bars of 16 mm diameter ($A_s = 24.12$ cm^2). So as in all previous specimens a plastic hinge formation would be expected in these zones (see Figure 5.50).

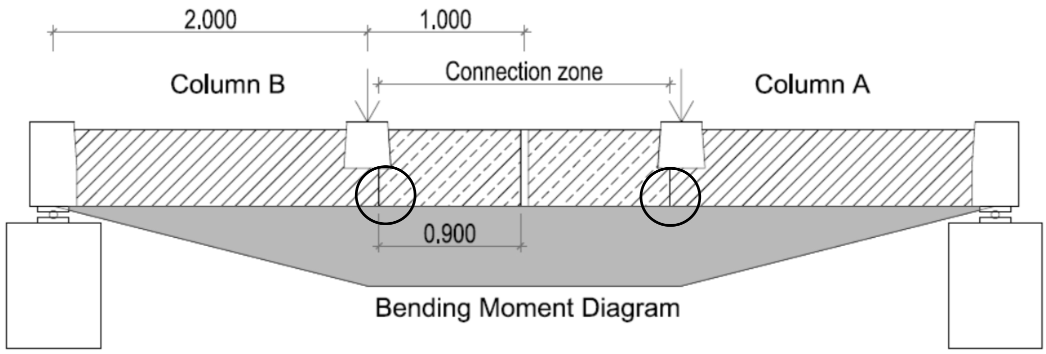

Legend:

Circular section with 12 longitudinal bars (Ø16);

Circular section with 24 longitudinal bars (Ø16);

Expected failure zones

Figure 5.55: Analysis of the behaviour of specimen S4.

However, specimen S4 failure occurred in the connection joint. Just like in specimen S1 this might have happened due to a 50 mm thick joint which led to absence of shear reinforcement at approximately 0.20 m from the middle of the connection joint. Consequently, on the column upper face, buckling of Trejor connections occurred, followed by concrete detachment caused by compression forces. With concrete detachment, occurred the decrease of compression area followed by decrease of section bending resistance, $M_{Rd,}$ which led to failure in the tensile side (column underside). In the figures below the failure mode of specimen S4 can be analysed in detail.

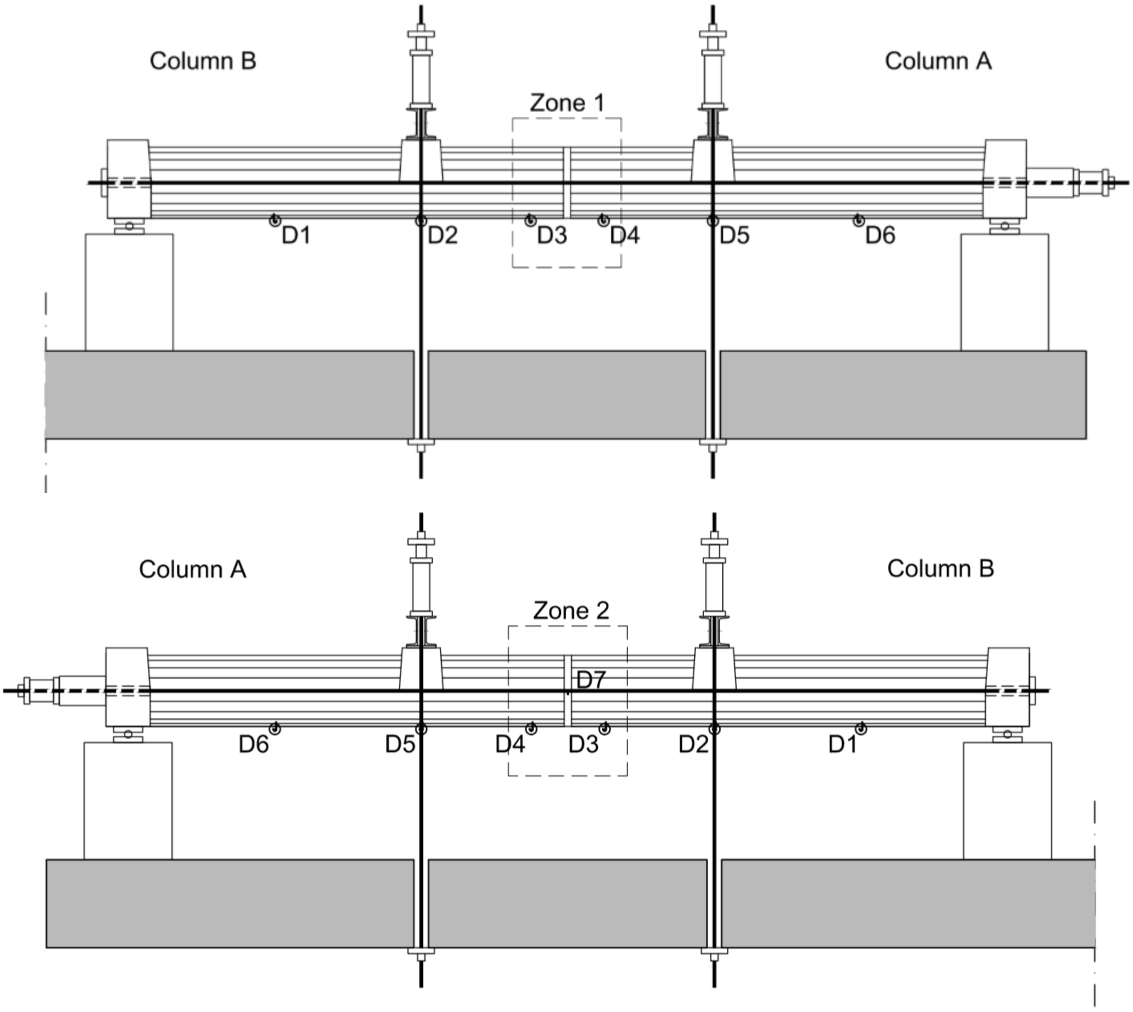

Figure 5.56: Identification of photographed zones of specimen S4.

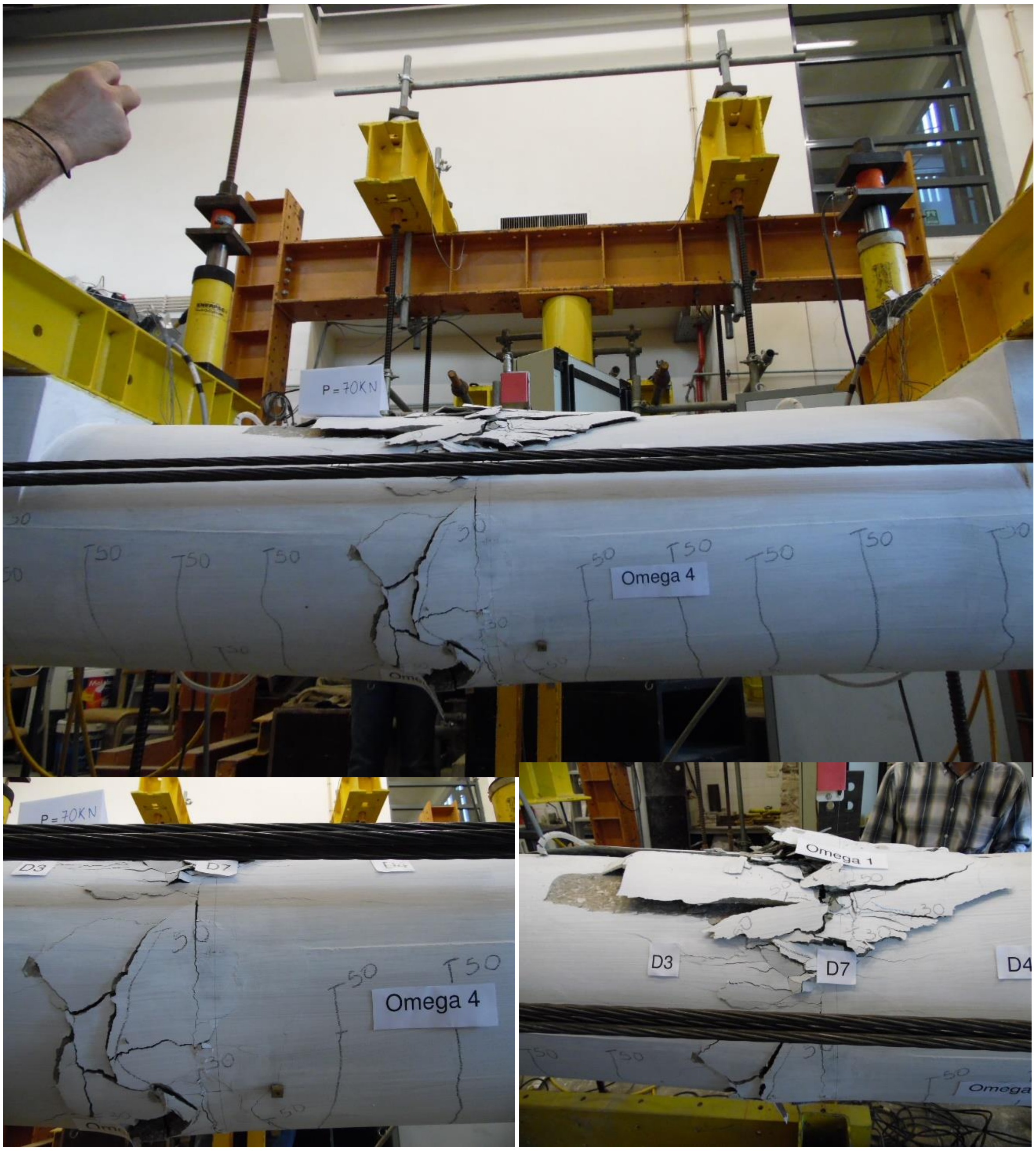

Figure 5.57: Overview of specimen S4 failure mode in connection joint (Zone 1): General scenery at mid-span.

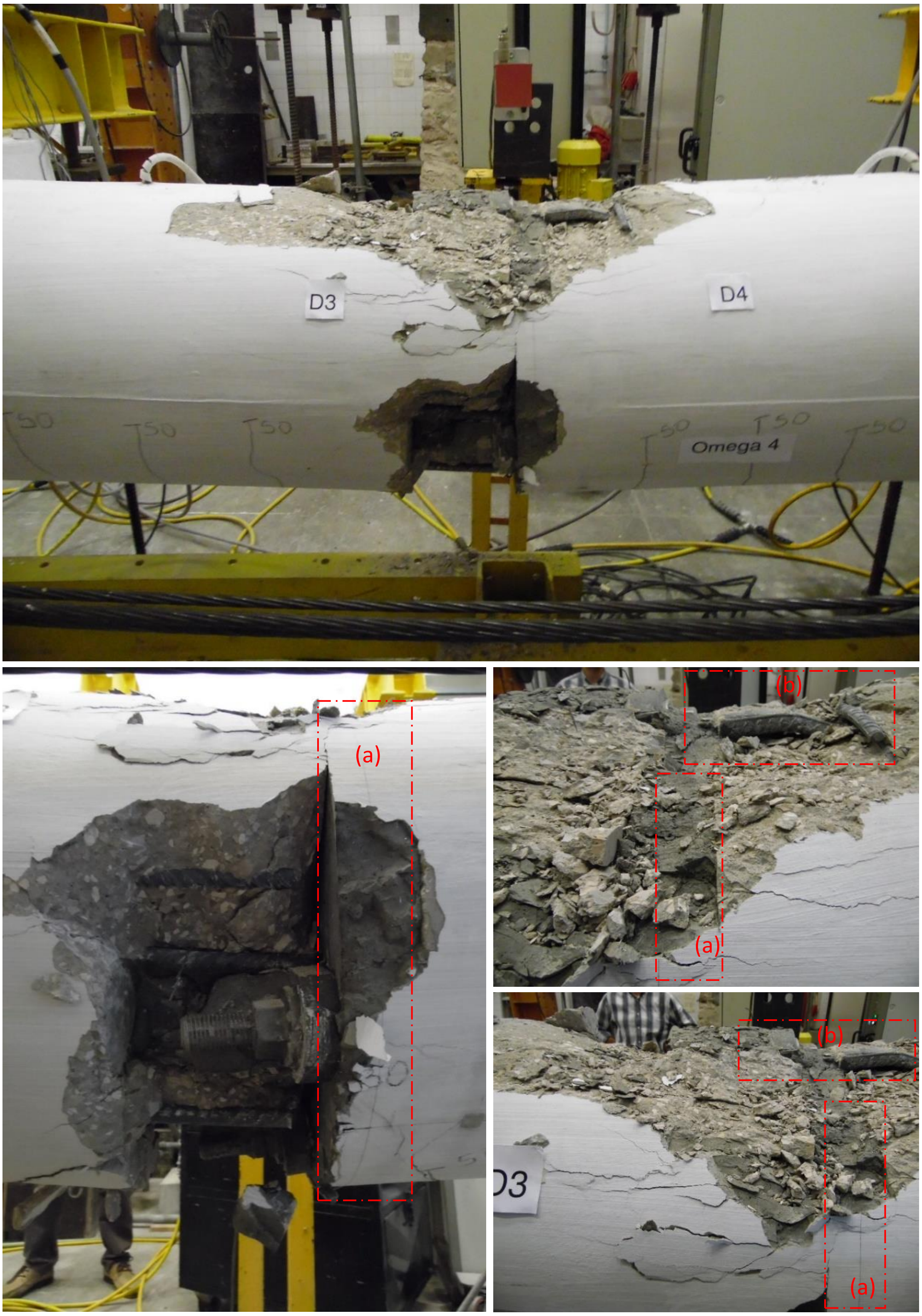

Legend: (**a**) joint with unidirectional fibre reinforcement grout; (**b**) buckling of Trejor male connection.

Figure 5.58: Overview of specimen S4 failure mode in the connection joint (Zone 1), after removing all crushed concrete.

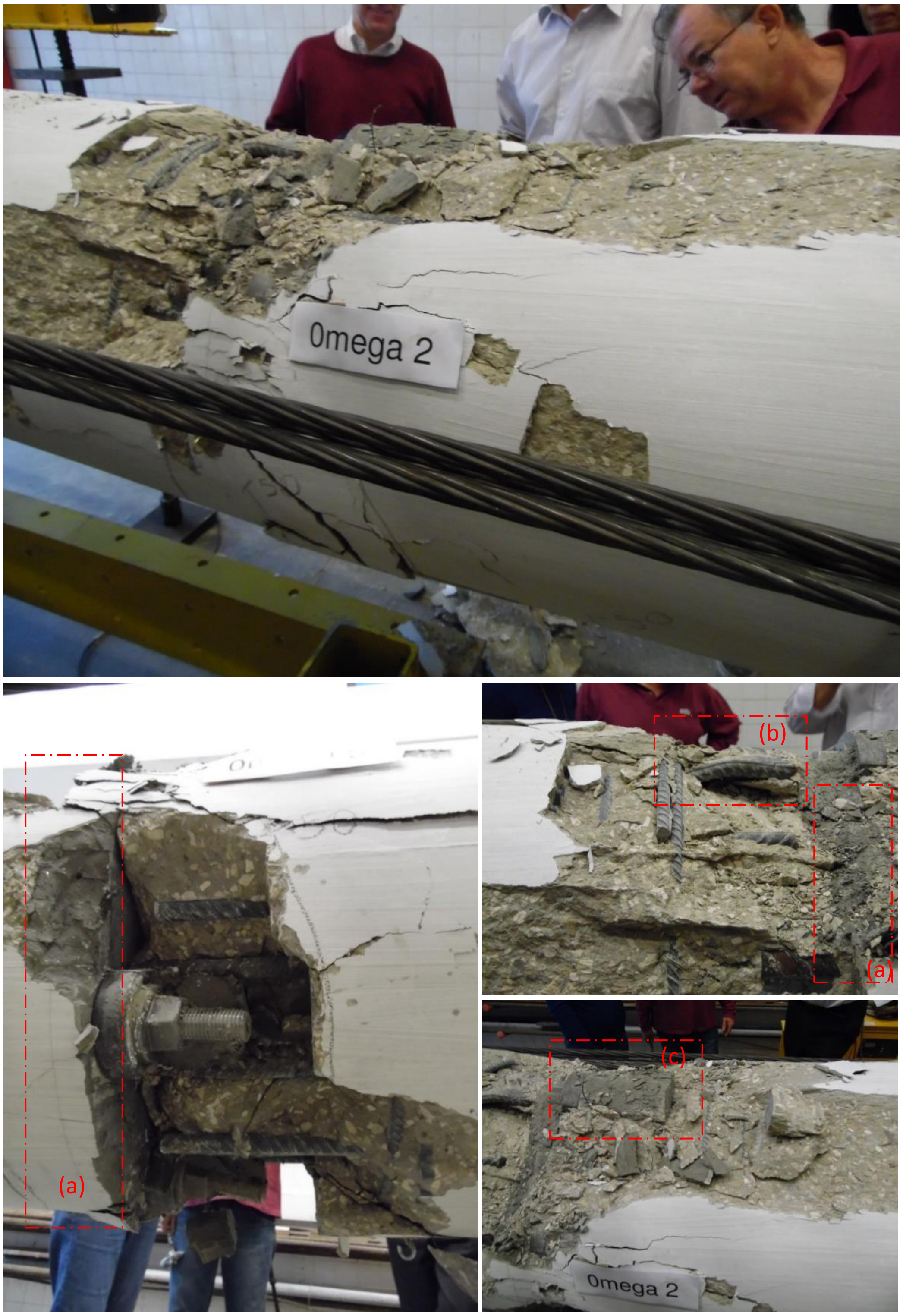

Legend: (**a**) joint with unidirectional fibre reinforcement grout (UFRG); (**b**) buckling of Trejor male connection; (**c**) hole in Trejor female connection filled with UFRG

Figure 5.59: Overview of specimen S4 failure mode in the connection joint (Zone 2), after removing all of the crushed concrete.

5.6.5 Comments

As shown in Figures 5.34, 5.39, 5.42 and 5.52 the use of unidirectional fibre reinforcement grout (UFRG) in specimens S1, S2 and S4, decreases the detachment of material in the joint and in the zone of anchor bolts holes.

As shown in Figures 5.34, 5.40 and 5.41, specimens S1 and S2 show a similar stiffness. However, the failure zones occurred in different places. In specimen S1 the failure occurred at the mid-span in connection zone while in specimen S2, with the reduction of connection joint thickness, failure in the connection zone was avoided and consequently occurred below the vertical load application zone of column A.

The failure in the 50 mm thick joint specimens S1 and S4 happened in the similar places: connection zone at mid-span due to buckling of the male anchor bolt connection. This problem can be avoided with the introduction of more links in this region, improving the confinement of anchor bolts (see Figures 5.34, 5.53 and 5.54).

Although there are differences between S3 and S4, namely, the type of connection and the type of joint, these specimens had a similar structural behaviour (nearly the same stiffness). Both had suffered failure in the connection joint at mid-span. However, if the buckling of anchor bolts in S4 had not occurred, or if the upper face of connection zone was completely filled, it is questionable if the structural behaviour of these two specimens would be similar.

As expected, the presence of cracks was always more significant and extensive in zones with less reinforcement. As mentioned, the only situations where this did not happen was in specimens S1 and S4 due to buckling of anchor bolts.

Chapter 6

Conclusions and Future Work

This chapter presents the conclusions of this study and some future work of interest in this area.

6.1 Conclusions

The increased use of precast concrete elements as a result of good quality control of products, economic viability and assemblage speed, calls for the need to use connection types to make the precast concrete solutions even more competitive and capable to given a good response to different types of actions which are subject during their life time.

According to the results obtained in this research, the use of these type of connections is perfectly acceptable and safe. In the case of commercial anchor bolts the positioning of links in the connection joint zone must be made with care to avoid the buckling of anchor bolts. Thus, it would be possible to have avoided the failure in the connection joint of specimen S2. In the case of specimen S3 with connections with protruding steel bars and corrugated sleeves: grout pouring, injection of resin and the bonding of lengths of sleeves must be undertaken with care. In this type of connection, the ideal would be the use of protruding steel bars in the two columns A and B. Thus, it would be possible to ensure the equal amount of reinforcement in the connection zone and this might avoid failure in connection zone.

Based on results it could be considered that the specimen S3 with 12 protruding steel bars would have the similar strength to the specimen S4 connection with 6 Trejor anchor bolts. However, it may be dangerous to come to this conclusion as the failure of specimen S3 happened due to the absence of resin in upper face of column in the connection joint and in specimen S4 it happened due to buckling of the male anchor bolt connections.

6.2 Future Work

In this dissertation, the proposed objectives were fulfilled. Below, possible future works with an aim to improve and develop the subject of this work are presented:

- more experimental tests in the specimens with 50 mm of thick wet joints to understand if it is possible to avoid the failure in the connection joint due to buckling of anchor bolts;
- more experimental tests on the use of protruding steel bars in the two columns A and B to understand what influences in failure mode could have;
- experimental tests with the same amount of reinforcement but with different thickness of joint, to guarantee the direct comparison between the 50 mm thick connection and the dry joint;
- experimental tests, similar to the ones performed in this study but avoiding the sharp transition of reinforcement to at least 1.0 m away from the cross section of maximum bending moment;
- testing the remnant connections of the truss towers in order to safely start their production;
- disseminate the present results to the scientific community.

References

[1] Global Wind Energy Council. (2014). Global Statistics. Fonte: GWEC. Representing The Global Wind Energy Industry: www.gwec.net.

[2] Lúcio, V. & Chastre, C. *Precast concrete wind tower structures-historic evolution, current development and future potential*; CPI - Concrete Plant International; June 2014.

[3] El Debs, M. K. *Precast concrete: design principles and uses*. São Carlos, SP, Publication EESC-USP, 2000. (In Portuguese)

[4] Reguengo, R., Lúcio, V., & Chastre, C. *Column-foundation connections for precast structures with protruded rebars from the column – monothonic and cyclic tests*. Encontro Nacional Betão Estrutural 2008.Guimarães, 2008 (In Portuguese);

[5] Fagà, E., Bianco, L., Bolognini D., & Nascimbene, R. *Comparison between numerical and experimental cyclic response of alternative column to foundation connections of reinforced concrete precast structures*; Proceedings of the Third International fib Congress and PCI Annual Convention and Bridge Conference; Washington, DC, USA, June 2010; ISBN: 9781617828218.

[6] Appleton, Júlio. *Estruturas de Betão-volume 1-1ª Edição*. Lisboa: Edições Orion, Julho de 2013 (In Portuguese).

[7] Magalhães, António J. S. *A Pré-fabricação em Betão em Edifícios*. Master's thesis, Instituto Superior de Engenharia do Porto, 2013 (In Portuguese).

[8] Proença, J. *Comportamento Sísmico de Estruturas Pré-fabricadas – Desenvolvimento de um Sistema Reticulado Contínuo*. Doctorate thesis, IST, Lisboa, 1996 (In Portuguese).

[9] Reis, P. R. S. R. *Ligação Contínua Viga-Pilar em Estruturas Pré-Moldadas de Betão*. Master's thesis, IST, Lisboa, 2000 (In Portuguese).

[10] Albarran, E. G. *Construção com Elementos Pré-fabricados em Betão Armado – Adaptação de uma Solução Estrutural "in situ" a uma Solução Pré-fabricada*. Master's thesis, IST, Lisboa, 2008 (In Portuguese).

[11] "Regulamento de Segurança Contra Incêndio", Porto Editora, Maio de 2009 (In Portuguese).

[12] "Tolerance Manual for Precast and Prestressed Concrete Construction". PCI, 2000.

[13] Pompeu dos Santos, S. G. *Comportamento de Ligações de Estruturas Prefabricadas de Betão*. Tese apresentada ao concurso para especialista do Laboratório Nacional de Engenharia Civil, LNEC (In Portuguese).

[14] Mokk, L. *Construcciones com materiales prefabricados de hormigón armado*. Bilbao: Ediciones Urmo, 1969. 555p.

[15] MURCHÚ, Brian Ó; QUINN, Caroline. Precast concrete: frames guide. Irish Precast Concrete Association (IPCA). Dublin.

[16] Björn, C. *Structural Connections for Precast Concrete Buildings*. CEB-FIB 43. Paper presented at FIB Guide to good practice . Switzerland. 2008.

[17] Instituto Português da Qualidade (IPQ): *Norma Portuguesa EN 1998-1-1 Eurocódigo 8: Projecto de Estruturas para resistência aos sismos- Parte 1-1: Regras gerais, ações sísmicas e regras para edifícios*. 2010 (In Portuguese).

[18] Ramos, A.P., & Lúcio, V. *Sebenta Estruturas de Betão Armado I e II*. Faculdade de Ciências e Tecnologia. September 2009 (In Portuguese).

[19] Elliot, Kim S. *Multi-storey precast concrete frame structures*. Blackwell Science. Oxford-UK.1996.

[20] Khandelwal, M. *Basic Forces Transfer Mechanism for Design of Structural Precast Connections*. The Masterbuilder Magazine. January 2015.Vol 17.

[21] Qing Zhi, Zhengxing Guo, Quandong Xiao, Fu Yuan, & Jingran Song. *Quasi-static test and strut-and-tie modeling of precast concrete shear walls with grouted lap-spliced connections*. Journal Construction and Building Materials. Volume 150, 2017.

[22] Elliott, Kim S. *Precast Concrete Structures*. Boston. Butterworth-Heinemann. 2002.

[23] Mostert, Louwrens Hubert. *Design and construction preferences for connections in the precast concrete industry of South Africa*. Master's thesis. Faculty of Engineering at Stellenbosch University. South Africa. 2014.

[24] Santos Silva, António M. *LIGAÇÕES ENTRE ELEMENTOS PRÉ-FABRICADOS DE BETÃO*. Master's thesis. Instituto Superior Técnico de Lisboa, 1998 (In Portuguese).

[25] National Cooperative Highway Research Program (NCHRP) Report 698: *Application of Accelerated Bridge Construction Connections in Moderate-to-High Seismic Regions – Appendix H - Detailed Evaluation of Connection Types*. Washington, DC. National Academies of Sciences, Engineering, and Medicine. 2011

[26] PCI: *PCI Design Handbook – Precast and Prestressed Concrete*. Precast/Prestressed Concrete Institute. Chicago. 1992.

[27] Stupré — Society for Studies on the Use of Precast Concrete. *Precast Concrete Connection Details*. Beton-Verlag GmbH, Düsseldorf, Netherlands, 1981.

[28] P. Sideris, A. J. Aref, & A. Filiatrault. *HYBRID SLIDING-ROCKING POST-TENSIONED SEGMENTAL BRIDGES: LARGE-SCALE QUASISTATIC AND SHAKE TABLE TESTING*. University at Buffalo – The State University of New York, U.S.A, 2012.

[29] Peikko Group: Anchor Bolt Connections. https://www.peikko.com/products/precast-products/column-connections, visited on 2018-01-25, (In Portuguese).

[30] Instituto Português da Qualidade (IPQ): *Norma Portuguesa NP EN1992 1-1: Eurocódigo 2: Projecto de estruturas de betão, Parte 1-1: Regras gerais e regras para edifícios*. 2010. (In Portuguese).

[31] Reis, Ana Rita. *LIGAÇÃO VIGA-PILAR DE ALTO DESEMPENHO SÍSMICO*. PhD thesis. Faculdade de Ciências e Tecnologia, Universidade Nova de Lisboa, 2012 (In Portuguese).

[32] Ficha técnica Sikadur-52 Injection. *RESINA DE EPOXI DE BAIXA VISCOSIDADE PARA INJECÇÃO*. versão n.º3, n.º de identificação: 07.608, Fevereiro de 2017 (In Portuguese).

[33] Instituto Português da Qualidade (IPQ): *NP EN 10002-1 - Materiais metálicos. Ensaio de tracção. Parte 1: Método de ensaio à temperatura ambiente*. 2006 (In Portuguese).

[34] Instituto Português da Qualidade (IPQ): *NP EN 12390-3 – Ensaios de Betão Endurecido. Parte 3: Resistência à Compressão de Provetes de Ensaio*. 2003 (In Portuguese).

[35] Instituto Português da Qualidade (IPQ): *Norma Portuguesa NP EN206-1: Betão, Parte I: Especificação, desempenho, produção e conformidade*. 2007. (In Portuguese).

[36] Instituto Português da Qualidade (IPQ): Norma Portuguesa NP EN196-1: Métodos de ensaio de cimentos, Parte I: Determinação das resistências mecânicas, 2006. (In Portuguese).

[37] Ficha técnica MasterFlow 765. *Argamassa fluída, de retracção compensada para enchimentos e ancoragens*. edição 11 de Maio de 2015 (In Portuguese).

[38] Gião, R., Lúcio, V., Chastre, C., & Brás, A. *UFRG-unidirectional fibre reinforced grout as strengthening material for reinforced concrete structures*. Lisboa: BEFIB2012, 2012. (In Portuguese).

[39] FAVIR: *Fábrica de plásticos, Lda*, 2015. http://www.favir.pt, visited on 2016-07-14, (In Portuguese).

[40] Monteiro, A., Cachim, Paulo., Morais, Miguel. *Desenvolvimento de um programa de cálculo de secções de betão armado em Estado Limite Último segundo o Eurocódigo 2*. Encontro Nacional Betão Estrutural 2012, FEUP, Outubro 2012. (In portuguese).

[41] Ramos, A.P., & Lúcio, V. *Sebenta Estruturas de Betão Armado I*. Faculdade de Ciências e Tecnologia. September. Chapter 7 - Pag.12. 2009 (In Portuguese).